A STUDY OF NEAR-SURFACE CURRENTS IN ENDICOTT ARM

A

THESIS

Presented to the Faculty of the

University of Alaska in Partial Fulfillment

of the Requirements

for the Degree of

MASTER OF SCIENCE

By

Robert R. Gleason, A.S., B.S.

College, Alaska

May, 1972

A STUDY OF NEAR-SURFACE CURRENTS IN ENDICOTT ARM

APPROVED:

____

____

____

____
Chairman

APPROVED: ______________________ DATE ____________
Dean of the College of Mathematics,
Physical Science and Engineering

____
Vice President for Research and Advanced Study

ABSTRACT

Currents in Endicott Arm were measured by parachute drogues and ice drift photogrammetry. The parachute drogues showed mean outflow speeds between 2 and 20 cm/sec. The mean outflow extended at reduced speeds to below ten meters and may have extended to sill depth at twenty meters.

From equations of drag and inertia, a differential equation was formed to describe tidal ice drift speeds. The equation was solved on an Analog computer and the solution shown as plotted. Coupling curves were used to measure the net tidal speed. Ice drift mean outflow speeds based upon these computations agreed with parachute drogue mean outflow speeds.

ACKNOWLEDGEMENTS

I wish to thank Dr. J. B. Matthews and Professor D. H. Rosenberg for their help and guidance during my graduate program. Further, I wish to thank Dr. R. F. Carlson and Dr. N. A. Lindberger for their assistance in solving the tidal ice drift problem and to thank Mr. John Lind for programming this problem on the analog computer.

I am indebted to Mr. R. E. Johnson for the editing and to Linda Bebee and Lavonia Wiele for the typing of this manuscript.

This work was made possible through funds provided by the Office of Naval Research, Contracts NONR 3010 (05) and N00014-67-A-0317-0002 and by the Institute of Marine Science, University of Alaska.

TABLE OF CONTENTS

Chapter III

RESULTS

Chapter IV

ANALYSIS OF THE DATA

Chapter V

SUMMARY AND CONCLUSIONS

Page

LIST OF FIGURES

Page

Page

Page

CHAPTER I

PHYSICAL OCEANOGRAPHY OF ENDICOTT ARM

1.1 Introduction

This study was undertaken to determine seasonal variations in the surface currents of a fjord estuary. The area selected for study was Endicott Arm. It was chosen because it is a fairly straight inlet with a sill. Measurements were restricted to surface and near-surface currents.

Endicott Arm is a fjord estuary located in Southeastern Alaska, 50 miles south of Juneau (figure 1). It forms a two-fjord system with Tracy Arm, sharing a common outlet to Stevens Passage through Holkam Bay (figure 2).

The data analyzed in this report were taken aboard the R/V ACONA and the R/V MAYBESO between November 1966 and March 1969. These research vessels are operated by the Institute of Marine Science, University of Alaska. In connection with the current data, bathymetric soundings were taken in March 1967 and November 1968. These were plotted and are discussed in Appendix A.

1.2 Water Masses

Matthews and Rosenberg (1968) have discussed the physical oceanography of Endicott Arm: the circulation is driven by the input of ice and fresh water from the North Dawes and South Dawes glaciers plus water from peripheral stream flow. The resultant accumulation of less dense water forms a seaward slope. The outflow of water downslope entrains

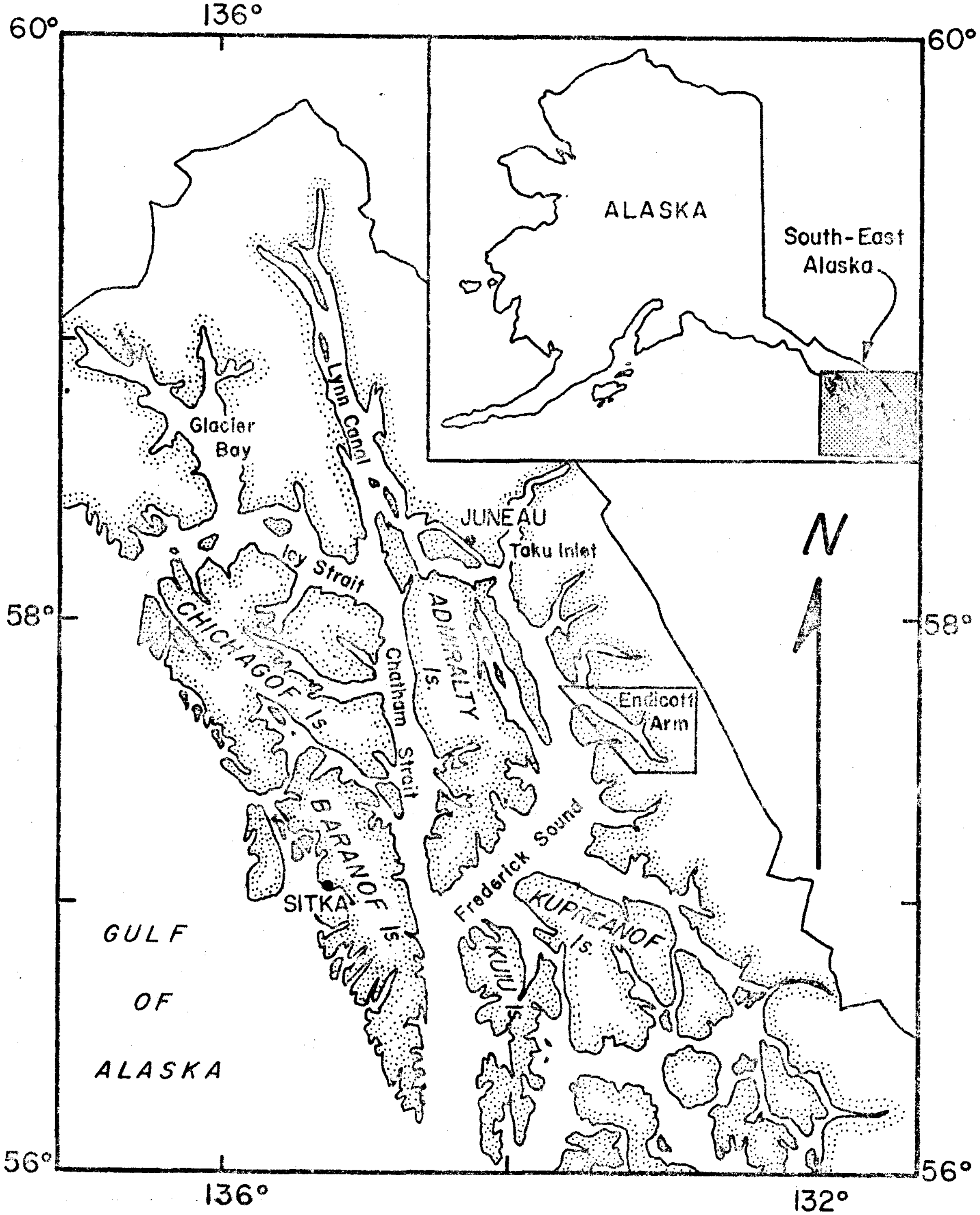

Figure 1 Map of Southeastern Alaska showing Endicott Arm south of Juneau

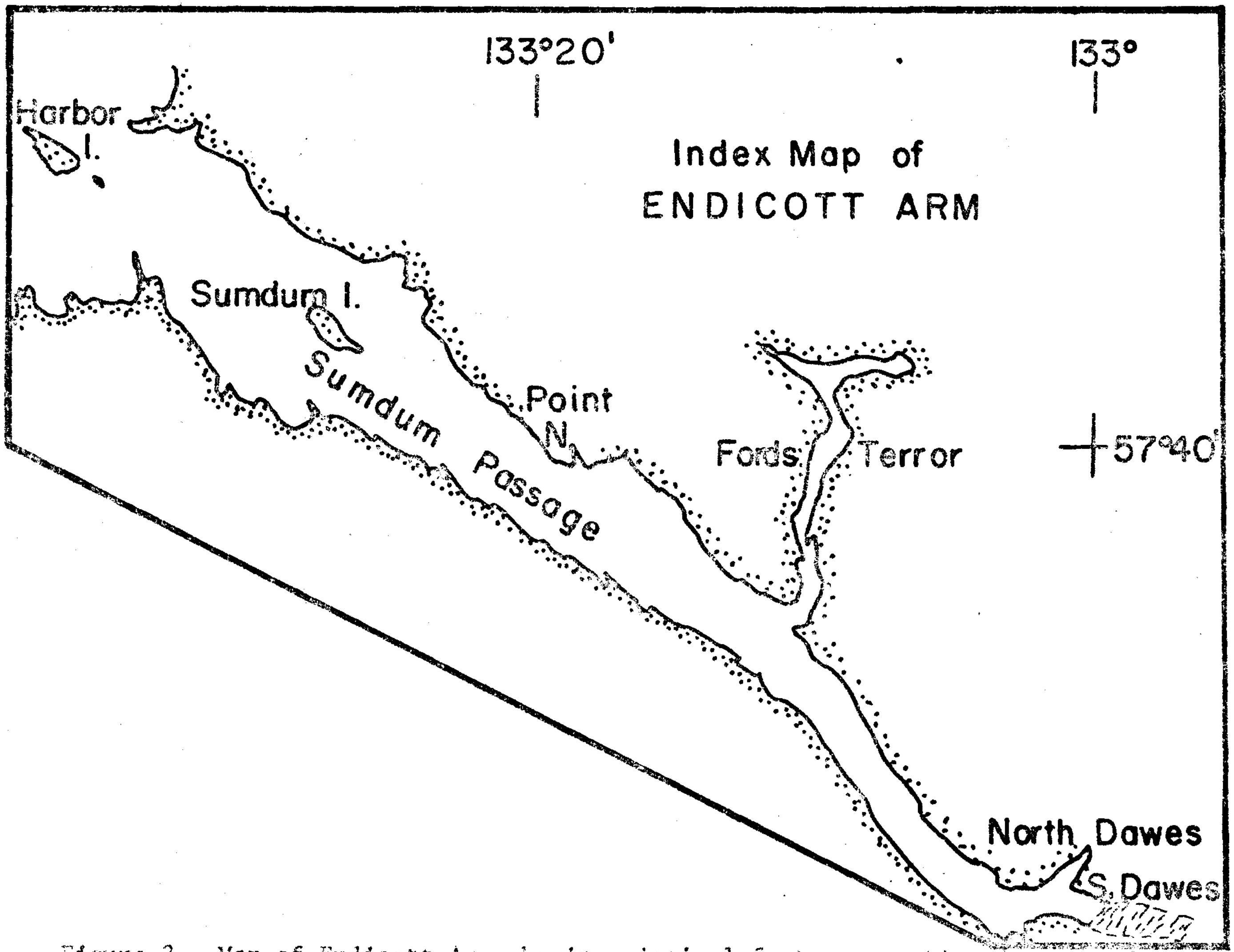

Figure 2. Map of Endicott Arm showin principal features mentioned in thesis.

salt water from beneath raising the salinity and volume of the outflow as it moves toward the mouth. To replace lost salt, saline water flows up-inlet under the outflow layer thus causing a two-layer flow.

The water masses in the inlet below 10 meters were grouped by Matthews and Rosenberg (1968) into the fall water mass (temperature above 4°C and slainity below 31.4°/₀₀) and the winter-spring water mass (temperature generally below 4°C, salinity 31.2°/₀₀). It appears that Pickard's (1967) ice inlet water mass represents a transition between the winter-spring water mass and the fall water mass seen in Endicott Arm (Matthews and Rosenberg, 1969).

Wallen and Hood (1968) stated that there are two seasonal maximums in run-off: the first, after Pickard (1961), occurs around June and is composed of melt from snow fields and glaciers. The second is in October when the maximum precipitation falls in the Juneau area. Wallen and Hood (1971) found that in glacial estuaries, such as Endicott Arm, the first maximum is usually delayed until July.

1.3 Currents

Currents in Endicott Arm are caused by two factors: fresh water outflow and tidal action. Fresh water supplied by streams and glacier discharge flows down inlet. As it flows it entrains salt water from the lower inflow layer and finally flows out into the larger body of water, Stevens Passage. The currents associated with this flow are longitudinally outward.

Superimposed upon this outflow are tidal oscillations. The tide alternately accelerates and retards the surface outflow. When the tidal amplitude is greater than the surface outflow, the surface currents reverse during the maximum flood current.

Currents are modified by the shape of the inlet. Where the inlet narrows or shoals sufficiently, the current increases. The passage between the southwest bank of Sumdum Island and the shore, "Sumdum Passage," as it is called herein, is an example of narrowing of the inlet. The sill is an example of narrowing and shoaling where the currents reach their maximum.

1.4 Tide

Tide in an estuary has distinctive characteristics depending upon the shape and size of the basin. In Southeastern Alaska, near Juneau, the tides have a semi-diurnal inequality: ie., there are two high tides and two low tides of unequal magnitude per lunar day (Tide Tables, USC&GS). In an estuary, the tide will have characteristics of a progressive or standing wave. In Endicott Arm it will be demonstrated later that the tide is close to a standing wave.

CHAPTER II

METHODS OF CURRENT MEASUREMENT

2.1 Instrumentation and Techniques

The standard method of parachute drogues was used primarily to measure currents (Volkman, Knauss, and Vine, 1956). Further, a secondary system of photographically monitoring the drift of icebergs was used to measure currents. The icedrift indicated currents were compared with the parachute drogue measured currents to indicate the usability of ice drift as a current measuring technique.

2.1.1 Parachute Drogues

The basic design of the parachute drogues used in this study is shown in Figure 3. The drogue consists of a submerged parachute attached to a surface float. This float is fitted with a mast, identification flags and a small flashing light for night tracking. The parachute has a greater area and drag coefficient than the rest of the drogue; thus the float and flags follow the movement of the parachute (Volkman, et al., 1956).

Knauss (1963) worked out the relationship between drag coefficient, area, and velocity for the drogue. This relationship is:

$$v - v_d = (V_s - v) \left(\frac{C_s A_s}{C_d A_d} \right)^{1/2}$$

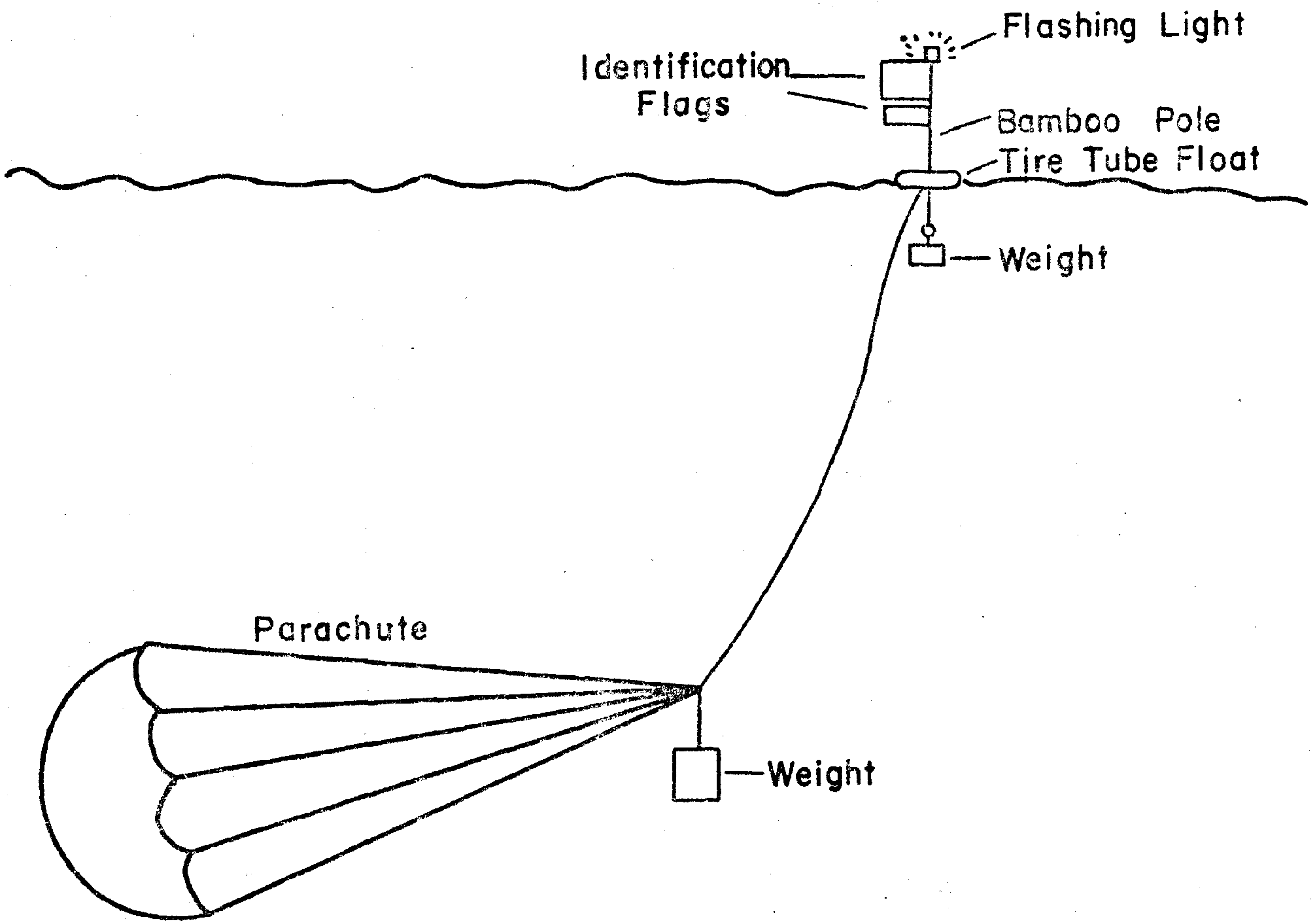

Figure 3. Schematic of Parachute Drogue showing float, pole, flags, line and parachute.

where v is the drogue velocity, v_s and v_d are the current velocities at surface and parachute depth, C_s and C_d are drag coefficients of the float and parachute, and A_s and A_d are the areas of float and parachute.

The parachutes used in these measurements were 28 feet (1.5 meters) diameter personnel parachutes with a frontal area of 57.2 m^2. They were attached to the float with a one quarter inch (0.62 centimeter) line, which for a 10 meter length has an area of about 0.06 m^2. The immersed area of the float and of the pole were about 0.08 and 0.12 m^2, respectively. Hoerner (1965) gives a maximum drag coefficient for a parachute as 1.7 (C_d). The drag coefficient of the rope is 1.5, for the pole 1.0 and for the float 1.1 (Roshko, 1961). (Reynold's numbers were $8 \times 10^{+1}$, $7 \times 10^{+2}$ and $8 \times 10^{+3}$, respectively.) Then C_sA_s=0.30 and C_dA_d-97.3. The ratio of the drags is:

$$\frac{C_sA_s}{C_dA_d}^{1/2} = 0.0555$$

Thus, for a ten meter drogue (parachute at ten meters) moving with a mean velocity of 1.5 cm/sec down-inlet, which the surface velocity is 5.0 cm/sec down-inlet, the error due to parasite drag would be 0.194 cm/sec or about 13% of the true 10 meter velocity.

The drogue positions are determined by running the ship alongside the drogue and then determining the ship's position by radar. The ship's position was determined by measuring the ship's heading with the gyro-compass and the range and bearing to a prominent known landmark with the radar. The range was measured to a tolerance of ± 18 meters at a distance of 0 to 5.5 kilometers and to ± 185 meters at a range of 5.5 to 11.0 kilometers. The bearings were measured to the nearest degree giving a maximum error of less than 2°. At a distance of 5.5 kilometers which was the longest range normally employed in positioning the drogues, the error was ± 185 meters, or about 3%.

On two occasions during the summer of 1968 the R/V ACONA was unavailable. The parachute drogues were then tracked from the R/V MAYBESO using a sextant to measure two angles between three prominent points. The error in determining positions by this method was estimated to be 365 meters, or about 7%.

2.1.2 Iceberg Photogrammetry

Photogrammetric methods have been adapted for use in numerous oceanographic applications. Keller (1963) and Swanson, Keller and Hicks (1963) reported measuring the tidal currents in several harbors via aerial photogrammetry. The technique give excellent resolution of current at all points where targets were placed. Forrester (1960) studied the application of aerial photogrammetry to water current patterns. Thorndyke and Ewing (1969) give illustrations of the uses of photogrammetry to measure ocean bottom currents.

The large number of icebergs in Endicott Arm provided excellent targets for an attempt to determine near-surface water movement using photogrammetric techniques.

Horizontal sequential pictures of icebergs were taken from land-based sites on opposite sides of the inlet during 10 July, 24 and 25

August 1968 and 6 March 1969. Horizontal, land-based, sequential photography has an advantage over aerial photography in that the cameras' orientation can be determined from a single picture and that high cloudiness does not impair the photo-mission.

Icebergs proved to be excellent targets since they had sufficient height to be identifiable for a distance of four miles. Drawbacks to their use as current indicators are that the exact depth and the coefficient of drag of each iceberg is unknown. Further, a knowledge of the current profile and the magnitude of tidal oscillations are needed in order to calibrate the general iceberg motion.

A technique requiring single photographs was used to measure positions of the icebergs. This technique (figure 4) required knowledge of the apparent distance of the iceberg below the shoreline, the distance from the center of the picture to the iceberg and to a known landmark as measured in the photograph; the height of the camera above water level, and the distance from the camera to the opposite shore in line with the iceberg. In addition, the camera was required to be level and the camera's and landmark's poisition to be determinable on a map.

Using the side of the picture as a arbitrary reference point (the vertical centerline was not easily marked on the film) the distances to the landmark and to the iceberg were measured. These were subtracted from one half the picture width to give D_1 and D_b, as seen in Figure 4.

A horizontal angle, as seen from the camera between the landmark and the iceberg (figure 4) was calculated with the following equation:

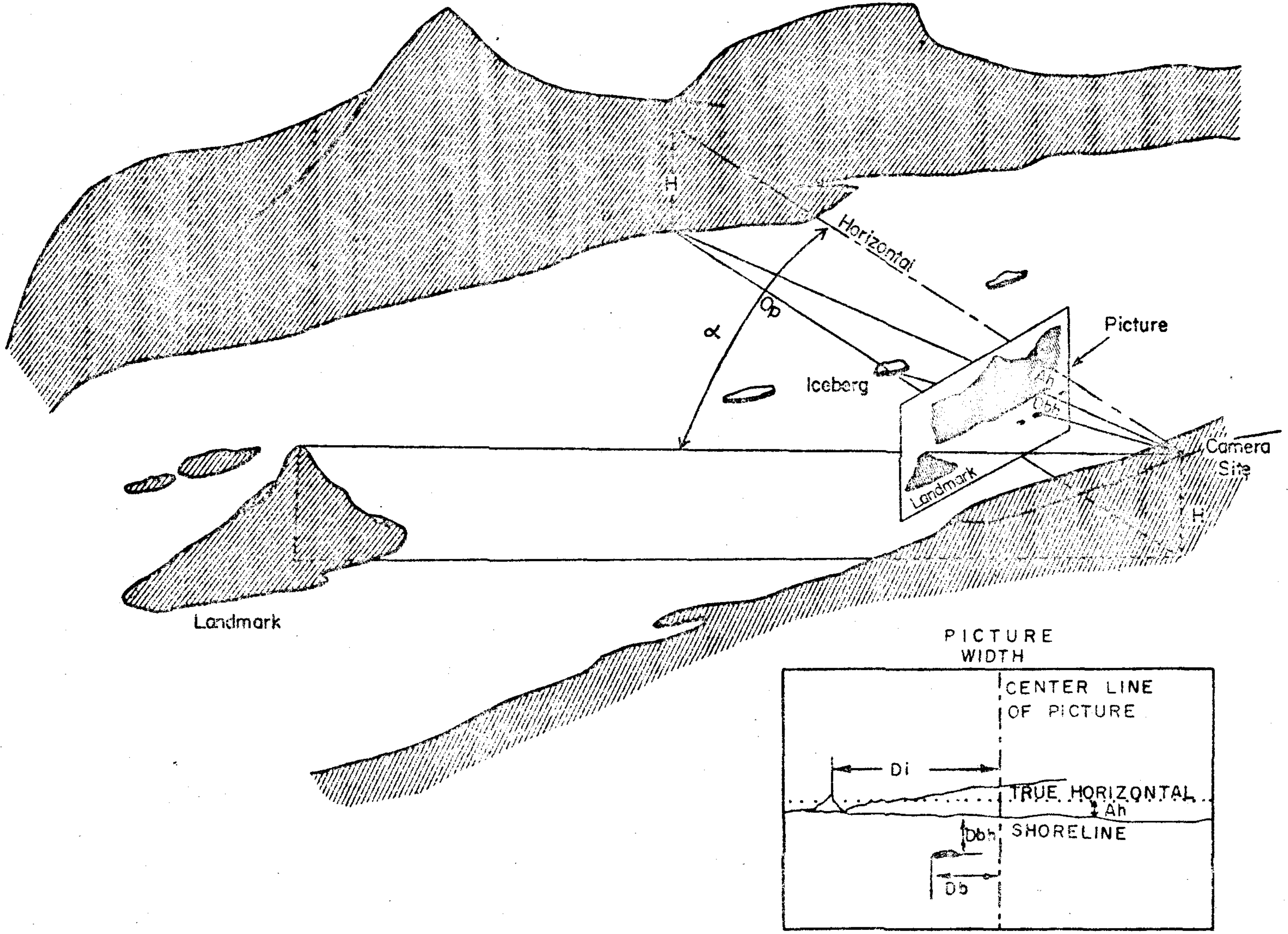

Figure 4 Schematic drawing of scene and measurements from camera vantage point, including photograph measurement

$$\alpha = \tan^{-1}(D_b/f) - \tan^{-1}(D_l/f)$$

where α is the horizontal angle, D_b is the distance from the centerline to the iceberg, D_l is the distance from the centerline to the landmark and f is the focal length of the camera.

The depression of the shoreline below the horizontal, as measured in the photograph, caused by the elevation of the camera was calculated by .

$$A_h = \frac{fH}{O_p}$$

where A_h is the distance on the photograph representing the depression of the shoreline below the horizontal, H is the height of the camera above water level and O_p is the horizontal distance from the camera to the opposite shore in line with the iceberg.

The horizontal distance from the camera to the iceberg was calculated by

$$D_i = Hf/(A_h + D_{bh})$$

where D_i is the horizontal distance from the camera to the iceberg, and D_{bh} is the distance of the iceberg below the shoreline, measured on the photograph.

Using the horizontal angle between the landmark and the iceberg and the horizontal distance from the camera to the iceberg, the position of the iceberg within the inlet can be measured. Successively-timed photographs allowed the movement of an iceberg to be plotted.

To facilitate handling the large number of iceberg positions, the foregoing procedure was programmed for computer processing (Appendix D).

This program included automatic selection of O_p (distance to opposite shore) values thus making it necessary to measure only D_b, D_l, and D_{bh}. The output was converted, in some cases, to X-Y positions relative to the inlet's axis.

If the camera lens axis is not horizontal, the photographic distances are correctable. When the camera is leveled, the focal distance — a line horizontal from the center of the lens to the film — is the same as the focal length (figure 5a). When the camera is out of level so that the film plane is not vertical, the focal distance and picture distances are lengthened (figure 5b) by the secant of the angle of deviation from the level in line with the lens axis (figure 5c). The depression of the apparent horizon (A_h) as seen in the picture and the apparent depression of the berg below the shoreline are also lengthened by the secant of this angle (figure 5d). Thus is the component of tilt in line with the lens axis is measured, the picture distances are corrected by multiplying the cosine of the tilt angle by the picture distances.

Two cameras were used in this experiment. The first, used during 10 July 1968, was a 125 x 95 millimeter format Graflex. The second two, used together, were Kalimar, Model SQ cameras.

The Graflex camera was calibrated by measuring a line along a building, setting the camera at a known distance at right angles from the center of the line, and taking a picture of this line. The focal length was then calculated from

$$f = \frac{Rd}{B}$$

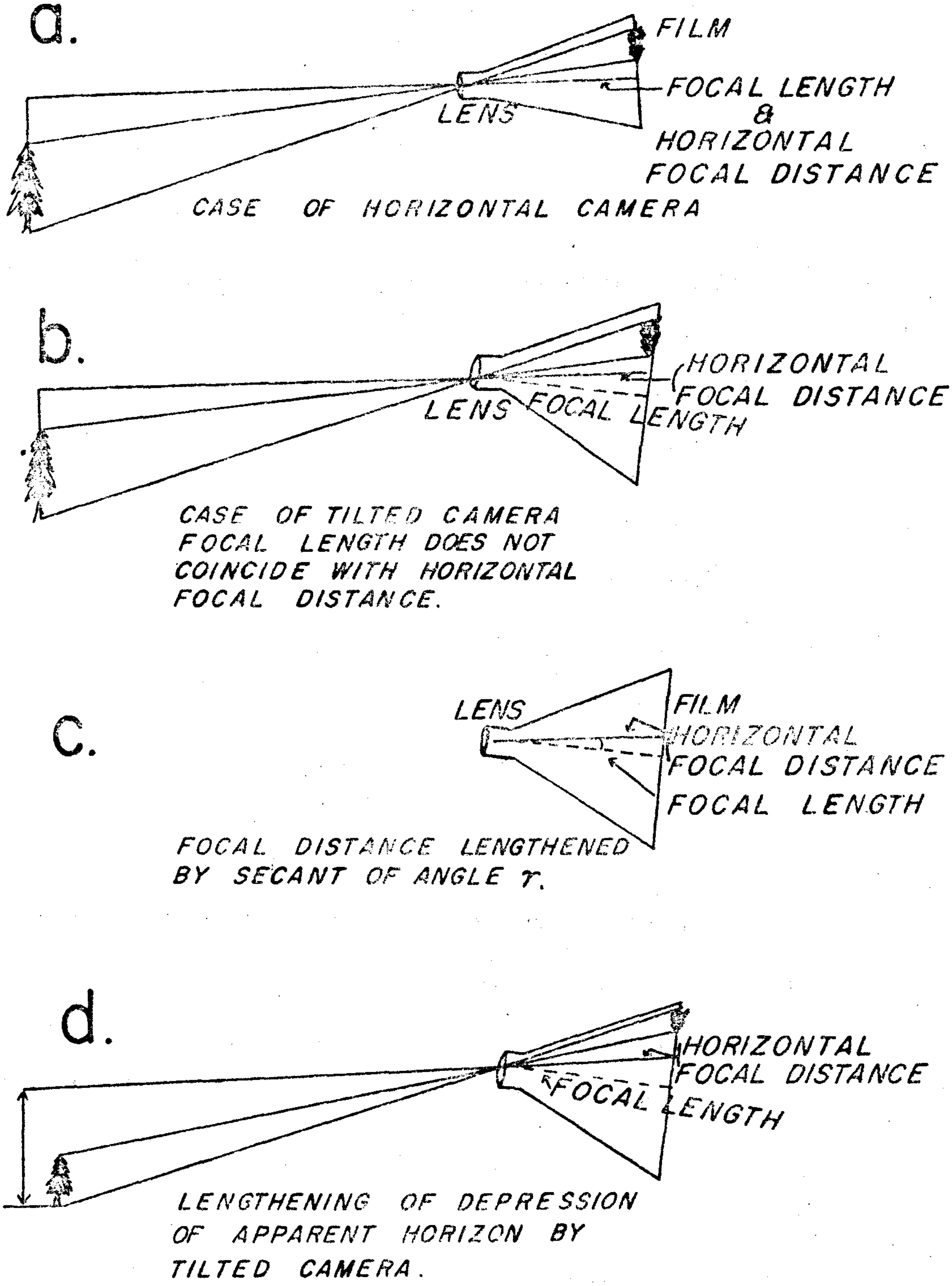

Figure 5 Distortion of picture distances caused by non-level camera

where f is the focal length, R is the range from the wall, d is the distance on the film, represented by the baseline, and B is the baseline distance measured on the wall.

The other two cameras were calibrated by setting up a transit an arbitrary distance from a building, measuring the angles to markers on the building, and photographing the measured points at the same level from the same point. The focal length was calculated from

$$f = \frac{a}{2\tan\alpha} + \frac{b}{2\tan\beta}$$

Here f is focal length, α and β are approximately equal angles on opposite sides of the center of the photograph, and a and b are the corresponding distances on film (Manual of Photogrammetry, 1952). These two angles had a common center close to the true center of the picture. The focal lengths of the two cameras were 78.1 and 77.9 millimeters by this method.

In addition, to test for lens distortion distances from the center of the picture were plotted against the measured angles (figure 6). These distances were measured to 0.1 millimeter and the angles to minutes of arc. A line was fitted to these points

$$\tan\theta = d/f$$

where d is the appropriate distance in the photograph and θ is the measured angle. Deviations of the points from the line indicate distortion were less than 1 millimeter and appeared random.

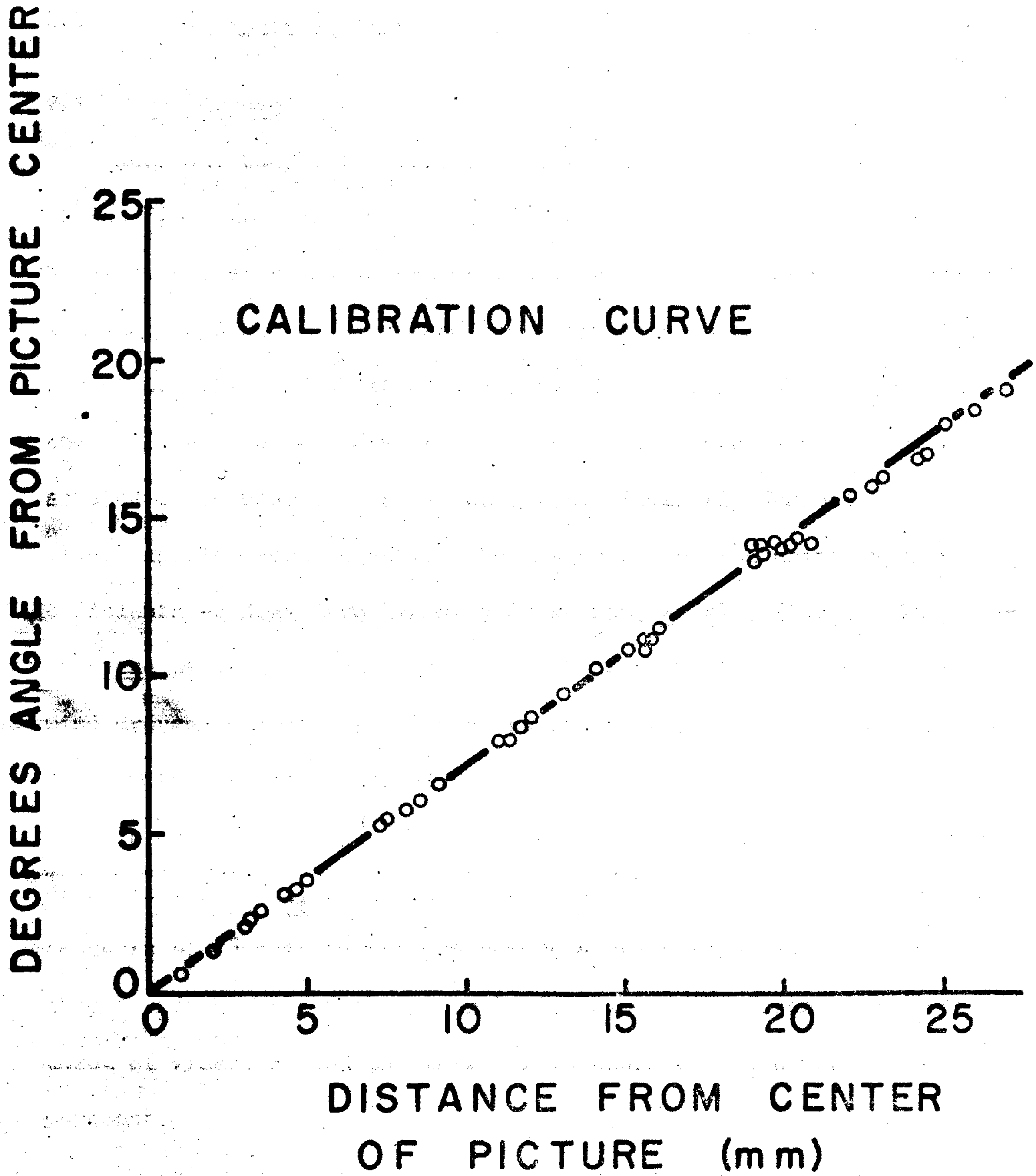

Figure 6 **Camera** calibration curve for 78.1 mm focal length camera. (Circles show measured positions.)

2.2 Ice Drift and Currents

2.2.1 Background

Reed and Campbell (1962) considered ice drift from the point of view of ice floes drifting in the arctic pack ice. They used the parameters of wind, currents and motion of the icepack to account for the motion of ice station Alpha. Using Reed and Campbell's model Ingram, et al., (1969) calculated the wind drift of ice floes in the Gulf of St. Lawrence. When the drift did not agree with calculated drift, the displacement was assumed to be caused by river currents. Similarly Gudkovich and Nikiforov (1967) applied force equations to a single ice floe using experimental coefficients of drag determined by Gudkovich, et al., (1967). They found that the wind-blown ice drift was turbulent and they derived equations for wind driven current, drift with respect to the water and the angle of this drift with respect to the wind.

In an analysis of iceberg drift in the North Atlantic Wolford and Moynehan (Abstract, 1969) found the iceberg under study drifted along contours of dynamic topography before a storm front crossed the area. They found that the iceberg partly followed drogue tracks, and with the onset of winds, a wind to excess of 10 knots affected the iceberg's movement.

In Endicott Arm the icebergs were affected by a mean outflowing current with superimposed tidal currents. These tidal currents were of significant magnitude and had to be accounted for in the analysis. Wind blew during the last photo-period and was also accounted for in the analysis.

2.2.2 Factors Affecting an Iceberg in an Oscillating Medium

The motion of an iceberg in an oscillating fluid is affected by the mass of the iceberg, its frontal area, its coefficient of drag, and magnitude and period of the oscillation. In this case the magnitude and period of the oscillation are the magnitude and period of the tidal currents. The shape, mass and drag coefficient must all be assumed from the visible part of the iceberg and some general observations of icebergs.

The magnitude of mean outflow and of the tidal currents need to be measured to depths ranging below that of the iceberg depth. Further, since there can be a current shear within the depth of the icebergs, this shear must be delineated to determine its effect on the icebergs. This is done by standard current measuring techniques.

The shape and mass of the iceberg is determined from the height and width of the visible part of the berg. Schvede (1966) established height-depth ratios for various icebergs. The height-depth ratio used in this thesis is 1:4 for flat and round-topped icebergs and 1:3 for pyramidal icebergs. The simplest subsurface shape assumes a rectangular frontal area based on calculations of height and width above water. The only other thing that can be said for subsurface shape is that it should be indicative of stability, i.e., the width should be a great or greater than the depth.

Drag coefficient is a virtual unknown for icebergs. The icebergs observed in Endicott Arm were generally of irregular shape (figure 7) and pitted at the water's surface by melting.

Figure 7. Photograph of Stranded Iceberg.

Gudkovich, et al., (1967) modeled hummocked ice floes and measured drag coefficients of 0.007 to 0.065. They found that increasing hummocking beyond 50 to 60% of the bottom area of the model iceberg caused the drag coefficient to decrease due to the hydrodynamic shadowing effect. They further indicated that 100% surface area hummock coverage coresponded to uniform plate roughness.

With irregular icebergs Gudkovich, et al's models are not satisfactory, since their models assumed trapezoidal hummocks of uniform height. Streeter (1958) shows drag coefficients of 0.2 to 0.6 for a submerged sphere moving in a fluid at similar Reynold's numbers ($R_e = UL/\nu = 10^4$ to 10^6). Further, for a disk moving through a fluid at these Reynold's numbers Streeter showed a drag coefficient of 1.1. Since the iceberg can have large concave areas, the drag coefficient could be related to that of a parachute where the coefficient is as high as 1.7, Hoerner (1967). This coefficient appears too high, however, since random choice would only face this area of the iceberg into the direction of motion part of the time. Probably the most reasonable drag coefficient is 1.0 given for Hoerner's blunt-ended barge moving with a similar Froude number ($f = U^2/gl = 10^{-4}$). The blunt-ended barge does not allow for roughness but is a blunt body pushing through the water as does the iceberg.

Assuming a drag coefficient of 1.0 and a reasonable subsurface shape for the iceberg, the drift of the iceberg in a tidal medium was programmed for the University of Alaska's EAI 380 Analog/Hybrid Computer.

The drag force on an iceberg moving relative to the water is

$$F = 1/2 C_D \rho A U^2.$$

Where F is the force, C_D is the drag coefficient, ρ is the density of the medium, A is the frontal area of the iceberg, U is the velocity of the iceberg relative to the water (Streeter, 1958). The inertial driving force is

$$F = \frac{m dv}{dt}$$

Where m is the mass of the iceberg, and v is the velocity of the iceberg. Equating the two forces

$$\frac{dv}{dt} = \frac{-C_D \rho A U^2}{2m}$$

(The minus sign indicates the forces are in opposition.) The velocity of the iceberg relative to the water is

$$U = v - v_0 \sin\omega t$$

v is the velocity of the iceberg, v_0 is the amplitude of the tidal current, ω is $2\pi/T$, where T is the tidal period, and t is time. This makes the differential equation

$$\frac{dv}{dt} = -k(v - v_0 \sin\omega t)^2$$

where k is $\frac{C_D \rho A.}{2m}$

The acceleration, dv/dt, is positive or negative in relation to the iceberg's relative velcoity U. Thus the actual relationship is

$$\frac{dv}{dt} = -k\ \mathrm{sgn}(v-v_o \sin\omega t)\ (v-v_o \sin\omega t)^2.$$

Where the sgn (or sign) function goes either +1 or -1 as $(v-v_o \sin t)$ goes positive or negative. This equation was programmed for the analog computer. (See Appendix G for details.)

Two typical traces are shown in figure 8. These traces illustrate two points: first the iceberg speed curve tends to flatten only as the tidal-current speed curve crosses it. Second, the iceberg speed curve is delayed in time and of lower amplitude than the tidal-current speed curve.

The iceberg does not stop accelerating when the tidal current reaches its maximum. When the tidal current is at its maximum velocity the acceleration of the iceberg is

$$\frac{dv}{dt} = \pm k(v-v_o)^2.$$

However, at this point v does not equal v_o and thus there is an acceleration. As the tidal current speed decreases, it reaches the magnitude of v

$$(v-v_o \sin\omega t)^2 = 0$$

Then there is no acceleration of the berg. As the current's speed becomes less than the iceberg's speed the iceberg is decelerated.

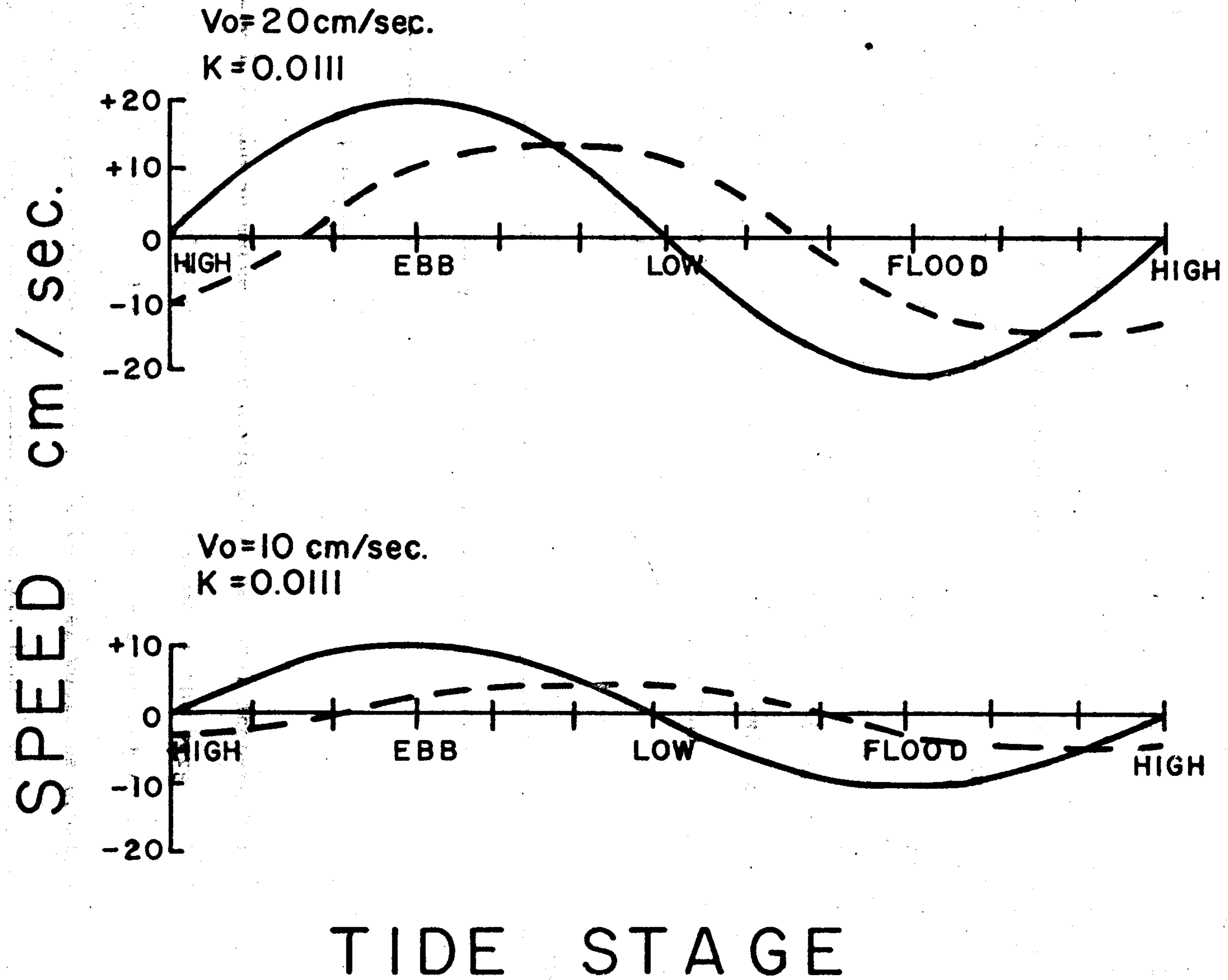

Figure 8. Tidal current speed and tidal ice drift speed curves. (Tidal current solid line, tidal ice drift dashed line.)

The lag and lower amplitude of the iceberg's speed curve, relative to the current speed curve are to be expected. The limiting cases are these: first, when the mass of the iceberg becomes very small (k becomes unity), the iceberg curve tends closely to the current speed curve in lag and amplitude; second, when the mass increases without limit (k goes to zero) the iceberg curve tends to zero amplitude and one quarter wave length lag.

A plot of the iceberg's lag and amplitude as percentages of the tidal period and tidal amplitude versus the k-number is presented in Figure 9, using v_o = 10 and 20 cm/sec and T = 12 hours.

The formula used for computing the k-number of the iceberg is

$$k = \frac{\rho C_D A.}{2m}$$

Since C_D is assumed to be 1.0, A is the submerged frontal area and the iceberg is assumed to have a density of 0.9 that of water; k may be rewritten

$$k = \frac{RA}{1.8V}$$

Where R is the submerged depth divided by the total iceberg height, A is the total frontal area, and V is the volume of the berg. If the height-depth ratio is 1:4, R is 4/5. Thus for a cubical 40 meter iceberg with a 1:4 height-depth ratio, the k-number would be 0.011, the lag would be about 14% of the tidal period (1.7 hours) and the speed amplitude would be 68% of the tidal current amplitude (13.5 cm/sec if v_o was 20.0 cm/sec).

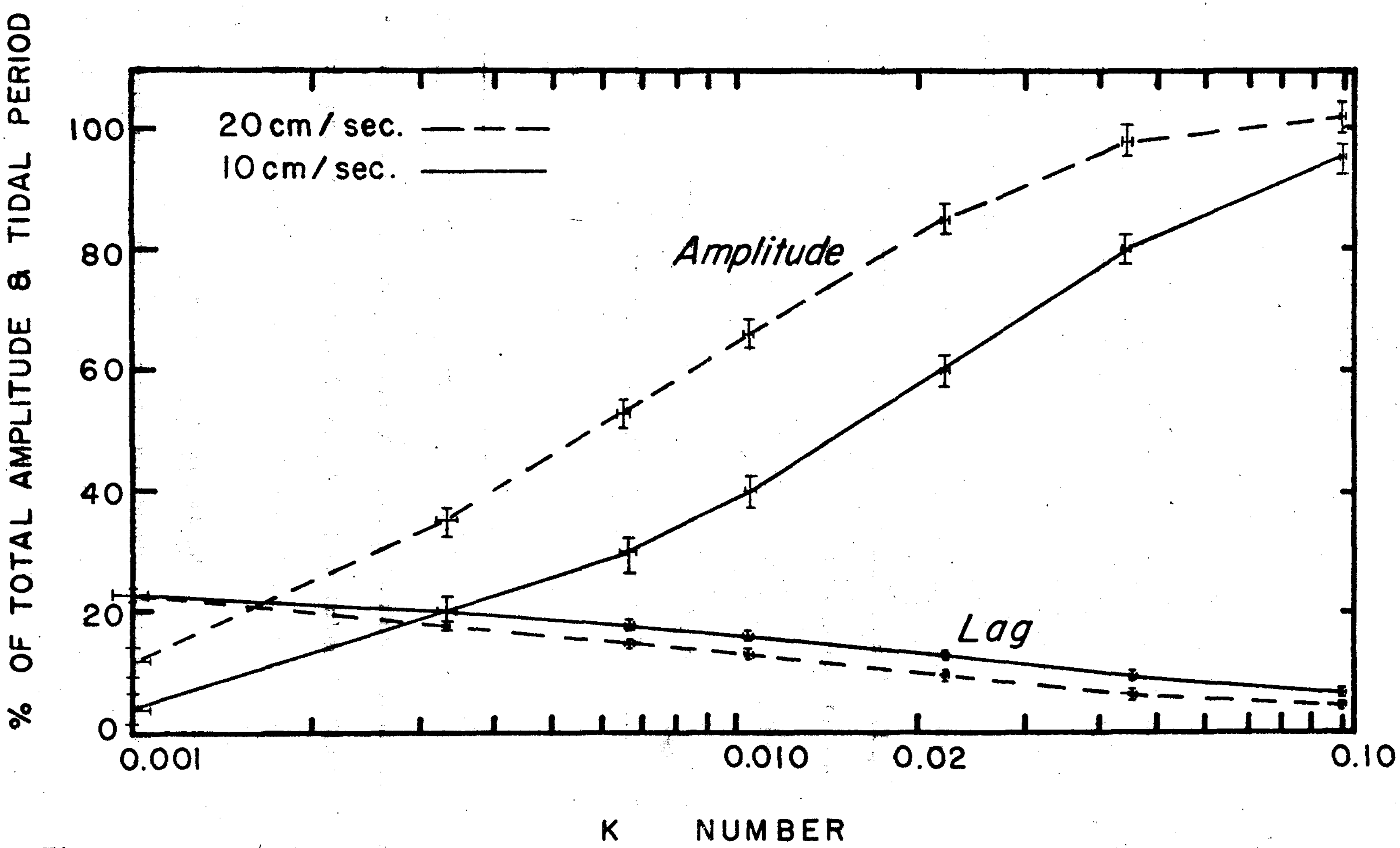

Figure 9. Iceberg's drift speed and lag expressed as percentages of total current speed and period versus k-number.

CHAPTER III

RESULTS

3.1 Data

The data taken between November 1966 and March 1969 which was used in this thesis are contained in Appendix B. The drogue positioning data are expressed in terms of the ship's heading, and direction and distance to known landmarks.

The data on ice drift given in Appendix A are expressed both as distances measured on the photograph as well as calculated bearings and distances from a known landmark to the iceberg, relative to the camera.

3.2 Plots

The plots of current drift are figures E1 to E8, and the plots of ice drift are figures E9 to E11. All plots are compiled with an insert showing tidal height vs. time.

3.3 Drogue Drift

The drogue drift data group into two sections: the data taken during 1966 and 1967 by Matthews and Rosenberg between Sumdum Island and the mouth of Endicott Arm (see figure 2) and the data taken by Gleason, Matthews and Rosenberg during 1968 and 1969 up-inlet from Sumdum Island.

3.3.1 Drogue Data Down-Inlet from Sumdum Island

The drogue data taken down-inlet from Sumdum Island were taken over short periods of time to determine the circulation near the mouth of Endicott Arm. These data were taken during November 1966, March and May

1967 (figures E1 to E3). The first two periods show the mean outflow velocities of currents leaving the mouth of the inlet. In addition, the 20 and 21 November drogues show currents on the northeast side of the inlet's sill (figure E1). On 5 May 1967 drogues planted on the southwest side of the inlet indicated the cross channel current speeds (figure E3).

3.3.2 Drogue Data Up-Inlet from Sumdum Island

The drogue data taken up-inlet from Sumdum Island were measured in March 1968 at 0, 10 and 20 meter depths, in June 1968 at 0 and 10 meter depths, in July at 0 and 10 meters, and in February 1969 at 0 and 10 meters. (The drogues were tracked for over 20 hours in each case.) These data are contained in figures E4 to E8. They were used to determine mean outflow currents, the increase in mean outflow down-inlet and the near surface velocity profile. These are discussed in the following chapter.

The March 1968 and February 1969 drogue data were taken aboard the R/V ACONA (figures E4, E5 and E8) using radar for positioning. This allowed drogue tracking to be carried on continuously. The June and July 1968 drogue data were measured by sextant aboard the R/V MAYBESO. Sextant positioning and the limitations of the vessel required anchoring at night. This is the reason for the 12 hour gap in these data (figures E6 and E7).

Descriptively these data fit into two groups: low mean outflow currents consisting of the March 1968 and June 1968 data and high mean outflow currents consisting of the July 1968 and February 1969 data.

Low mean outflow currents ranged between 1.0 and 9.0 cm/sec at the surface, were reversed by the flooding tidal current and were increased by the ebbing tidal current. The typical pattern (figure E4) is down-inlet during high, ebb and low tide stages and up-inlet drift when the tidal current exceeds the mean outflow current.

The high run-off currents were generally between 9.0 and 20.1 cm/sec, and showed no reversal of direction at flood tide (figures E7 and E8). In both July 1968 and February 1969 the ten meter drogues showed similar patterns of flow with slower speeds. (The ten meter drogue used in July 1968 was retreived with a fouled parachute making its speed data suspect.)

3.4 Ice Drift Data

Photography of ice drift was taken on three different cruises: 10 July, 24 and 25 August 1968 and 6 March 1969. The data taken in August were the most extensive but were not checked by drogue data. The ice drift data of July 1968 and March 1969 were taken on the same cruise as the drogue data.

3.4.1 10 July 1968 Ice Drift Data

The July ice drift data were taken with a 95 x 125 millimeter format Graflex camera using a 127 millimeter lens. This camera gave large clear pictures and made the taks of interpretation relatively easy. A typical picture is shown in figure 10. From these pictures five icebergs were tracked. These are shown in figure E9.

Figure 10 Typical photograph of inlet.

3.4.2 24 and 25 August 1968 Ice Drift Data

On 24 and 25 August photographs of ice drift were taken from both sides of the inlet (positions b and c, figure E10). The individual icebergs proved unrecognizable from one side to the other. For this reason and because position c had limited visibility the photography from position b was used.

From the photographs eight icebergs were tracked. Numbers 3 through 8 showed movement and were plotted (the circled number in figure E10). Numbers 5 through 8 reversed direction at about 1700 and dirfted up-inlet apparently against an ebbing tidal current.

From the photographs taken on 25 August the icebergs tracked (marked with boxed numbers) showed steady outflow from 0835 to 1400 against what should have been a flooding tidal current.

3.4.3 6 March 1969 Ice Drift Data

On 6 March 1969 photography was taken from position d for about four hours (figure E11). Six icebergs were tracked which showed predictable trends. There was a ten knot (5.1 m/sec) intermittent wind blowing down-inlet. The effect was to increase velocities by 1cm/sec at about 30° to the right (Gudkovich and Nikiforov, 1967).

CHAPTER IV

ANALYSIS OF THE DATA

4.1 Drogue Data

As stated previously, the drogue data were grouped into those taken up-inlet from Sumdum Island in 1968 and 1969 and the data taken down-inlet from Sumdum in 1966 and 1967.

4.1.1 Plots of Current Up-Inlet from Sumdum Island

Plots of current versus time for the data taken up-inlet from Sumdum Island are shown in figures 11 and 14. These plots show tidal oscillations superimposed on an outflow current. (The positive speed axis indicates outflow.) Tidal current maxima and tidal high and low stages are labeled on the time axis.

The agreement between the predicted and actual tidal current maxima was not clear due to the braod peaks and troughs in the curves. (The peaks and troughs appear sharper in the June and July 1968 data because there are fewer data points.) The times of maximum flood current were calculated (Appendix F) ignoring the effect of large eddies, by assuming the current maximum occurs half-way between the reversals in direction of the drogue drift (figures E4 to E6). Using these assumptions the maximum surface flood current was found to be 3 hours 40 minutes after low tide and the maximum ten meter flood current 3 hours 40 minutes to 5 hours after low tide. The surface tidal amplitudes ranged from about 4 cm/sec in February 1969 to about 20 cm/sec in June 1968, and the ten meter amplitudes ranged similarly from 4 cm/sec in February 1969 to over 10 cm/sec in June 1968.

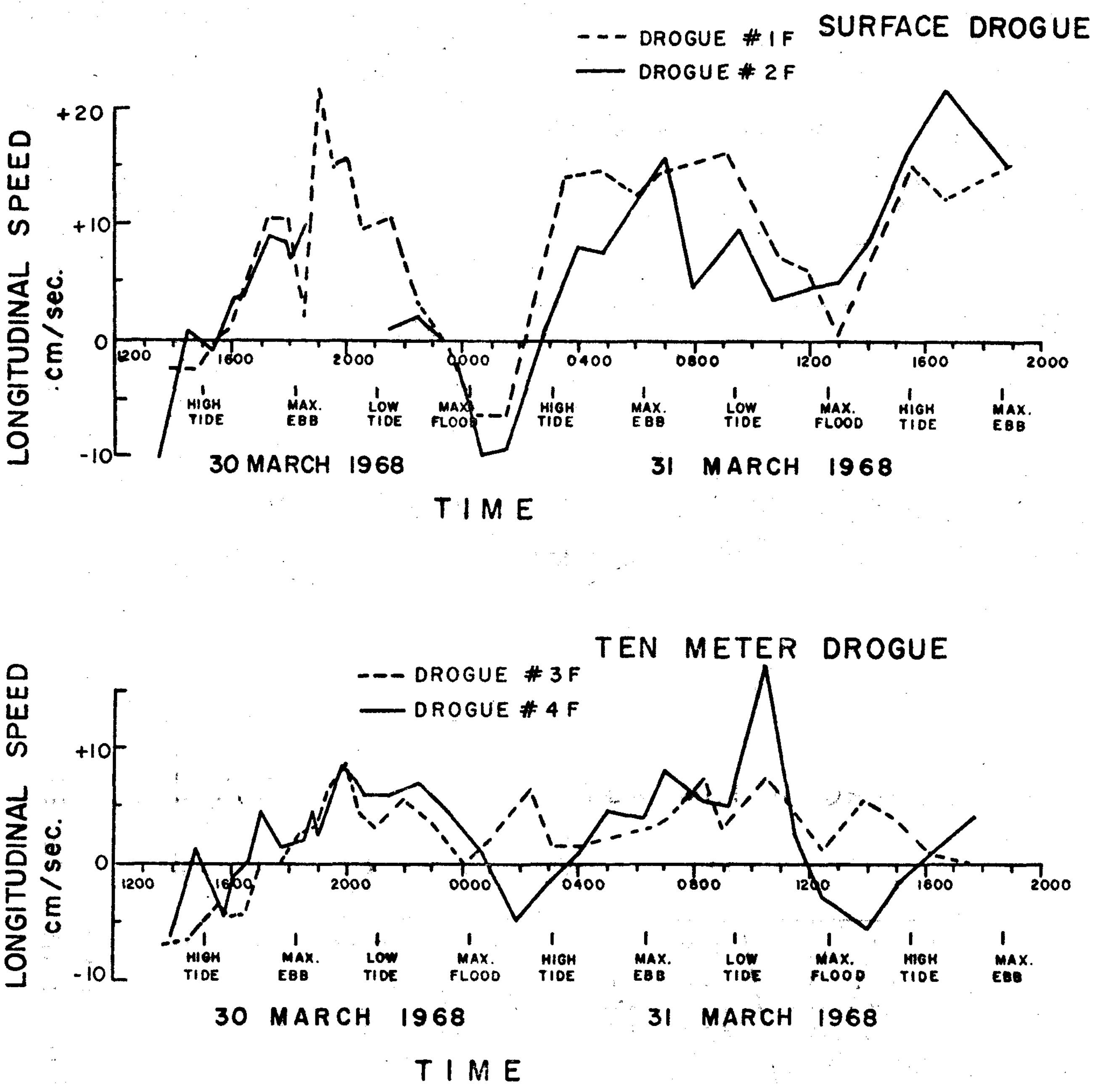

Figure 11. Drogue speed versus time plots for surface and 10 meters; 30 and 31 March 1968.

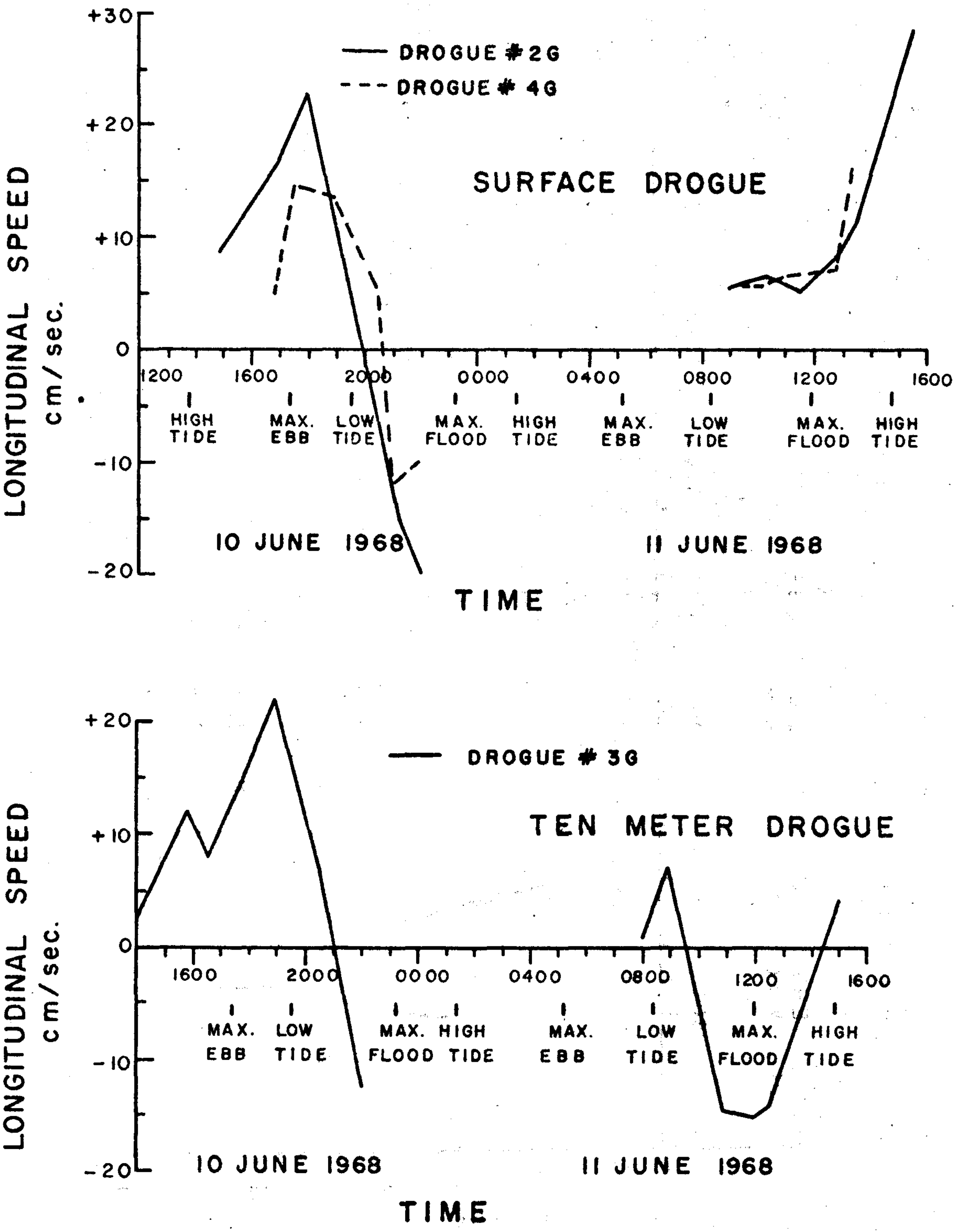

Figure 12. Drogue speed versus time plots for surface and 10 meters; 10 and 11 June 1968.

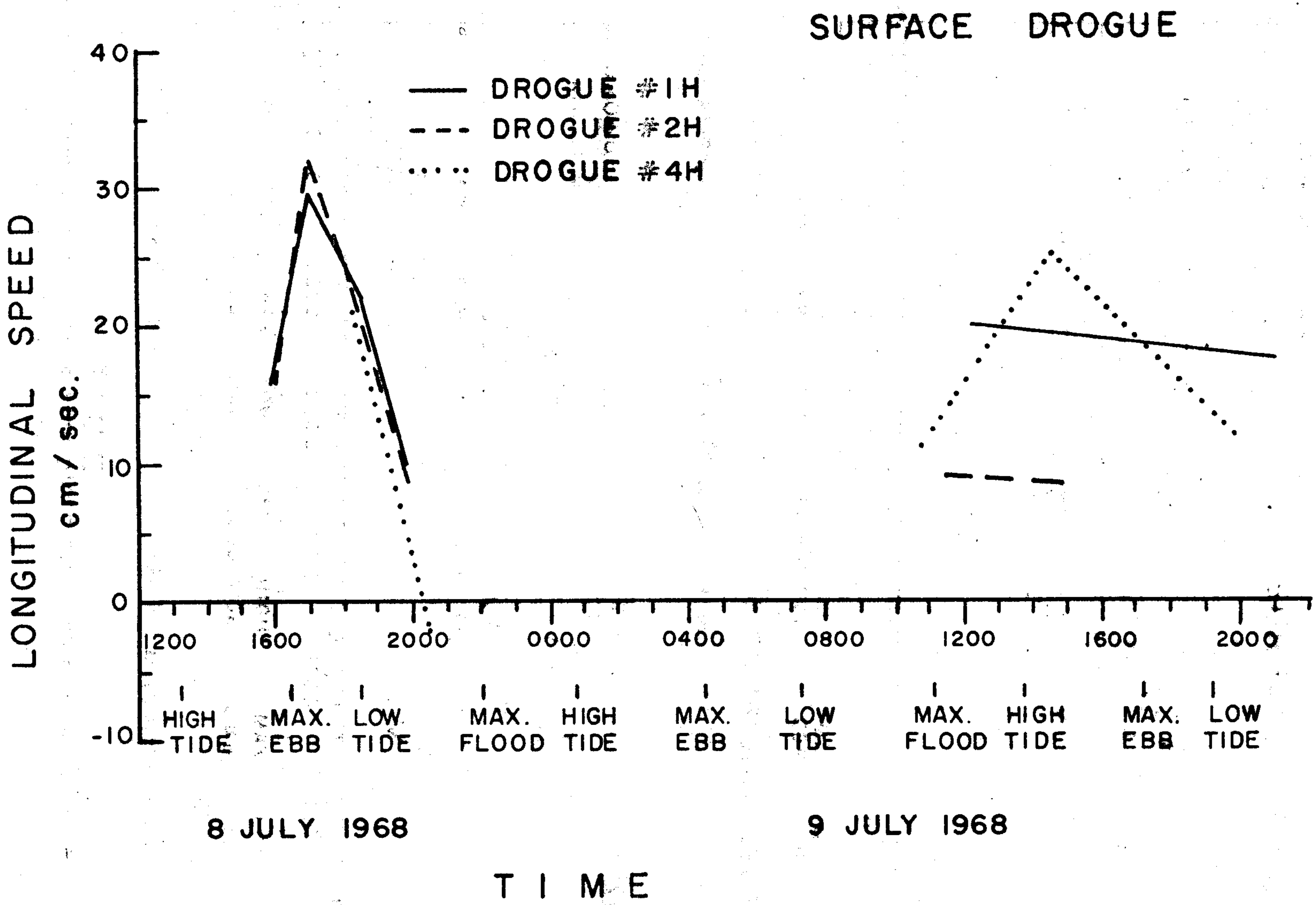

Figure 13. Drogue speed versus time plot for surface; 8 and 9 July 1968.

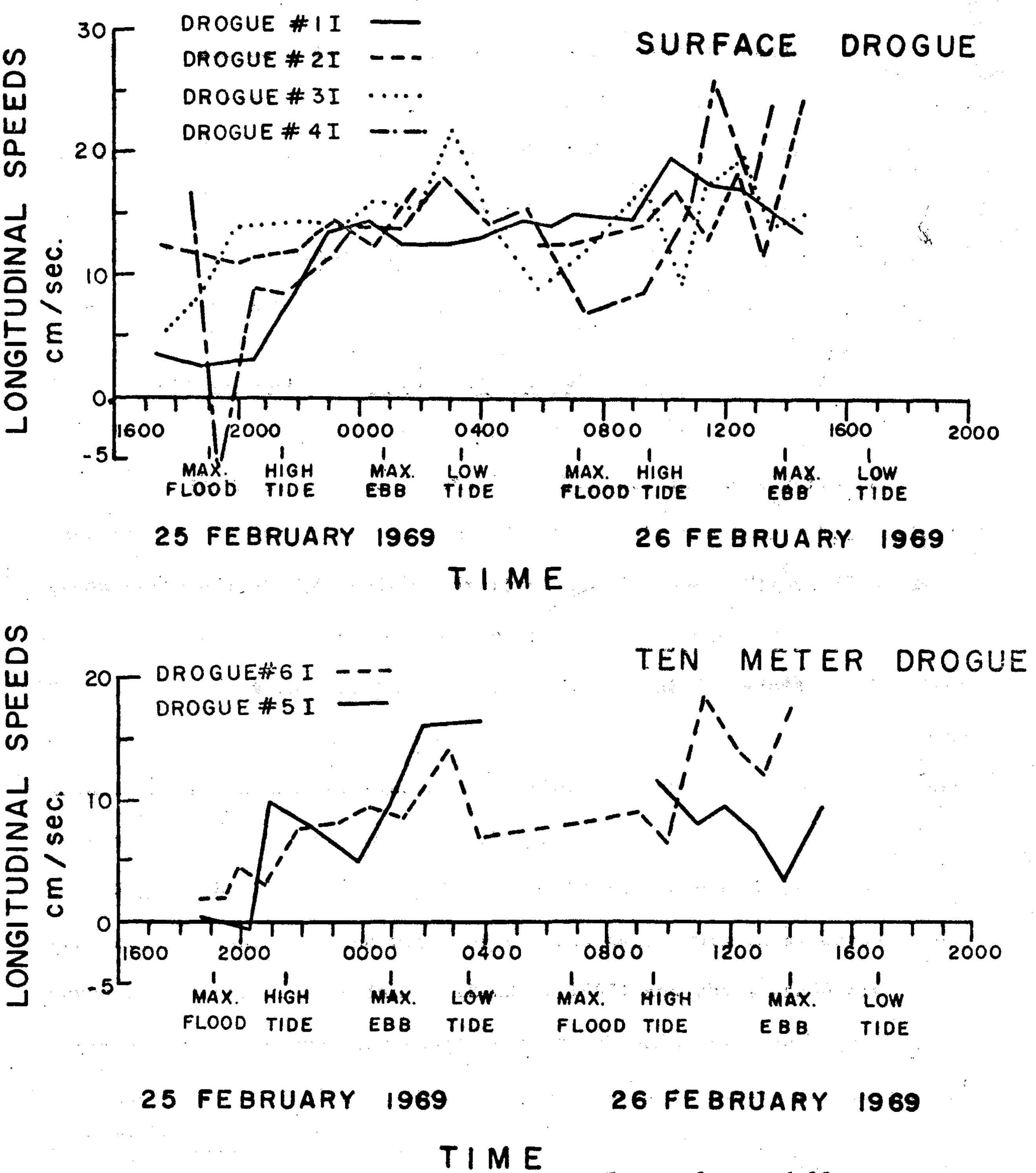

Figure 14. Drogue speed versus time plots for surface and 10 meters; 25 and 26 February 1969.

From these data and a short tidal stage record (Appendix F) which indicates the tide in North Dawes was within one half hour of Juneau's predicted tide it was concluded that the tide in Endicott Arm is close to a standing wave. (A standing wave has current maxima at half tide stages: i.e., the maxima of current are halfway between high and low tide. Kinsman, 1965a.)

4.1.2 Means of Current Up-Inlet from Sumdum Island

Twelve hour means of the current data measured up-inlet from Sumdum Island are shown in figures 15 and 16. The bars in the figures show the mean of the data taken between the time intervals enclosed. The positive speed axis indicates down-inlet drift of the drogues. Figure 17 shows six-hour means taken from maximum ebb to maximum flood current and vice versa. The plots show an increase in mean current down-inlet. The plots are annotated Sumdum Passage where the drogues had to pass between Sumdum Island and the southwest side of the inlet. In this area current speeds increased due to the narrowing of the passage.

Figure 18 illustrates the effect on "ideal" currents as affected strictly by changes in the width of the passage. This ideal current removes the effect of entrainment (Bowden, 1967) and shows gradually decreasing current speeds down-inlet except in Sumdum Passage. This plot suggests that the increase in current speed seen in figure 17 was caused by entrainment.

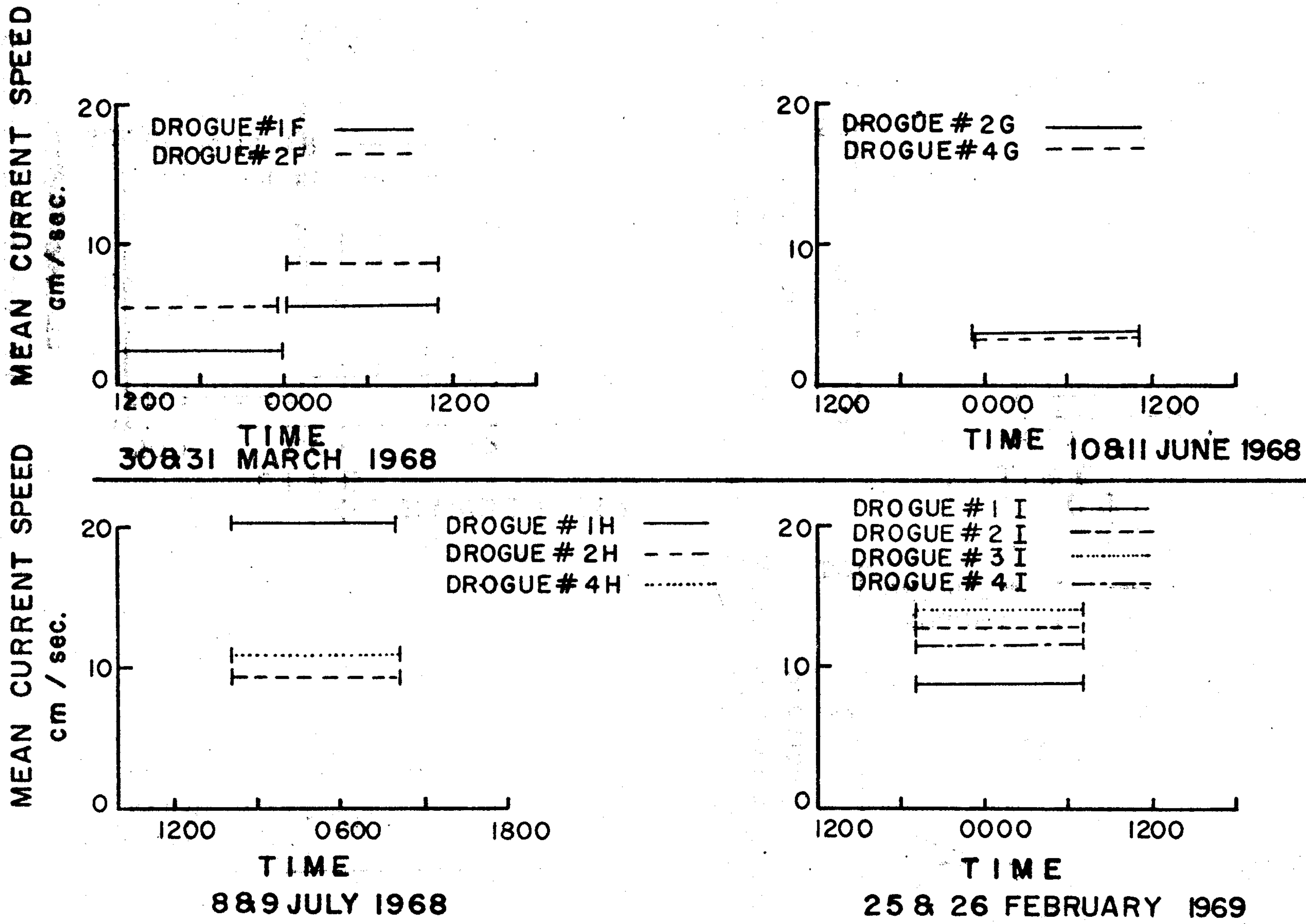

Figure 15. Twelve hour means of surface current's speed.

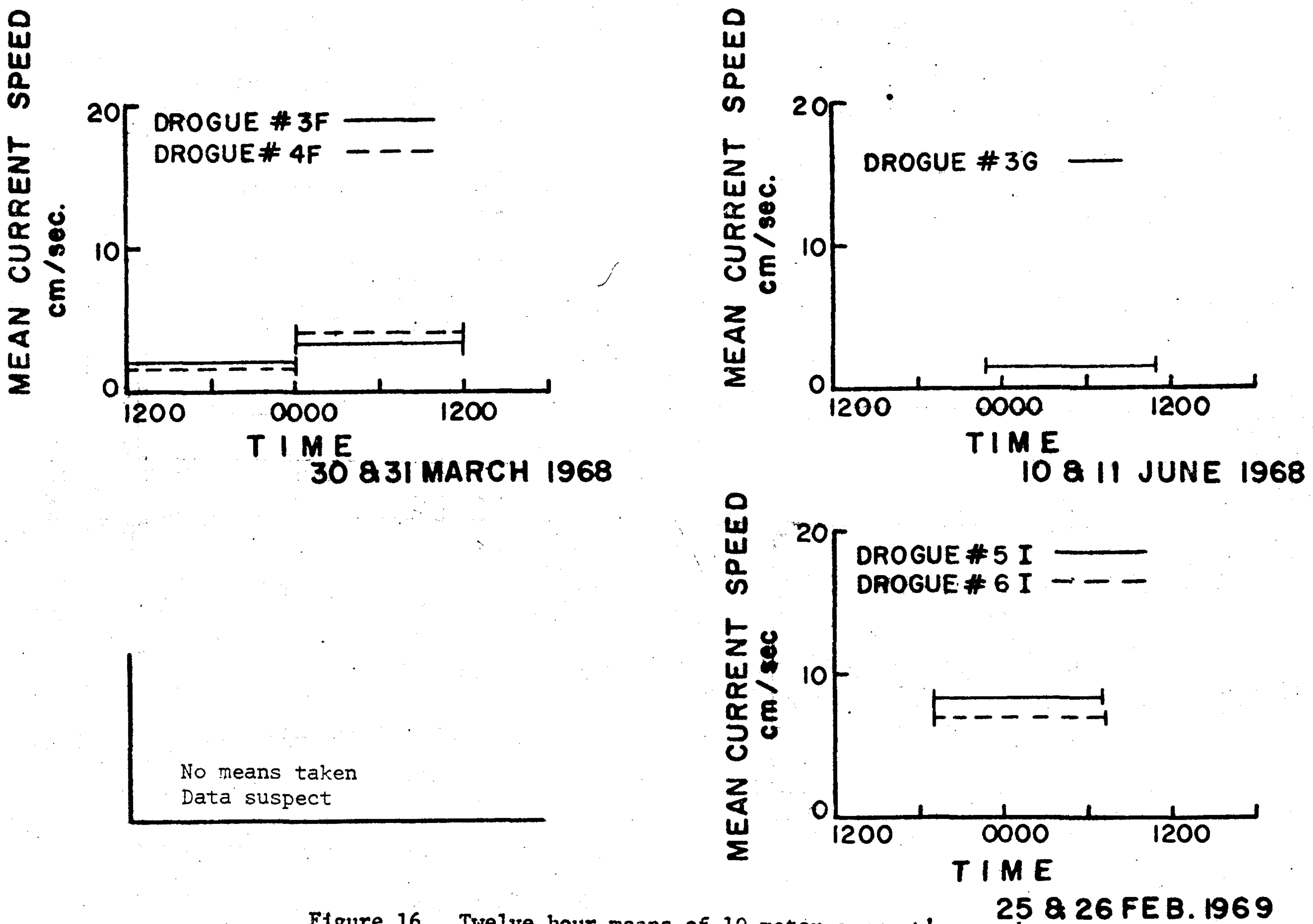

Figure 16. Twelve hour means of 10 meter current's speed.

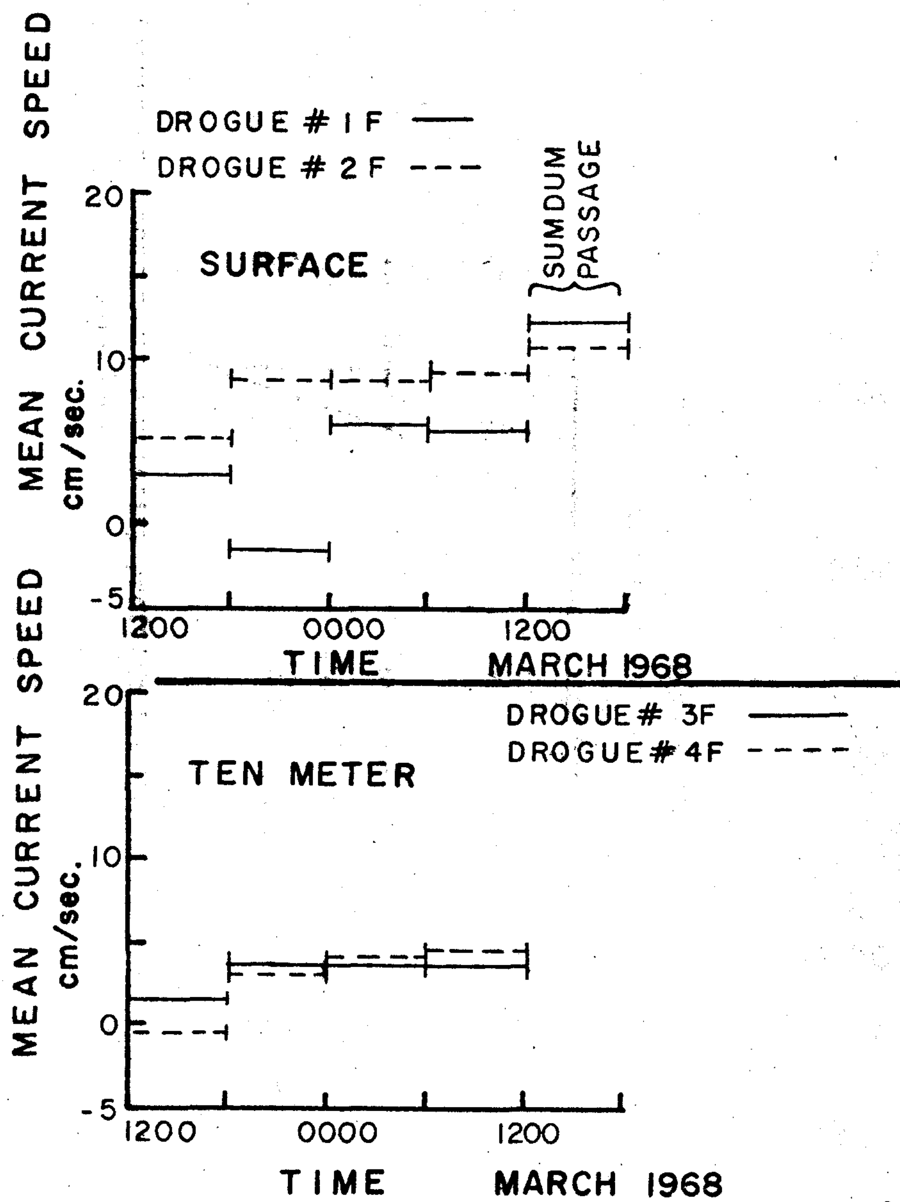

Figure 17 Six hour means of surface and 10 meter current's

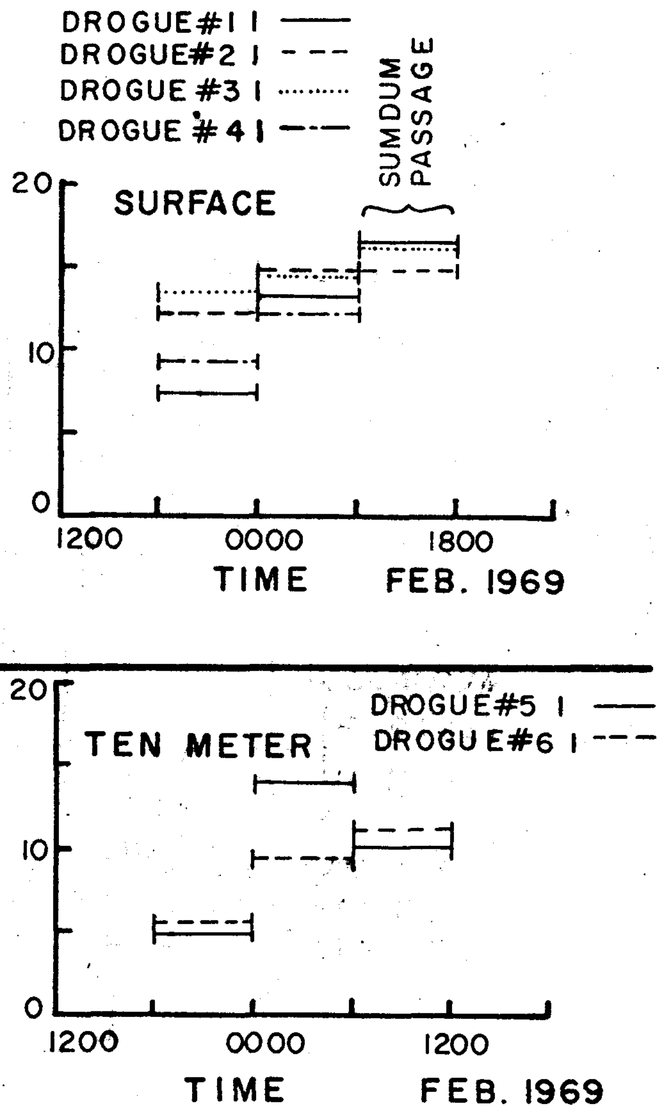

s speeds for March 1968 and February 1969

Figure 18. Changes in 5 and 10 cm/sec current affected by changes in inlet width. "Sumdum Passage" indicates the passage between Sumdum Island and the inlet's southwest shore.

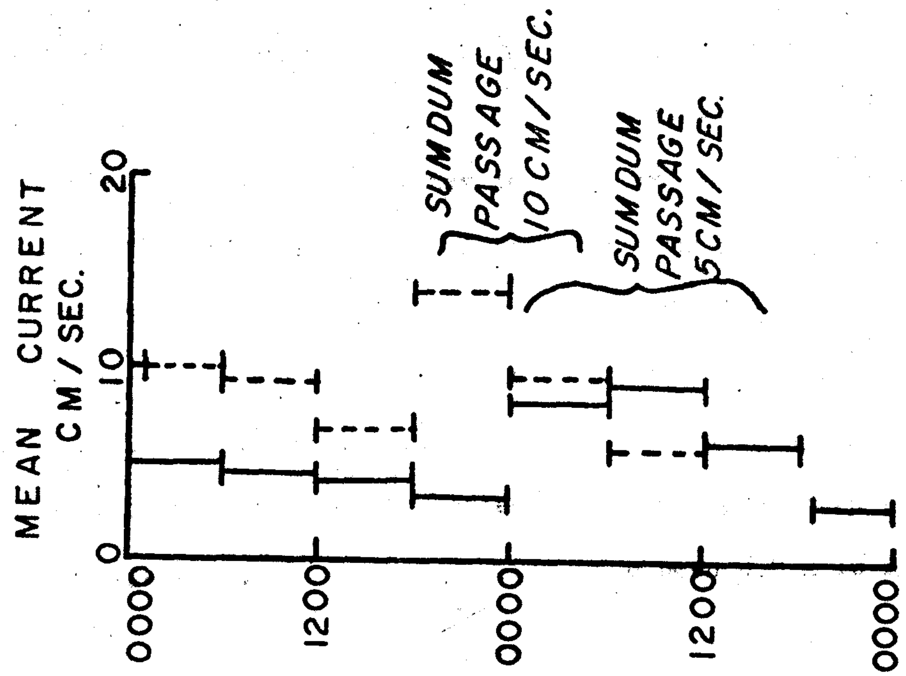

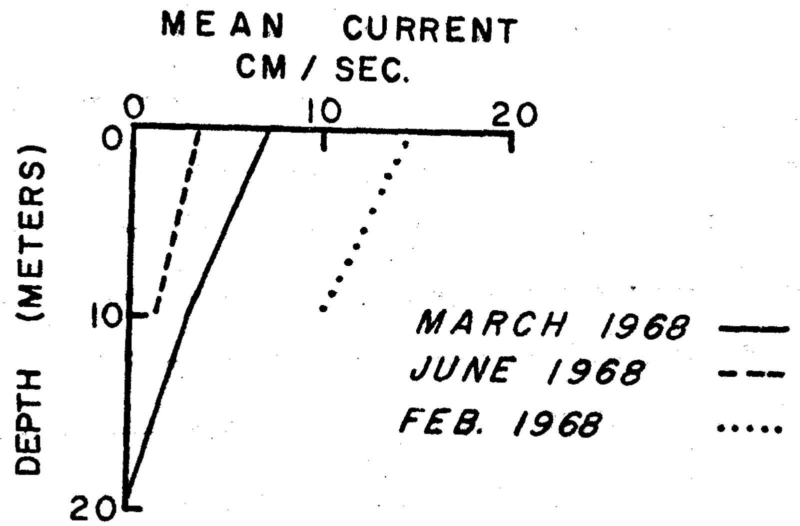

Figure 19. Near-surface velocity profiles for March and June 1968 and February 1969.

Drogues planted on 21 November 1966 (figure E1) at twenty and forty meters drifted from the mouth of the inlet at high tide. The twenty meter drogue left the inlet at 28.6 cm/sec and the forty meter drogue at 9.5 cm/sec. Assuming that the 20 meter drogue represented the current speed of the total volume of water leaving the inlet at high tide, the volume outflow from the inlet at this time was $5.3 \times 10^3 m^3$/sec.

Similarly on 6 March 1967 a surface drogue left the inlet on the ebb tide (figure E2) at 70 cm/sec. This exit speed was converted to an exit speed at high tide of 43 cm/sec by means outlined in Appendix F. Assuming that the surface drogue's corrected speed represented the volume outflow at high tide, this outflow would have been $8.0 \times 10^3 m^3$/sec.

4.2 Ice Drift Measurements

The ice drift measured from the photography showed tracks similar to those of the drogues (figures E9 to E11). The photograph-to-photograph movements, however, did not show tidal trends in the velocity-time plots (figures 20 to 22). The level of error (figure F1 to F3) proved as great as the iceberg's movement between photographs.

Instead of speed versus time plots, mean speed versus time plots were constructed (figure 23). These plots use the total drift per time of photography as the mean speed. In figure 22, with the exception of 24 August 1968, the iceberg's mean speeds tended to group around certain values: in July, 23 cm/sec; on 25 August, 8 cm/sec; and on 6 March, 8 cm/sec. On 24 August the icebergs reversed direction near ebb tide, showing speeds up to +19 and -17 cm/sec. (These speeds are considered

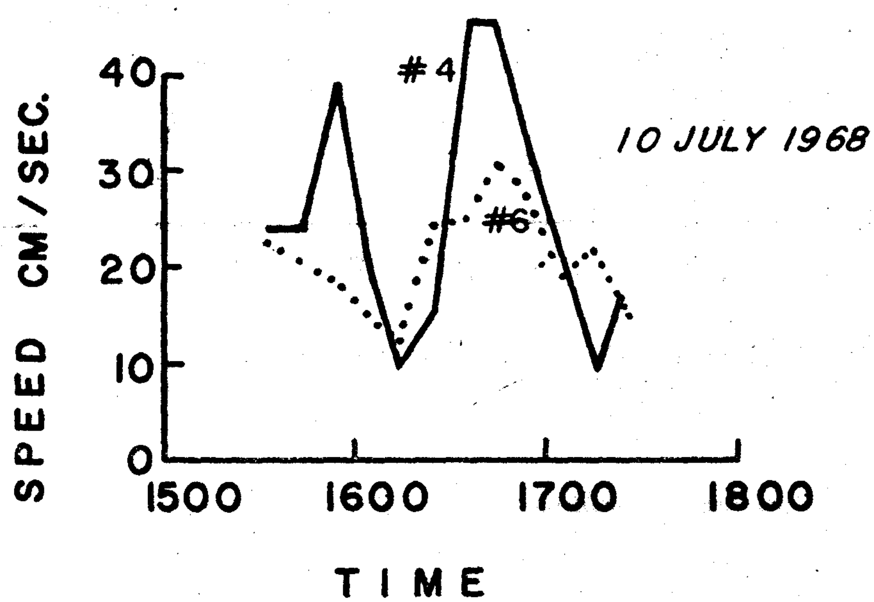

Figure 20. Typical iceberg speed curves, 10 July 1968.

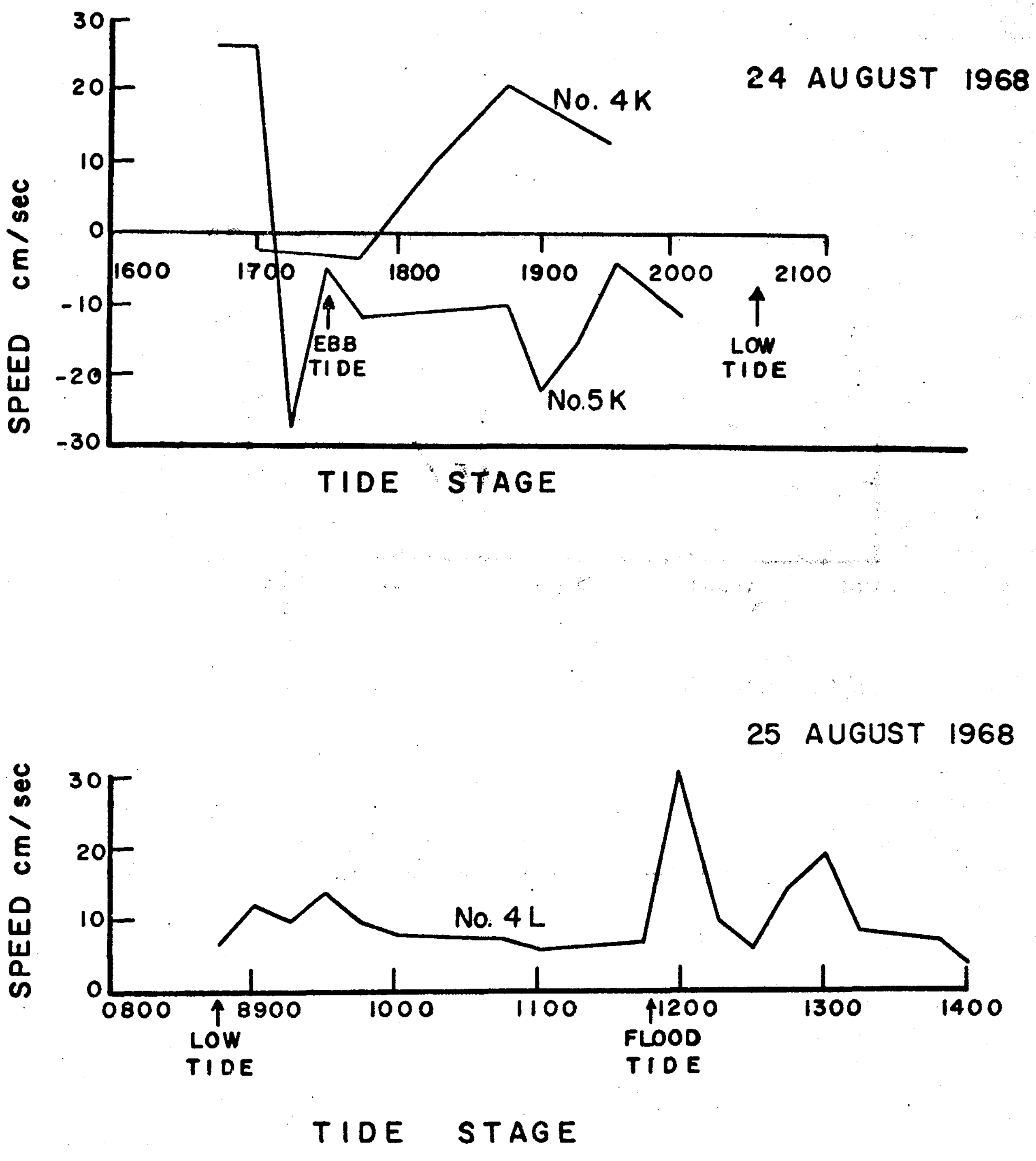

Figure 21. Typical iceberg speed curves, 24 and 25 August 1968.

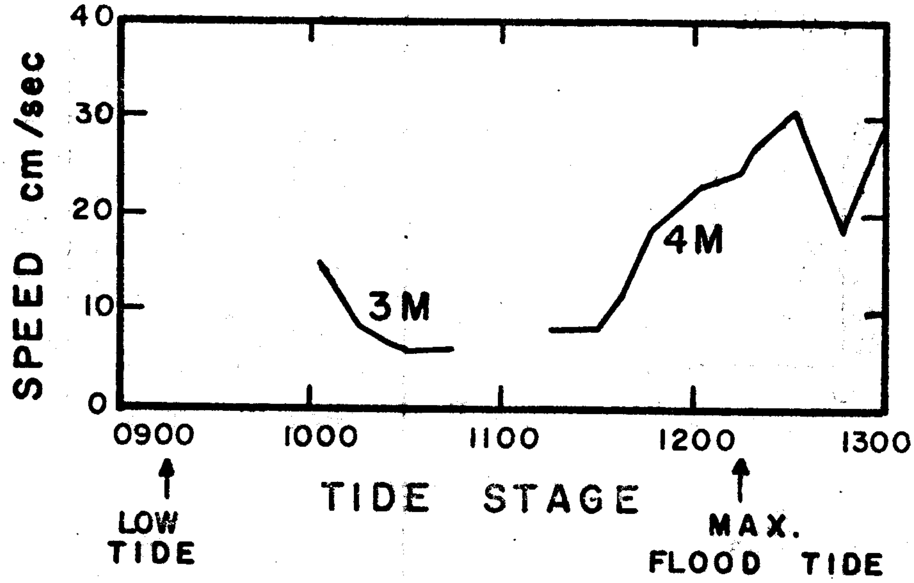

Figure 22. Typical iceberg speed curves, 6 March 1969.

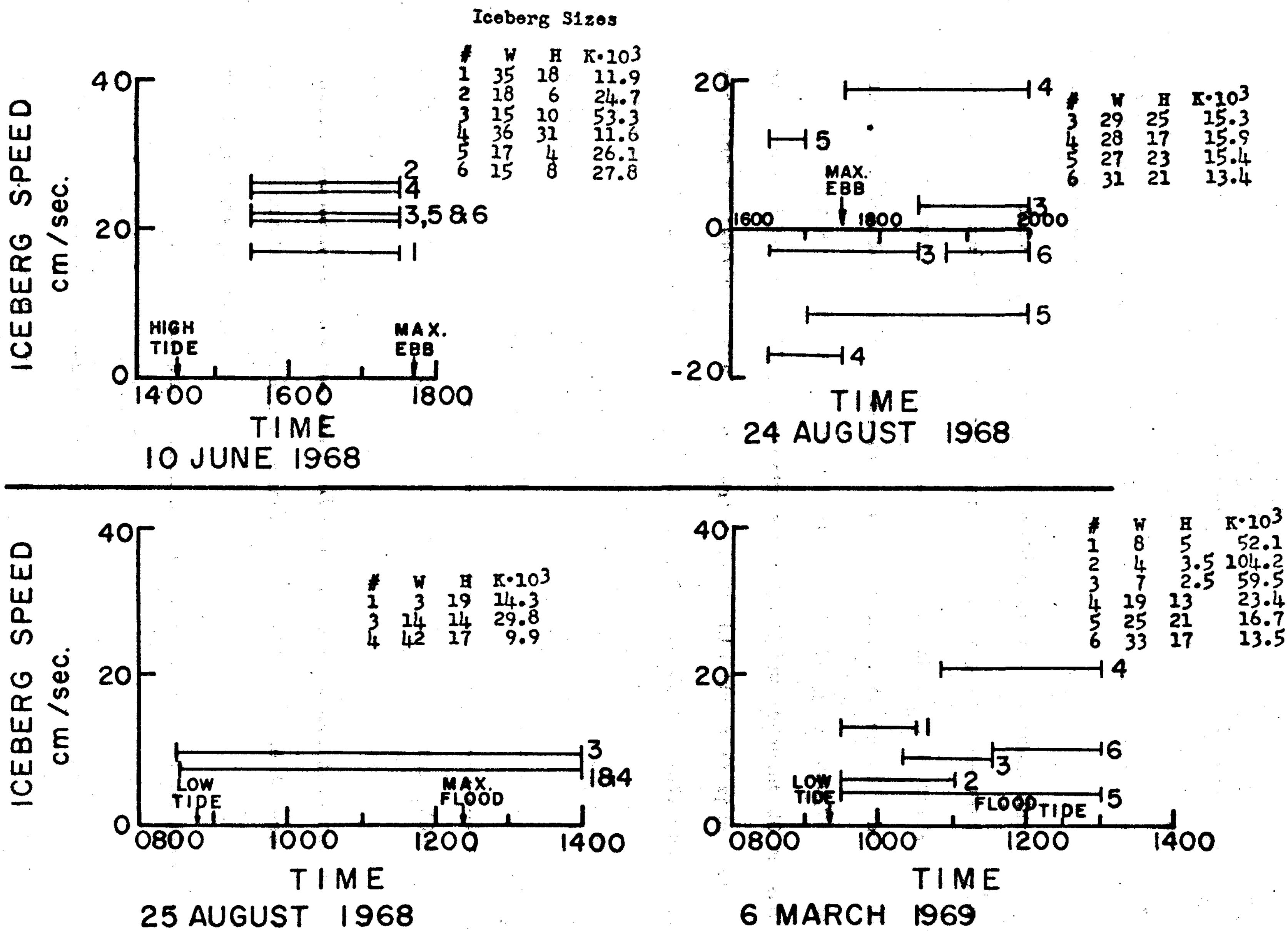

Figure 23. Mean iceberg speeds for 10 July, 24 and 25 August 1968 and 6 March 1969.

dubious but the direction change was clearly evident in the photographs.)

Comparing figures 23 and 8 and assuming the tidal oscillation is superimposed on a mean outflow gives some indication of the true mean outflow currents.

On 10 July 1968, assuming a 20 cm/sec tidal amplitude during photography, the iceberg's tidal oscillation speed should have varied from -10 to +10 cm/sec (figure 8, 20 cm/sec plot). This means the tidal component of the iceberg's speed was zero over the interval of photography. The icebergs with similar k-numbers as that of the plot had mean speeds of 17 and 25 cm/sec. This suggests a mean outlfow of about 20 cm/sec reaching to twenty meters. This value is within the mean speeds measured by the surface drogues of the previous two days. This mean further suggests that the ten meter mean outflow speed was the same as at the surface.

The ice drift of 24 August is not explicable by the tide ice drift curves. The reversal of the icebergs in the center of the inlet occured near maximum ebb current (figure E10). The iceberg's mean tidal drift should have been down inlet at about 2 cm/sec which should have reinforced the mean outflow current. The reversal of these icebergs may have been caused by sub-surface currents but there is no independent data to check this possiblity.

During the photography period of 25 August the tidal oscillation speed of the icebergs varied from +4 to -4.5 cm/sec. Taking the mean area under the two curves gives a mean tidal current of about -1 cm/sec assuming the tidal current amplitude was about 10 cm/sec. (The area-under-the-curve mean was used because the time interval extended beyond the negative maximum of the iceberg speed curve.) The mean ice drift speed during the time was about 8 cm/sec, giving a mean outflow current speed of about 9 cm/sec.

On 6 March 1969 icebergs 5 and 6 (figure 23, text and figure E11) with k-numbers similar to the figure 8 iceberg were used. (A ten cm/sec tidal current amplitude was assumed.) Iceberg 5 covered a tidal oscillation from about +4 to -4 cm/sec giving zero tidal correction. Iceberg 6 covered a tidal oscillation from 0 to -4 cm/sec giving a tidal correction of +2 cm/sec. The wind was blowing intermittently at about 10 knots (5 m/sec). Since the wind was intermittent, one half of Gudkovich and Nikiforov's (1967) correction was applied (-1 cm/sec). From these corrections and mean outflow current measured by icebergs 5 and 6 was 3 and 11 cm/sec respectively (figure 23). (Since iceberg 4 had a high mean speed, it was checked. Its tidal correction was taken from plots in Appendix G and found to be -3 cm/sec. Applying this and the wind correction gives a mean outflow velocity of 17 cm/sec.) The mean surface outflow current from the 25 and 26 February data was 7 to 17 cm/sec, and the mean ten meter outflow current was 5 to 11 cm/sec (figure 16). Apparently the icebergs (except number 4) drifted at a speed near the mean ten meter outflow current speed.

4.3 Iceberg Melt as it Affects Measurements

The icebergs were measured about two thirds of the way down the inlet. Assuming a linear melt rate the icebergs measured here could have been three times as large at the glacier. Also assuming that the icebergs melt completely in the inlet make a 40 meter wide iceberg measured by photography 120 meters wide at the glacier. Further, if this iceberg drifted down-inlet at 5 cm/sec, its complete melting would give a melt rate of 9.2 m/day for 13 days. Since the longest interval one iceberg was tracked was 5 hours, the iceberg should have melted 1.9 meters in width. This would be hard to detect and rotation of rectangular icebergs would confuse such measurements.

In the same five hours the iceberg's coupling with the tidal current would have changed also. This change, in the case of the 40 meter iceberg would be from 0.0111 to 0.0117 in k-number. This represents a 6% change in amplitude and about 2% change in lag (figure 9).

CHAPTER V

SUMMARY AND CONCLUSIONS

5.1 Summary of Drogue Drift Measurements

Drogue drift measurements were made on 30 and 31 March 1968; 10 and 11 June 1968; 8 and 9 July 1968; and 25 and 26 February 1969. All the surface and 10 meter drogues showed tidal oscillations with superimposed mean outflow.

The maxima of current proved close to the predicted maxima but the broad peaks and troughs precluded accurate timing except by reversal times of the drogues. The mean outflow was measured by use of 12-hour means of the data. Six-hour means, between current maxima, showed an increase in mean outflow down-inlet. Since the inlet widens towards the mouth, this increase was related to entrainment.

Velocity-depth profiles were derived from the six- and twelve-hour means of current. The March 1968 and February 1969 profiles and similar slopes of about 0.4 cm/sec/m between the surface and ten meters.

The 1968 data show a seasonal summertime increase in mean current speed. The March and 10 June drogues showed low mean outflow speeds. The 11 June data showed a sudden increase in speed on a flooding tide which was related to the onset of the summer run-off period. The July data showed high mean outflow currents which were considered normal for this time of year (Wallen and Hood, 1971).

The February 1969 data did not fit this pattern but instead showed high mean outflow speeds similar to those of July 1968. This may have been an unusual occurrence for this time of year but that is not known.

The drogue data taken down-inlet from Sumdum Island indicated there is little flow over the shallows northeast of the mouth of the inlet. The current measured through the mouth of the inlet in November 1966 of 28.6 cm/sec indicated at total outflow volume at high tide of 5.3 x $10^3 m^3$/sec. The current measured on 6 March 1967 and corrected to high tide suggested an outflow of 8.0 x $10^3 m^3$/sec.

5.2 Summary of Photogrammetry

Photogrammetric interpretation of currents from ice drift proved a complex procedure. First, the standard considerations of photogrammetry had to be made including site selection and camera-pointing. Second, the current regime with depth needed measuring independently of the ice drift. Third, measurements on the photographs were made of the movement of the icebergs, their width, height and general shape. Fourth, calculations were made of the coupling between the iceberg and the water. Finally, the total drift with time was used to minimize measurment errors.

The cameras used were calibrated and two were measured for distortion errors. The cameras used were a Graflex and two Kalimar, SQ cameras. Site selection required the photographer to be as high as convenient where the view was unobstructed. Cameras were pointed generally down-inlet so one iceberg could be tracked as long as possible. This, however, proved a nuisance since often the iceberg was moving nearly away from the camera, the direction in which the error was greatest.

Currents were measured by parachute drogues, as previously discussed, and these measurements were used as an independent check on the iceberg photogrammetry. This points up the fact that icedrift photogrammetry was used to gather auxiliary data. This technique measures the current only in the mean and is not practical for measuring tidal currents.

Measurements of the photographs consisted of measuring distances from the side of the photograph to the iceberg and the known landmark, and measuring the distance of the iceberg below the shoreline. These distances were converted to distance from the camera and angle at the camera, between the landmark and the iceberg. In addition, the width and height-above-water of the iceberg were measured to determine its true size. From the positions of the iceberg with time the photograph-to-photograph and total drift speeds of the icebergs were determined.

From the equations of drag and inertia, a differential equation was formed to describe the iceberg's motion in the tidal current. This differential equation was simulated on the University of Alaska's analog computer. The coefficients of drag, frontal area, volume and density were lumped into one coefficient, k. For the solution of the differential equation, k was varied with the tidal amplitude at 10 and 20 cm/sec.

Since the icebergs were affected by both tidal and mean outflow currents, the position-to-position movements were checked. Unfortunately, the error in measurement was often as large as the iceberg's movement negating trend measurements. The times of photography generally covered both positive and negative tidal movement, so net drift with time was used. This net drift was corrected by the iceberg coupling curves to indicate mean outflow currents. These indicated currents were checked against the existing drogue data. The agreement was good which indicates the ice drift photogrammetry technique is probably a reliable method of gathering auxiliary current data.

5.3 Conclusions

5.3.1 The Drogue Study

The tide staff record shows that low tide at North Dawes inlet of Endicott Arm is within one-half hour of low tide at the mouth. Further, the current drogue data indicate the tidal wave is close to a standing wave in Endicott Arm.

The drogue drift patterns, showing a general outflow with small or no reversals at maximum flood current, show the mean outflow is of similar magnitude to the tidal currents. The mean outflow showed an expected summer increase in July 1968, but the February 1969 data showed unusually high mean outflow currents.

The current profiles indicated a roughly similar 0-10 meter slope. This slope suggests there may be an increase in depth of the mean outflow layer with an increase in the mean outflow current. This suggests a concurrent depression of the mean inflow layer. McAlister, Rattray, and Barnes (1959), observed the opposite effect in Silver Bay during 1956. They observed a surface current of about 10 cm/sec and a mean outflow layer of about 30 meters in March and a surface current of about 18 cm/sec with the main outflow layer depth of about 5 meters from the surface and a second between about 35 and 90 meters in July. The data do not suggest a reason for this difference.

5.3.2 The Ice Drift Study

As stated previously the ice drift study proved complex. It was evident from the error curves that the cameras were pointed too much down-inlet. The height-of-camera to range-of-iceberg ratio of 1:50 combined with the fact that the icebergs moved primarily away from the cameras made the photograph-to-photograph velocities of the icebergs useless.

A further difficulty was the loss of the horizon. The photographs were taken on black and white film which caused the quiet water to blend with the mountain behind. This difficulty could have been readily corrected by the use of color film.

The cameras used did not produce film adapted to automated processing. The best camera for this work would have been a 35 millimeter camera where the film would have been left in strips after development. Thirty-five millimeter film is easily and accurately measured on systems such as the OSCAR.

The technique did prove workable for gathering supplementary current data. As with all remote sensing, the interpretation requires independent measurements to test and calibrate the remote measurements. However, if the current profile with depth and the tidal amplitude and frequency are known, photogrammetric icedrift measurements will provide workable supplementary current data.

REFERENCES CITED

Bowden, K. F., 1967. Circulation and Diffusion, Estuaries, AAAS #83, G.H. Lauff, Ed., 15-36.

Forrester, W. D., 1960. Plotting Water Current Patterns by Photogrammetry, Photo Engr. 26, 726-736.

Gudkovich, Z. M., G. I. Melkonyan and E. G. Nikiforov, 1967. Aerodynamic Investigations of Ice Flow Models, Hydrometeorology of the Polar Regions, G. Ya. Vangengeim and A. F. Laktionov, 1963, NSF by Israel Prog. Sci. Trans., Jerusalem, 237-259.

Gudkovich, Z. M. and E. G. Nikiforov, 1967. Steady-State Drift of a Single Ice Floe, Hydrometeorology of the Polar Regions, G. Ya. Vangengeim and A. F. Laktionov, Ed., Leningrad, 1963, NSF by Isreal Prog. Sci. Trans., Jerusalem, 214-226.

Hoerner, S. F., 1958. Fluid Dynamic Drag, Published by Author, 148 Bustead Dr., Midland Park, N. J., 07432.

Ingram, R. G., O. M. 1969. Johannessen and E. R. Pounder, Pilot Study of Ice Drift in the Gulf of St. Lawrence, J. Geophys. Res., 74, 5453-5459.

Keller, M., 1963. Tidal Current Studies by Photogrammetric Methods, USC&GS Tech. Bul. 22, 20 p.

Kinsman, B., 1965. Notes on Tides, Seiches and Long Waves, Unpublished Notes, Dept. Ocean., Johns Hopkins U., 258 p.

Knauss, J. A., 1963. Drogues and Neutral-Buoyant Flots, The Sea, M. N. Hill, Ed., 303-305.

Maunual of Photogrammetry, Amer. Soc. of Photogrammetry, Box 286, Benj. Franklin Sta., Wash., D.C., 1952.

Matthews, J. B. and D. R. Rosenberg, 1969. Numeric Modeling of a Fjord Estuary, Inst. Mar. Sci., U. of Alaska, Prog. Rept., Mar. 1966 to Jun 1968, 24-40.

McAllister, W. B., M. Rattray, Jr., and C. Barnes, 1959. The Dynamics of a fjord Estuary: Silver Bay, Alaska, Tech. Rept. 62, Dept. of Ocean., U. of Washington, 70 p.

Reed, R. J. and W. J. Campbell, 1962. The Equilibrium Drift of Ice Station Alpha, J. Geophys. Res., 67, 281-297.

Roshko, A., 1961. Experiments on the Flow Past a Circular Cylinder at Very High Reynolds Number, J. Fluid Mech., 10, 345-356.

Schvede, Ye. Ye., 1966. Icebergs in the Northwest Atlantic, Oceanology, 6, 499-504.

Streeter, V. L., 1958. Fluid Mechanics, McGraw Hill, Inc., New York, 705 p.

Swanson, L. W., M. Keller and S. D. Hicks, 1963. Photogrammetric Measurement of Tidal Currents, USC&GS, Int. Un. of Geod. and Geophys., 13 Gen. Assbly., Berkeley, Cal., Aug 19-31.

Thorndyke, E. M. and M. Ewing, 1969. Photographic Determination of Ocean Bottom Current Velocity, Mar. Tech. Soc. J., 3.

Tide Tables, West Coast of North and South America, U.S. Dept. of Commerce, U.S. Govt. Print. Off., Wash., D.C., 20401, 1966-1969.

Volkman, G., J. Knauss and A. Vine, 1956. The Use of Parachute Drogues in the Measurement of Subsurface Ocean Currents, Trans. Am. Geophys. Un., 37, 573-577.

Wallen, D. D. and D. W. Hood, 1968. Descriptive Oceanography of the Southeastern Alaskan Waters, Prog. Rept., Inst. Mar. Sci., U. of Alaska, Mar 1966 to June 1968, 1-18.

Wallen, D. D. and D. W. Hood, 1971. Tech. Rept. R 71-1, Inst. Mar. Sci., U. of Alaska.

Walford, T. C. and M. J. Moynehan, 1969. The Influence of Directly Measured Currents, Geostrophic Currents and Winds on Iceberg Drift, (Abstract) Trans. Am. Geophys. Un., 50, 192.

APPENDIX A

BATHYMETRY

The only published soundings in Endicott Arm (U.S. Coast and Geodetic Survey Chart 8201) shows little sounding information. In addition it shows the North and South Dawes Glaciers nearly meeting at the point of land between them.

This chart has been brought up to date with soundings taken aboard the University of Alaska's ship, R/V ACONA, during March 1967 and November 1968. Figure 1A shows the new bathymetric chart of Endicott Arm. Bathymetry data was gathered with a model Precision Depth Recorder attached to a UQN EDO Fathometer. The sounding tracks are shown as an insert.

Soundings were positioned by radar using prominent landmarks as references. The data taken during the November 1968 cruise were considered the most accurate and the other data were adjusted to them.

The basic configuration of the inlet was obtained from U.S. Geological Survey Topographic Maps (Sumdum C3, C4 and C5). Sounding tracks were plotted on this outline chart and sonic profiles were then adjusted to fit the length of each track. The adjusted sounding profiles were read at 20 fathom (37 meter) intervals; the position of each 20 fathom interval was plotted on the chart, and the chart was contoured. Positioning of the soundings is considered accurate to ±0.1 nautical miles (±185 meters). Depth accuracy is considered to be ±2 fathoms (4 meters).

The bathymetry is characterized by two basins separated by a rise near Point N (figure 1A). The outer basin is wide, irregular and terminated by a sill at the mouth of the inlet. The sill at the mouth is 8 to 12 fathoms (14 to 22 meters) in the deepest area. The inner basin, separated from the outer by an 80 fathom (293 meter) deep rise, is a U-shaped valley typical of fjords. The deepest point (195 fathoms — 714 meters) in the inlet is found in this basin. Bathymetry near the head of the inlet is unknown due to lack of data.

APPENDIX B

DROGUE POSITION AND SPEED DATA

B.1 Drogue Position Data

The drogue position data are listed for observations used in this thesis as time of observation, azimuth and distance from a known landmark. The azimuths are in degrees and the distances are in nautical miles.

19 November 1966

Surface Drogues

Positions based on NW End of Sumdum Island

Drogue #1			Drogue #2			Drogue #3a		
Time	Az.	Dist.	Time	Az.	Dist.	Time	Az.	Dist.
0822	29	1.46	0830	44	0.91	0839	266	0.55
0903	355	1.1	0910	352	0.6	0855	196	0.97
0930	20	0.87	0937	20	0.34	0917	249	0.55
1005	24	1.6	1000	55	1.7	0934	214	0.57
1035	10	0.25	1027	05	0.21	1020	270	0.6
1208	06	0.96	1040	308	0.34	1045	Assumed Lost	
1340	340	0.5	1200	292	0.65	1610	341	0.83

Drogue #3b			Drogue #4			Drogue #5		
Time	Az.	Dist.	Time	Az.	Dist.	Time	Az.	Dist.
1045	261	0.51	0850	220	1.1	0856	216	1.7
1153	266	0.7	0935	199	1.02	0933	194	1.7
1220	255	1.5	0955	176	0.65	0944	190	1.8
1400	273	1.45	1117	243	0.99	0955	171	1.28
1535	294	1.60	1150	231	1.05	1125	175	0.35
			1225	248	2.1	1255	224	0.95
			1405	277	1.50	1510	224	2.85
			1420	277	1.50			
			1545	295	1.42			

20 November 1966

Positions Based on Wood Spit Light

Drogue #3 20 m			Drogue #4 10 m			Drogue #5 20 m		
Time	Az.	Dist.	Time	Az.	Dist.	Time	Az.	Dist.
1020	26	1.5	1155	20	1.18	1235	18	1.11
1050	30	1.37	1400	13	1.1	1420	38	0.99
1125	30	1.3	1531	23	1.24	1550	38	1.09
1410	08	1.1	1604	14	1.23	1624	36	1.52
1538	21	1.4	1700	118	0.68	1730	52	1.3
			1725	30	1.32			

21 November 1966

Drogue #3 20 m Drogue set 20 Nov. Posit. on SE and Harbor Island			Drogue #4 10 m Drogue set 20 Nov. Posit. on Wood Spit Light			Drogue #5 20 m Drogue set 20 Nov. Posit. on Wood Spit Light		
Time	Az.	Dist.	Time	Az.	Dist.	Time	Az.	Dist.
0835	183	1.7	1040	105	0.90	0945	182	0.62
1005	193	1.7	(aground)					

Drogue #3a Surf Posit. on Wood Spit Light			Drogue #5a 20 m Posit. on Wood Spit Light			Drogue #6 40 m Posit. on Wood Spit Light		
Time	Az.	Dist.	Time	Az.	Dist.	Time	Az.	Dist.
1025	140	0.7	1040	141	0.72	0830	189	0.85
1140	56	1.14	1125	115	1.21	0920	181	0.55
1300	45	2.10	1205	111	1.43	1110	175	0.49
			Posit. on 26F Pt.			1150	132	0.46
			Near Pt. Coke			1325	63	0.64
			1400	258	1.03	1430	72	0.85

6 March 1967

All Positions based on Wood Spit Light

Drogue #1 Surf			Drogue #2 Surf			Drogue #3 50 m		
Time	Az.	Dist.	Time	Az.	Dist.	Time	Az.	Dist.
1330	70	0.93	0900	62	1.95	1015	82	1.55
1445	60	0.95	1028	55	2.00	1120	98	1.50
1510	64	0.91	1130	52	2.19	1305	94	1.40
1630	31	0.96	1200	51	2.14	1330	90	1.30
			1255	56	1.83	1400	82	1.59
			1320	50	2.00			
			1415	48	2.00			

Drogue #4 Surf		
Time	Az.	Dist.
1005	114	1.25
1020	92	0.90
1123	83	0.85
1150	77	0.81
1215	61	0.68
1250	70	0.66
1310	58	0.64
1336	49	0.73
1405	32	0.70
1500	330	0.57
1555	297	2.22

5 May 1967

Surface Drogues

All Positions based on NW End Sumdum Island

Drogue #1			Drogue #2			Drogue #3		
Time	Az.	Dist.	Time	Az.	Dist.	Time	Az.	Dist.
1200	233	1.70	1215	247	1.90	1230	249	1.77
1250	240	1.81	1325	251	1.89	1330	254	1.78
1445	245	2.21	1437	260	2.31	1430	262	2.02
1545	246	2.47	1530	263	2.83	1525	266	2.60
						1555	299	2.71

5 May 1967

Drogue #4			Drogue #5		
Time	Az.	Dist.	Time	Az.	Dist.
1150	248	1.88	1145	262	1.10
1235	256	1.75	1246	267	1.58
1330	262	1.92	1333	274	2.00
1420	267	2.40	1500	277	2.06

30 & 31 March 1968

All Positions Based on SE end Sumdum Island except where indicated

Drogue #1 Surf.			Drogue #2 Surf.			Drogue #3 10 m		
Time	Az.	Dist.	Time	Az.	Dist.	Time	Az.	Dist.
1239	130	2.49	1245	128	2.62	1237	128	2.51
1335	133	2.69	1350	128	2.67	1350	128	2.65
1431	136	2.70	1443	132	2.71	1439	127	2.61
1536	137	2.72	1533	132	2.72	1542	126	2.70
1617	136	2.67	1614	133	2.70	1602	126	2.71
1641	137	2.64	1638	133	2.66	1633	125	2.71
1714	137	1.54	1712	134	2.54	1707	124	2.67
1752	138	2.44	1750	134	2.41	1744	124	2.65
1805	136	2.40	1807	133	2.37	1812	124	2.63
1833	137	2.31	1835	138	2.35	1840	124	2.59
1858	139	2.45	1900	138	2.17	1904	125	2.56
1943	--	--	1924	144	2.05	1951	124	2.44
2011	--	--	2003	144	1.85	2017	124	2.37
2035	142	1.78	2034	145	1.75	2043	125	2.32
2125	148	1.67	2125	148	1.57	2137	124	2.22
2233	144	1.58	2237	149	1.51	2239	127	2.08
2337	143	1.58	2335	148	1.52	2345	127	1.98
0036	141	1.76	0033	147	1.65	0043	127	1.96
0137	144	1.97	0133	149	1.78	0145	130	2.06
0247	145	1.97	0239	155	1.71	0255	128	2.09
0345	148	1.84	0339	163	1.43	0359	124	2.08
0450	153	1.73	0442	172	1.12	0503	123	1.98
0602	160	1.51	0554	182	0.80	0614	119	1.90
0657	169	1.32	0651	194	0.52	0706	116	1.78
Posit. on Wood			Posit. on Wood			0813	115	1.66
Spit Light			Spit Light			0907	118	1.55
0802	126	5.72	0753	131	5.14	1034	114	1.41
0919	131	5.50	0925	135	4.81	1132	112	1.38
1047	130	5.40	1053	133	4.61	1238	109	1.44
1146	131	5.31	1151	131	4.49	1351	112	1.56
1255	131	5.19	1302	132	4.49	1459	114	1.59
1408	133	5.00	1413	133	4.43	1613	114	1.56
1521	132	4.60	1525	134	3.97	1740	107	1.51
1633	135	4.10	1636	138	3.69			
1849	139	3.45	1854	140	3.01			

30 & 31 March 1968

All Positions Based on SE end Sumdum Island

Drogue #4 10 m			Drogue #5 20 m		
Time	Az.	Dist.	Time	Az.	Dist.
1242	129	2.53	1249	128	2.60
1349	131	2.69	1353	129	2.75
1437	130	2.79	1447	129	2.94
1531	130	2.85	1539	127	3.00
1604	128	2.88	1620	128	3.02
1631	128	2.92	1645	128	3.00
1704	128	2.92	1717	129	3.00
1740	129	2.92	1755	125	3.03
1814	127	2.89	1803	127	3.02
1842	128	2.86	1830	126	3.03
1907	129	2.81	1854	129	3.00
1954	133	2.69	1930	128	2.86
2020	132	2.64	2001	128	2.93
2101	131	2.59	2030	129	2.87
2143	132	2.52	2115	128	2.82
2245	132	2.44	2220	129	2.78
2352	133	2.44	2331	126	2.81
0050	133	2.49	0023	128	2.93
0220	132	2.68	0127	126	3.05
0303	131	2.70	0231	125	3.02
0406	130	2.72	0332	127	3.03
			0428	127	3.03
0620	126	2.59	0549	126	3.01
0712	126	2.52	0644	125	3.01
0819	127	2.35	0747	127	2.95
0902	130	2.31	0937	129	2.93
1025	130	2.10	1101	129	2.85
1126	130	2.01	1204	129	2.83
1230	130	1.96	1312	129	2.67
1344	129	2.10	1427	129	3.05
1453	130	2.19	1534	129	3.09
1607	129	2.21	1643	129	3.03
1725	126	2.21	1926	130	3.04

10 & 11 June 1968

Sextant Readings

Sextant readings were taken as angles between two or more sets of two points. These are read as successive angles between known landmarks (figures E6 and E7). Drogue #1 at 1420 was 41° between #5 and Cabin Point; 15° between Cabin Point and Sumdum Island, etc.

Time	Mark 1	Mark 2	Mark 3	Mark 4	Mark 5	Mark 6
Drogue #1						
1420	#5	Cabin Pt.	Sumdum	Waterfall	#1	
		41°	15°	43°		
1535	#6	#5	#4	Sumdum	Waterfall	#X
		71°	72°	21°		97°
Drogue #2						
1350	Released 300 yards at 140° (magnetic) from #3					
1550	#4	Sumdum	Waterfall	#X	#5	
		29°	49°		100°	
1657	#4	Sumdum	Waterfall	Creek 3		
		33°	58°	37°		
1758	#5	#4	Sumdum	Waterfall	#X	
		72°43'	84°	71°86'	82°46'	
1900	Sumdum	Waterfall	#X	#4	Sumdum	
		86°05'	74°21'	74°36'	125°58'	
2052	#5	#4	Sumdum	Waterfall	#1	#5
		78°00'	73°01'	66°57'	97°37'	55°13'
2157	#5	#4	Waterfall	#1	#5	
		115°49'		103°26'	55°05'	

11 June 1968

Time	Mark 1	Mark 2	Mark 3	Mark 4	Mark 5	Mark 6
0908	#5	#4	Sumdum	Waterfall	Creek 3	#4
		23°23'	133°12'	103°02'	40°22'	82°16'
1025	Sumdum	Waterfall	#1	#4		
		105°55'	64°16'	45°22'		
1123	Sumdum	Waterfall	#4			
		109°23'	102°22'			
1259	Sumdum	#2	Waterfall	#4		
		33°12'	84°29'	75°29'		
1320	Sumdum	#2	Waterfall	#4		
		33°59'	82°03'	78°41'		
1527	Sumdum	#2	Waterfall	#3	Sumdum	
		92°52	41°00'		24°22'	

10 June 1968

Drogue #3

1410	#5	#4	Sumdum	Waterfall	#6	#5
		46°	17°		215°	103°
1545	#5	#4	Waterfall	#X		
		103°	71°	68°		
1648	#4	Waterfall	Creek 3			
		77°	34°	Lie on a circle assumed in line with previous		
1745	#4	Sumdum	Waterfall	#X		
		31°05'	62°00'	84°27'		

Time	Mark 1	Mark 2	Mark 3	Mark 4	Mark 5	Mark 6
1851	#5	#4	Sumdum	Waterfall	#X	#5
		70°57'	100°04'	73°40'	76°39'	(39°44')
2035	#5	#4	Sumdum	Waterfall	#1	#4
		37°45'		79°35'	83°11'	70°53'
2205	#5	#4	Waterfall	#1	#5	
		101°44'		89°04'	29°33'	

11 June 1968

Time	Mark 1	Mark 2	Mark 3	Mark 4	Mark 5	Mark 6
0853	#5	#4	Sumdum	Waterfall	#X	
		43°28'	121°59'	79°47'	76°00'	
1043	#5	#4	Sumdum	Waterfall	#X	
		104°27'	50°40'	62°57'	88°37'	
1146	#5	#4	Sumdum	Waterfall		
		100°25'	33°39'	53°34'		
1227	#5	#4	Sumdum	Waterfall		
		90°41'	28°15'	49°35'		
1411	#5	#4	Sumdum	Waterfall	#6	#5
		75°08'	29°54'	47°00'		155°50'
1450	#5	#4	Sumdum	Waterfall		
		77°49'	31°37'	48°15'		

10 and 11 June 1968

Drogue #4 Sextant Readings

Time	Mark 1	Mark 2	Mark 3	Mark 4	Mark 5	Mark 6
1530	#6	#5	#4	Sumdum	Waterfall	
		86°		23°	42°	
1640	#5	#4	Sumdum			
		66°	27°			
1731	#4	Sumdum	Waterfall	#4	#2	
		30°40'	49°49'		38°49'	
1837	#5	#4	Sumdum	Waterfall	#X	
		100°43'	44°40'	59°12'	91°22'	
2025	#5	#4	Waterfall	Creek 3	#1	#5
		85°37'		44°03'		48°29'
2108	#5	#4	Sumdum	Waterfall	#1	#5
		98°10'	45°56'	58°44'	105°26'	(53°19')
2157	#5	#4	Waterfall	#1	#5	
		115°49'		103°36'	55°05'	

11 June 1968

Time	Mark 1	Mark 2	Mark 3	Mark 4	Mark 5	Mark 6
0920	#5	#4	#1	Waterfall	Sumdum	
		13°39'	36°58'	67°29'	95°34'	
1013	Sumdum	Waterfall	#1	#4		
		98°02'	64°33'	30°27'		
1100	Sumdum	Waterfall	Creek 3	#4		
		100°30'	31°57'	61°08'		
1247	Sumdum	Waterfall	Creek 3	#4		
		107°15'	29°37'	61°54'		
1338	Sumdum	Waterfall	#4	#2	Waterfall	
		114°23'	72°08'		(72°08')	

8 and 9 July 1968

Sextant Readings

Time	Mark 1	Mark 2	Mark 3	Mark 4	Mark 5	Mark 6
	Drogue #1	8 July				
1421	#10	#1	Waterfall 2			
		116°12'	36°20'			
1553	#5	Sumdum	#10	Waterfall 2		
		22°49'	59°35'	111°55'		
1655	#6	#5	Sumdum	#10	#1	Waterfall 2
		60°37'	26°56'	102°25'	48°42'	65°42'
1834	Sumdum	Waterfall 1	#10	Waterfall 2	#6	
		36°52'	97°24'	37°06'	41°39'	
1948	Water-fall 1	#10	#1	Waterfall 2	#6	#5
		99°37'	25°13'	6°39'	33°51'	87°58'
			9 July 1968			
1215	Wood Spit Light	Sumdum	Bushy Right Side	Point N #2		
		10°45'	23°20'	128°04'		
1323	San-ford Cove	~~Sumdum~~	~~Bushy~~ Right Side	Point N #2		
		44°20'	29°20'	120°22'		
2105	Wood Spit Light	West End Sumdum	East End Sumdum	Building Sanford Cove		
		67°38'	58°49'	83°40'		

8 and 9 July 1968

Time	Mark 1	Mark 2	Mark 3	Mark 4	Mark 5	Mark 6
	Drogue #2	8 July				
1418	#10	#1	Waterfall 2			
		109°33'	39°41'			
1602	#5	Sumdum	#10	Waterfall 2		
		21°29'	61°57'	108°44'		
1702	#6	#5	Sumdum	#10	Waterfall 2	
		68°27'	25°42'	103°59'	63°26'	
1834	Sumdum	Waterfall 1	#10	Waterfall 2	#6	
		36°52'	97°24'	37°06'	41°39'	
1955	#10	Waterfall 2	#6	#5	Sumdum	
		32°28'	40°41'	83°57'	146°22'	
			9 July 1968			
1124	Sumdum	#2	Waterfall 1	Waterfall 2	#4	
		50°39'	3°21'	54°07'	5°40'	
1450	#2	Waterfall 1	#4			
		45°50'	48°49'		500 ft. offshore	
1900	Sumdum	#2	Waterfall 1	#6		
		52°19'	55°21'	57°31'		

8 and 9 July 1968

Sextant Readings

Time	Mark 1	Mark 2	Mark 3	Mark 4	Mark 5	Mark 6
			Drogue 3			
			8 July 1968			
1429	Waterfall 1	#10	#1	Waterfall 2		
		199°05'	137°22'	24°49'		
1541	Sumdum	#10	#1	Waterfall 2		
		34°27'	(119°25')	15°20'		
1715	#10	Waterfall 2	#6	#5	Sumdum	
		39°41'	76°40'		49°35'	
1822	#5	Sumdum	Waterfall 1	Waterfall 2	#5	
		71°19'	28°27'		103°23'	
2008	Waterfall 2	#5	#4	Sumdum		
		75°58'	39°40'	54°25'		
			9 July 1968			
1059	#4	#3	Sumdum	#2		
		113°51'	33°11'	75°02'		
1354	On line #2 to drogue. Sumdum is 22°27' Right About 1 mile from #2 (fog)					
1815	#3	Sumdum	#2	Waterfall 2		
		81°31'	178°33'	6°55'		
2002	#2	#3	Sumdum			
		100°30'	75°20'			

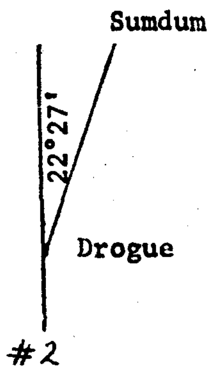

10 July 1968

1115	Wood Spit	W. End Sumdum	E. End Sumdum
		29°35'	75°56'

25 and 26 February 1969

Drogues 1 and 2 (Surface)

Drogue #1

Time	Azimuth	Distance
Azimuths relative to Tide Gauge		
1617	111°	1.05
1739	113°	0.95
1848	106°	0.93
1943	98°	0.93
2036	95°	0.91
2142	82°	0.81
2306	61°	0.52
0017	20°	0.40
0133	347°	0.55
Azimuth based on east end of Sumdum		
0254	142°	2.05
0407	148°	1.78
0526	156°	1.46
0620	161°	1.27
0657	169°	1.16
0912	201°	0.89
1017	228°	1.11
1121	242°	1.37

Drogue #2

Time	Azimuth	Distance
Azimuths relative to Tide Gauge		
1615	98°	1.06
1726	86°	0.85
1957	46°	0.62
2046	29°	0.59
2203	02°	0.65
2318	340°	0.86
0029	328°	1.08
0141	319°	1.36
Azimuth based on east end of Sumdum		
0605	194°	0.60
0706	216°	0.63
Azimuth based on Wood Spit		
0921	122°	3.61
1026	122°	3.25
1127	123°	2.99
1225	123°	2.64
1322	123°	2.40
1430	118°	1.90

Drogue #1

Time	Azimuth	Distance
Azimuth based on Wood Spit		
1221	126°	3.30
1318	127°	2.79
1421	127°	2.60

25 and 26 February

Drogue 3 (Surface)			Drogue 4 (Surface)		
Time	Azimuth	Distance	Time	Azimuth	Distance
Azimuths based on Tide Gauge Point			Azimuths based on Tide Gauge Point		
1612	75°	1.30	1710	72°	1.58
1722	75°	1.08	1833	56°	1.44
1840	65°	0.95	1927	62°	1.30
2000	44°	0.73	2025	55°	1.25
2052	26°	0.75	2134	46°	1.13
2159	04°	0.83	2255	30°	1.01
2333	343°	1.04	0005	10°	0.98
0033	327°	1.30	0121	346°	1.03
0144	321°	1.63	Azimuths based on east end of Sumdum		
Azimuths based on east end of Sumdum			0242	137°	1.48
0306	166°	0.70	0415	147°	1.06
0425	197°	0.62	0535	151°	0.70
Azimuths based on Wood Spit Light			0725	165	0.49
0545	116°	4.23	Azimuths based on Wood Spit Light		
0712	116°	3.88	0933	116°	4.27
0925	119°	3.15	1042	118°	3.91
1034	120°	2.90	1145	121°	3.36
1131	119°	2.61	1241	121°	3.02
1228	117°	2.20	1335	120°	2.60
1325	114°	1.89	1449	118°	2.24
1437	114°	1.51			

26 February 1969

Drogue 1a Surface

Time	Azimuth	Distance
Azimuth based on east end of Sumdum		
1602	139°	2.75
1703	137°	2.76
1801	136°	2.75
1905	135°	2.76
2005	135°	2.76
2104	135°	2.76
2202	136°	2.79

Drogue 2a Surface

Time	Azimuth	Distance
Azimuth based on east end of Sumdum		
1610	132°	2.65
1707	131°	2.47
1806	135°	2.28
1911	146°	2.08
2014	145°	1.93
2113	146°	1.78
2218	147°	1.65

Drogue 3a Surface

Time	Azimuth	Distance
Azimuth based on east end of Sumdum		
1620	127°	2.64
1710	126°	2.40
1809	125°	2.11
1915	127°	1.79
2019	127°	1.50
2119	129°	1.27
2229	132°	1.13

Drogue 4a Surface

Time	Azimuth	Distance
Azimuth based on east end of Sumdum		
1628	119°	2.34
1714	118°	2.62
1813	118°	2.50
1920	118°	2.31
2025	117°	2.11
2126	117°	1.94
2241	117°	1.70

25 and 26 February 1969

Drogue 5 (10m.)

Time	Azimuth	Distance
Azimuths based on Tide Gauge Point		
1717	75°	1.37
1835	75°	1.36
2019	80°	1.25
2104	71°	1.20
2217	64°	1.10
2340	59°	0.94
0051	45°	0.83
Azimuths based on east end of Sumdum		
0158	128°	2.51
0333	143°	2.08
0940	170°	0.85
1050	183°	0.79
1154	199°	0.71
1245	210°	0.72
1345	216°	0.60
1506	237°	0.66

Drogue 6 (10m.)

Time	Azimuth	Distance
Azimuths based on Tide Gauge Point		
1736	105°	0.83
1846	97°	0.85
1936	95°	0.82
2007	94°	0.78
2040	88°	0.78
2146	77°	0.69
2305	62°	0.55
0014	38°	0.49
0129	14°	0.53
Azimuths based on east end of Sumdum		
0250	137°	2.39
0349	140°	2.26
0521	143°	2.05
0645	146°	1.84
0901	154°	1.50
1006	153°	1.34
1112	174°	1.16
1211	185°	1.03
1312	199°	0.92
1406	220°	0.86

B.2 Drogue Speed Data

The drogue speed data were calculated from the position data. They are listed as time and speed to that time in cm/sec. The speed data for 19 November 1966 was not listed for the positions were dubious and speeds excessively high.

The speeds from 19 November 1966 to 5 May 1967 were calculated as position to position velocities while those for 1968 and 1969 were listed as longitudinal velocities based on a 128° Azimuth.

Current Speeds

20 November 1966

Drogue 3

Time	Speed cm/sec
1050	16.4
1125	6.2
1410	34.2
1538	17.4
1612	31.1
1715	6.2

Drogue 4

Time	Speed cm/sec
1400	4.2
1531	8.5
1604	18.7
1722	14.3

Drogue 5

Time	Speed cm/sec
1420	11.0
1550	2.7
1624	40.3
1730	21.0

21 November 1966

Drogue 3

Time	Speed cm/sec
1005	6.9
Drogue 3 Reset	
1330	38.6
Drogue 5	
0945	9.1
1040	33.1
1205	31.9
1400	72.9

Drogue 6

Time	Speed cm/sec
1110	2.0
1150	26.9
1325	19.1
1430	11.7

6 March 1967

	Drogue 1	Surface
Time	Veloc. Kn.	Vol. cm/sec
1445	0.13	6.5
1510	0.16	8.2
1630	0.27	13.5

	Drogue 2	Surface
1028	0.14	7.2
1130	0.22	11.3
1200	0.14	7.2
1255	0.38	19.6
1320	0.64	33.0
1350	0.18	9.3
1415	0.28	14.7

	Drogue 3	50 m.
1120	0.35	17.6
1145	0.17	9.0
1205	0.30	15.6
1305	0.11	5.6
1330	0.36	18.4
1400	0.70	36.0

	Drogue 4	Surface
Time	Veloc. Kn.	Vol. cm/sec
1020	2.00?	103?
1123	0.16	8.5
1150	0.25	12.9
1215	0.48	24.4
1250	0.17	9.2
1310	0.45	23.2
1336	0.35	17.8
1405	0.34	17.5
1500	0.72	37.0
1555	1.94	99.7

5 May 1967

Drogue 1

Time	Vel (cm/sec)
1250	13.6
1445	24.5
1545	12.9

Drogue 4

Time	Vel (cm/sec)
1235	30.2
1330	14.0
1420	32.2

Drogue 2

Time	Vel (cm/sec)
1325	8.4
1437	21.3
1530	28.2

Drogue 5

Time	Vel (cm/sec)
1240	27.4
1333	26.8
1500	37.0

Drogue 3

Time	Vel (cm/sec)
1330	8.2
1430	19.0
1525	34.1
1555	43.2

Longitudinal Velocities (cm/sec)

30 and 31 March 1968

Drogue 1 Surf		Drogue 2 Surf		Drogue 3 (10 m.)		Drogue 4 (10 m.)	
Time	Vel.	Time	Vel.	Time	Vel.	Time	Vel.
1335	10.4	1350	-2.6	1350	-2.6	1349	-7.2
1431	0.5	1443	-2.6	1439	1.5	1437	-6.7
1536	-1.0	1533	-0.5	1542	-4.6	1531	-3.6
1617	3.7	1614	1.5	1602	-1.5	1604	-4.6
1641	3.8	1638	5.1	1633	0	1631	-4.6
1704	13.4	1712	10.8	1707	4.6	1704	+0.0
1752	7.1	1750	10.8	1744	1.5	1740	+0.0
1805	7.1	1807	7.2	1812	2.1	1814	2.5
1833	10.3	1835	2.1	1840	4.6	1842	3.1
1858	14.8	1900	22.1	1904	2.6	1907	6.2
1943	--	1924	15.4	1951	8.8	1954	9.3
2011	--	2003	15.9	2017	7.2	2020	4.6
2035	--	2034	9.8	2043	6.2	2101	3.1
2135	8.7	2125	10.8	2137	6.2	2143	5.7
2233	2.7	2231	2.6	2239	7.2	2245	4.1
2337	-0.5	2335	-0.5	2345	4.1	2352	0.0
0036	8.9	0033	-6.7	0043	1.0	0050	2.0
0137	-9.1	0133	-6.7	0145	-5.1	0220	6.7
0247	0.4	0239	3.1	0255	-1.5	0303	1.5
0345	6.0	0339	14.4	0359	1.0	0406	1.5
0450	7.6	0442	14.9	0503	4.6	0620	3.1

Longitudinal Velocities (cm/sec)

30 and 31 March (continued)

Drogue 1 Surf		Drogue 2 Surf		Drogue 3(10 m)		Drogue 4(10 m)	
Time	Vel.	Time	Vel.	Time	Vel.	Time	Vel.
0602	12.4	0504	12.9	0614	4.1	0712	4.1
0657	15.4	0651	14.9	0706	8.3	0819	7.7
0802	4.6	0753	15.4	0813	5.7	0902	3.1
0919	10.3	0925	16.5	0907	5.1	1025	7.7
1047	3.6	1053	7.2	1034	17.5	1126	4.6
1146	4.6	1151	6.2	1132	2.6	1230	1.0
1255	5.1	1302	0.0	1238	2.1	1344	5.7
1408	8.2	1413	6.7	1351	5.7	1453	4.1
1521	16.5	1525	15.4	1459	2.1	1607	1.0
1633	22.1	1636	12.4	1613	1.0	1725	0.0
1849	15.4	1854	15.4	1740	4.1		

Longitudinal Velocities

10 and 11 July 1968

Drogue 2 Surf		Drogue 3 (10 m)		Drogue 4 Surf	
Time	Vel.	Time	Vel.	Time	Vel.
1550	8.8	1410	2.6	1640	5.1
1657	17.0	1545	12.5	1731	14.9
1758	23.2	1648	8.2	1857	13.9
1900	15.9	1745	14.9	2025	5.1
2052	-12.4	1851	22.6	2108	-11.3
2157	-20.6	2035	7.2	2157	-10.3
0908	5.7	2205	-12.8	0920	5.7
1025	6.6	0755	1.0	1013	5.7
1123	5.1	0852	7.2	1100	6.7
1259	8.7	1043	-14.9	1247	7.2
1330	11.8	1146	-16.0	1338	16.5
1527	27.8	1227	-14.4		
		1411	-3.1		
		1457	4.1		

Longitudinal Velocities

8 and 9 July 1968

Drogue 1 Surface

Time	Vel
1553	16.0
1658	28.8
1834	21.1
1948	9.8
1215	20.0

Drogue 1 New Surface

1325	
2105	14.9

Drogue 2 Surface

1602	15.5
1701	32.4
1834	21.1
1955	8.7
1124	9.3
1450	8.7

Drogue 3 10 M.

No Speeds Calculated

Drogue 4 Surface

1814	21.1
2032	-2.0
1046	10.8
1425	25.2
1945	12.3

Drogue 5 Surface

2019	12.9
2048	-3.1

Surface Longitudinal Velocities

25 and 26 February 1969

Drogue 1 Time	Vel cm/sec	Drogue 2 Time	Vel cm/sec	Drogue 3 Time	Vel cm/sec	Drogue 4 Time	Vel cm/sec
1739	3.6	1726	12.4	1722	5.6	1833	16.5
1848	2.5	1957	11.0	1840	8.6	1927	-5.0
1943	3.2	2046	11.1	2000	13.7	2025	9.1
2036	2.9	2203	11.9	2052	13.7	2134	8.9
2141	9.0	2318	14.4	2159	14.4	2255	11.4
2306	13.2	0029	12.2	2323	14.1	0005	14.6
0017	14.4	0141	17.1	0033	16.3	0121	13.6
0133	12.5	0605	12.4	0144	15.6	0242	18.0
0254	12.2	0706	12.2	0306	22.6	0415	14.2
0407	12.9	0921	14.0	0425	13.6	0533	15.3
0526	14.4	1026	16.9	0545	9.4	0725	7.3
0620	14.3	1127	12.7	0712	11.3	0933	8.7
0657	14.8	1225	18.7	0925	17.2	1042	14.9
0912	14.4	1322	11.2	1034	9.9	1145	25.8
1017	19.5	1430	25.0	1131	16.8	1241	17.2
1121	17.5			1228	20.6	1335	22.8
1221	17.0			1325	13.7	1449	18.5
1318	23.4			1437	14.9		
1412	13.2						

Surface and Longitudinal Velocities

25 and 26 February 1969

Drogue 1a		Drogue 2a		Drogue 3a		Drogue 4a	
Time	Vel cm/sec	Time	Vel cm/sec	Time	Vel cm/sec	Time	Vel cm/sec
1703	-1.0	1707	9.3	1710	11.3	1714	10.3
1701	-0.5	1806	11.3	1809	15.4	1813	6.2
1905	-1.0	1911	12.3	1915	14.4	1920	8.7
2005	0.0	2014	7.2	2019	15.4	2025	9.8
2104	0.0	2113	8.2	2119	11.3	2126	9.3
2202	3.1	2218	4.6	2229	5.5	2241	9.8

10 Meter Longitudinal Speeds (cm/sec)

25 and 26 February 1969

Drogue 5		Drogue 6	
1835	0.3	1846	2.3
2019	-0.3	1936	2.1
2104	10.5	2007	4.4
2217	8.3	2040	3.0
2340	5.2	2146	7.8
0051	9.7	2305	8.1
0159	16.0	0014	9.8
0353	16.5	0129	8.8
0940	13.0	0250	13.8
1050	8.4	0349	7.4
1154	9.7	0521	7.9
1245	7.8	0645	8.1
1345	3.4	0901	9.1
1506	9.8	1006	6.6
		1112	18.5
		1211	14.3
		1312	11.8
		1406	17.5

Appendix C

Iceberg Position Data

C.1 Photographic Distances

The iceberg position data is listed as photographic distances and real distances. The photographic distances are the distances from the center of the photograph to the landmark and to the iceberg (D_l and D_b respectively). Further, the distance of the iceberg below the horizon is tabulated. These distances permit calculation of the position of the iceberg as described in the thesis.

Photo Distances

10 July 1968

Iceberg 1 Iceberg 2

D_b and D_1 calculated from center of photograph

Time	D_1	D_b	D_{bh}	D_1	D_b	D_{bh}
1525	29.8	-13.5	2.45	29.8	-27.5	1.34
1535	29.8	-12.44	2.30	29.8	-25.36	1.27
1545	29.8	-10.09	2.25	29.8	-22.76	1.08
1555	29.8	- 8.34	1.96	29.8	-20.98	0.90
1605	29.8	- 5.49	1.76	29.8	-18.88	0.75
1615	29.8	- 3.74	1.73	29.8	-17.43	0.79
1625	29.8	- 2.37	1.70	29.8	-15.71	0.83
1635	29.8	- 0.71	1.61	29.8	-14.33	0.67
1645	29.8	1.22	1.56	29.8	-13.22	0.64
1655	29.8	2.94	1.44	29.8	-12.42	0.48
1705	29.8	4.04	1.39	29.8	-11.85	0.44
1715	29.8	5.03	1.33	29.8	-10.93	0.37
1725	29.8	5.88	1.28	29.8	-10.20	0.28

Photo Distances

10 July 1968

D_b and D_1 calculated from center of photograph

	Iceberg 3			Iceberg 4		
Time	D_1	D_b	D_{bh}	D_1	D_b	D_{bh}
1525	29.8	-20.4	0.93	29.8	-25.1	1.59
1535	29.8	-19.03	0.87	29.8	-22.73	1.53
1545	29.8	-18.03	0.85	29.8	-19.94	1.40
1555	29.8	-16.53	0.80	29.8	-17.89	1.26
1605	29.8	-15.55	0.70	29.8	-15.07	1.18
1615	29.8	-14.44	0.60	29.8	-13.57	1.15
1625	29.8	-13.42	0.65	29.8	-11.89	1.10
1635	29.8	-12.12	0.60	29.8	- 9.98	0.95
1645	29.8	-10.66	0.55	29.8	- 8.10	0.80
1655	29.8	- 9.21	0.45	29.8	- 6.45	0.70
1705	29.8	- 8.01	0.57	29.8	- 5.07	0.67
1715	29.8	- 6.55	0.52	29.8	- 4.03	0.67
1725	29.8	- 5.40	0.55	29.8	- 3.38	0.62

Photo Distances

10 July 1968

D_b and D_1 calculated from center of photograph

	Iceberg 5			Iceberg 6		
Time	D_1	D_b	D_{bh}	D_1	D_b	D_{bh}
1525	29.8	- 9.8	9.32	29.8	- 9.6	14.7
1535	29.8	- 1.98	8.24	29.8	4.93	12.40
1545				29.8	15.23	11.00
1555	29.8	8.22	6.82	29.8	19.25	10.00
1605	29.8	14.66	5.92	29.8	25.77	8.93
1615	29.8	19.85	5.41	29.8	30.81	8.38
1625	29.8	22.65	5.18	29.8	36.41	7.53
1635	29.8	25.70	5.02	29.8	41.65	6.84
1645	29.8	30.33	4.82	29.8	46.65	6.33
1655	29.8	34.00	4.47	29.8	51.90	5.68
1705	29.8	34.86	4.22	29.8	54.85	5.34
1715	29.8	35.46	4.00	29.8	56.90	4.99
1725				29.8	56.75	4.66

Photo Distances

24 August 1968

Measured from side of photographs

	Iceberg 3			Iceberg 4		
Time	Side to Land-mark	Side to Ice-berg	D_{bh}	Side to Land-mark	Side to Ice-berg	D_{bh}
1633	18.3	43.0	0.1	18.3	36.3	0.2
1645	18.4	43.3	0.1	18.4	38.0	0.1
1700	18.7	43.8	0.1	18.7	38.7	0.2
1715	18.5	44.1	0.05	18.5	39.0	0.2
1730	18.6	44.8	0.1	18.6	39.1	0.2
1745	19.0	46.1	0.1	19.0	40.1	0.15
1800	18.9	46.4	0.05	18.9	40.7	0.2
1815	19.0	46.7	0.1	19.0	40.8	0.2
1832	19.0	46.3	0.1	19.0	38.7	0.2
1845	18.6	46.2	0.1	18.6	38.2	0.1
1900	18.5	45.5	0.1	18.5	37.6	0.1
1916	18.7	45.4	0.1	18.7	37.9	0.1
1937	18.6	44.6	0.1	18.6	37.5	0.1
1945	18.5	--	--	18.5	37.1	0.1
2000	18.4	44.5	0.1	18.4	37.1	0.05

Photo Distances

24 August 1968

Measured from side of photographs

	Iceberg 5			Iceberg 6		
Time	Side to Land-mark	Side to Ice-berg	D_{bh}	Side to Land-mark	Side to Ice-berg	D_{bh}
1633	18.3	33.2	2.5	18.3	19.4	0.8
1645	18.4	30.4	2.2	18.4	19.2	0.8
1700	18.7	28.1	2.0	18.7	19.9	0.8
1715	18.5	25.7	1.7	18.5	19.9	0.7
1730	18.6	24.7	1.7	18.6	20.4	0.8
1745	19.0	25.5	1.7	19.0	21.1	0.8
1800	18.9	26.2	1.8	18.9	20.9	0.8
1815	19.0	27.3	1.9	19.0	20.1	0.8
1832	19.0	27.9	2.0	19.0	20.9	0.8
1845	18.6	28.2	2.3	18.6	20.5	1.0
1900	18.5	29.1	2.6	18.5	20.2	1.0
1916	18.7	30.3	2.9	18.7	20.2	1.0
1937	18.6	31.7	3.0	18.6	20.2	1.0
1945	18.5	32.3	3.2	18.5	20.1	1.0
2000	18.4	33.2	3.4	18.4	20.1	1.0

Photo Distances

24 August 1968

Measured from side of photographs

	Iceberg 7			Iceberg 8		
Time	Side to Land-mark	Side to Ice-berg	D_{bh}	Side to Land-mark	Side to Ice-berg	D_{bh}
1633	18.3	26.3	0.4	18.3	18.6	0.7
1645	18.4	26.2	0.4	18.4	18.7	0.7
1700	18.7	26.9	0.4	18.7	19.5	0.7
1715	18.5	27.4	0.4	18.5	19.8	0.6
1730	18.6	27.8	0.3	18.6	20.2	0.7
1745	19.0	28.9	0.3	19.0	20.2	0.75
1800	18.9	29.3	0.3	18.9	20.1	0.8
1815	19.0	29.6	0.4	19.0	19.7	0.8
1832	19.0	29.6	0.4	19.0	19.1	0.8
1845	18.6	30.6	0.4	18.6	18.4	0.9
1900				18.5	18.2	0.9
1916				18.7	19.0	0.9
1937				18.6	19.2	0.9
1945				18.5	19.2	0.9
2000				18.4	19.2	0.85

Photo Distances

25 August 1968

Measured from side of photographs

	Iceberg 1			Iceberg 2		
Time	Side to Land-mark	Side to Ice-berg	D_{bh}	Side to Land-mark	Side to Ice-berg	D_{bh}
0835	18.8			18.8	22.9	0.05
0845	18.8			18.8	22.7	0.05
0900	18.7			18.7	22.7	0.05
0915	18.6			18.6	22.7	0.05
0930	18.7			18.7	22.6	0.05
0945	18.7	32.9	0.45	18.7	22.5	0.05
1000	18.7	31.3	0.50	18.7	22.6	0.10
1015	18.7	29.7	0.40	18.7	22.7	0.10
1030	18.7	28.4	0.30	18.7	22.7	0.10
1045	18.7	27.5	0.30	18.7	22.7	0.10
1100	18.6	26.7	0.30	18.6	22.6	0.10
1115	18.7	25.8	0.30	18.7	22.7	0.10
1130	18.6	24.9	0.30	18.6	22.6	0.10
1145	18.6	24.0	0.30	18.6	22.5	0.10
1202	18.4	23.1	0.35	18.4	22.4	0.10
1215	18.0	21.9	0.35	18.0	22.0	0.10
1230	18.0	20.9	0.30	18.0	21.9	0.10
1246	17.9	18.8	0.30	17.9	21.8	0.10

1300	17.5	18.2	0.30	17.5	22.0	0.10
1315	18.4	17.7	0.40	18.4	22.2	0.10
1330	18.3	15.8	0.40	18.3	22.0	0.10
1345	18.2	13.8	0.35	18.2	22.0	0.10
1400	18.3	12.2	0.40	18.3	22.1	0.10

Photo Distances

25 August 1968

Measured from side of photographs

	Iceberg 3			Iceberg 4		
Time	Side to Land-mark	Side to Ice-berg	D_{bh}	Side to Land-mark	Side to Ice-berg	D_{bh}
0835	18.8	33.0	0.20	18.8	40.4	1.00
0845	18.8	32.0	0.20	18.8	39.1	0.95
0900	18.7	30.6	0.15	18.7	37.4	0.90
0915	18.6	29.8	0.15	18.6	35.8	0.85
0930	18.7	29.0	0.15	18.7	34.0	0.85
0945	18.7	28.3	0.10	18.7	32.2	0.85
1000	18.7	28.0	0.10	18.7	31.2	0.90
1015	18.7	27.4	0.10	18.7	30.5	0.80
1030	18.7	27.0	0.10	18.7	30.0	0.80
1045	18.7	26.8	0.10	18.7	29.3	0.80
1100	18.6	26.3	0.10	18.6	28.6	0.80
1115	18.7	25.7	0.10	18.7	28.2	0.80
1130	18.6	25.2	0.05	18.6	27.7	0.80
1145	18.6	24.4	0.05	18.6	27.1	0.70
1202	18.4	23.5	0.05	18.4	26.5	0.65
1215	18.0	22.7	0.05	18.0	25.8	0.65
1230	18.0	22.6	0.05	18.0	25.1	0.65
1246	17.9	22.7	0.05	17.9	24.1	0.65

1300	17.5	22.2	0.05	17.5	23.1	0.60
1315	18.4	23.2	0.05	18.4	23.5	0.55
1330	18.3	23.2	0.05	18.3	22.7	0.50
1345	18.2	23.2	0.05	18.2	22.1	0.50
1400	18.3	23.2	0.05	18.3	21.2	0.50

Photo Distances

25 August 1968

Measured from side of photographs

Iceberg 5

Time	Side to Landmark	Side to Iceberg	D_{bh}
0835	18.8	19.4	0.30
0845	18.8	19.0	0.25
0900	18.7	18.3	0.20
0915	18.6	17.8	0.20
0930	18.7	17.3	0.20

Photo Distances

6 March 1969

Iceberg 1 / Iceberg 2

Time	Iceberg 1: Side to Landmark	Iceberg 1: Side to Iceberg	Iceberg 1: D_{bh}	Iceberg 2: Side to Landmark	Iceberg 2: Side to Iceberg	Iceberg 2: D_{bh}
0945	13.1	2.5	4.3	13.1	13.5	18.5
1000	11.3	5.7	3.4	11.3	14.0	9.8
1015	12.3	8.7	4.5	12.3	21.5	7.8
1030	14.0			14.0	26.1	7.0
1045	11.7			11.7	29.7	6.1
1100	11.5			11.5	33.1	5.4
1115	15.3			15.3		
1130	15.3			15.3		

Iceberg 3

Time	Side to Landmark	Side to Iceberg	D_{bh}
1015	12.3	13.1	3.6
1030	14.0	26.1	3.0
1045	11.7	30.6	2.7
1100	11.5	32.1	2.6
1115	15.3	36.8	2.4

Photo Distances

6 March 1969

	Iceberg 4			Iceberg 5		
Time	Side to Landmark	Side to Iceberg	D_{bh}	Side to Landmark	Side to Iceberg	D_{bh}
0945	13.1			13.1	19.2	0.30
1000	11.3			11.3	17.3	0.30
1015	12.3			12.3	18.4	0.29
1030	14.0			14.0	20.2	0.25
1045	11.7			11.7	17.9	0.25
1100	11.5	13.6	0.6	11.5	17.3	0.24
1115	15.3	19.4	0.6	15.3	20.7	0.24
1130	15.3	22.1	0.6	15.3	20.5	0.23
1145	15.4	24.4	0.55	15.4	20.3	0.23
1200	13.8	24.8	0.5	13.8	18.8	0.22
1215	13.1	26.2	0.45	13.1	17.8	0.22
1230	13.0	28.1	0.4	13.0	17.7	0.21
1245	13.0	29.3	0.4	13.0	17.5	0.20
1300	12.4	30.0	0.35	12.4	16.9	0.20

Photo Distances

6 March 1969

Iceberg 6

Time	Side to Land-mark	Side to Ice-berg	D_{bh}
1130	15.3	15.6	0.75
1145	15.4	17.1	0.78
1200	13.8	17.0	0.69
1215	13.1	17.8	0.68
1230	13.0	20.0	0.64
1245	13.0	21.9	0.62
1300	12.4	23.1	0.62

C.2 Iceberg Positions

The iceberg positions, calculated from the picture distances, are presented as angle at the camera from the landmark to the iceberg and distances from the camera to the iceberg. The angles are in degrees and minutes, the distances in nautical miles.

Iceberg Positions

10 July 1968

	Iceberg 1		Iceberg 2	
Time	**Angle**	**Distance Nautical Mi.**	**Angle**	**Distance Nautical Mi.**
1525	19°26'	1.28	25°39'	1.67
1535	18°58'	1.33	24°42'	1.73
1545	17°54'	1.36	23°34'	1.88
1555	17°06'	1.48	22°47'	2.05
1605	15°49'	1.58	21°51'	2.19
1615	15°01'	1.59	21°12'	2.16
1625	14°24'	1.61	20°26'	2.13
1635	13°38'	1.65	19°49'	2.29
1645	12°46'	1.68	19°19'	2.33
1655	11°59'	1.76	18°57'	2.51
1705	11°29'	1.80	18°42'	2.56
1715	11°02'	1.85	18°17'	2.67
1725	10°38'	1.88	17°57'	2.80

Iceberg Positions

10 July 1968

	Iceberg 3		Iceberg 4	
Time	Angle	Distance Nautical Mi.	Angle	Distance Nautical Mi.
1525	22°24'	2.04	24°26'	1.57
1535	21°48'	2.09	23°25'	1.64
1545	21°21'	2.11	22°11'	1.72
1555	20°43'	2.16	21°17'	1.81
1605	20°16'	2.26	20°03'	1.87
1615	19°46'	2.37	19°23'	1.90
1625	19°19'	2.32	18°38'	1.94
1635	18°41'	2.39	17°48'	2.07
1645	18°05'	2.46	16°58'	2.21
1655	17°26'	2.59	16°13'	2.31
1705	16°54'	2.46	15°36'	2.37
1715	16°15'	2.53	15°07'	2.39
1725	15°44'	2.50	14°50'	2.46

Iceberg Positions

10 July 1968

	Iceberg 5		Iceberg 6	
Time	Angle	Distance Nautical Mi.	Angle	Distance Nautical Mi.
1525	17°43'	0.48	17°37'	0.32
1535	14°12'	0.54	11°06'	0.38
1545			6°31'	0.42
1555	9°38'	0.63	4°45'	0.46
1605	6°46'	0.72	1°54'	0.51
1615	4°29'	0.77	0°15'	0.54
1625	3°16'	0.80	*-2°36'	0.62
1635	1°56'	0.82	-4°45'	0.69
1645	*-0°03'	0.86	-6°45'	0.79
1655	-1°36'	0.97	-8°48'	0.88
1705	-1°57'	1.02	-9°56'	0.93
1715	-2°12'	1.07	-10°42'	1.00
1725			-10°39'	1.06

*Negative angles indicate positions to the left of the landmark.

Iceberg Positions

24 August 1968

	Iceberg 3		Iceberg 4	
Time	X Nautical Mi.	Y Nautical Mi.	X Nautical Mi.	Y Nautical Mi.
1633	2.61	1.72	2.55	1.39
1646	2.57	1.70	2.76	1.57
1700	2.57	1.71	2.51	1.44
1715	2.75	1.80	2.50	1.46
1730	2.54	1.74	2.50	1.46
1745	2.52	1.76	2.30	1.37
1800	2.64	1.86	2.11	1.49
1815	2.49	1.77	2.34	1.28
1832	2.47	1.78	2.59	1.40
1845	2.49	1.76	2.76	1.57
1900	2.52	1.76	2.79	1.56
1916	2.53	1.75	2.77	1.56
1937	2.55	1.73	2.55	1.73
1945	2.55	1.75	2.80	1.55
2000	2.55	1.74	2.94	1.63

Iceberg Positions

24 August 1968

	Iceberg 5		Iceberg 6	
Time	X Nautical Mi.	Y Nautical Mi.	X Nautical Mi.	Y Nautical Mi.
1633	0.85	0.42	2.09	0.60
1646	0.96	0.43	2.24	0.65
1700	1.04	0.42	2.09	0.62
1715	1.04	0.42	2.02	0.59
1730	0.85	0.32	1.96	0.57
1745	1.19	0.43	1.96	0.56
1800	1.19	0.44	1.96	0.54
1815	1.14	0.43	1.85	0.50
1832	1.08	0.43	1.85	0.50
1845	2.82?	1.13?	1.85	0.51
1900	0.95	0.39	1.84	0.52
1916	0.87	0.37	1.84	0.52
1937	0.78	0.35	1.90	0.54
1945	0.75	0.35		
2000	0.71	0.34		

Iceberg Positions

24 August 1968

	Iceberg 7		Iceberg 8	
Time	X Nautical Mi.	Y Nautical Mi.	X Nautical Mi.	Y Nautical Mi.
1633	2.42	0.94	3.09	1.12
1646	2.63	1.01	3.09	1.13
1700	2.48	0.97	3.04	1.14
1715	2.37	0.95	2.88	1.11
1730	2.57	1.04	2.97	1.18
1745	2.95	1.23	2.95	1.20
1800	2.67	1.13	2.95	1.21
1815	2.45	1.04	3.11	1.27
1832	2.45	1.04	2.95	1.21
1845	2.36	1.06	3.11	1.27

Iceberg Positions

25 August 1968

	Iceberg 1		Iceberg 2	
Time	X Nautical Mi.	Y Nautical Mi.	X Nautical Mi.	Y Nautical Mi.
0835			3.59	1.19
0845			3.59	1.18
0900			3.59	1.18
0915			3.59	1.19
0930			3.59	1.18
0945	2.18	1.05	3.60	1.18
1000	2.14	0.98	3.39	1.11
1015	2.38	1.03	3.39	1.12
1030	2.68	1.11	3.39	1.12
1045	2.58	1.03	3.39	1.12
1100	2.63	1.02	3.39	1.12
1115	2.64	0.99	3.39	1.12
1130	2.68	0.97	3.39	1.12
1145	2.68	0.96	3.39	1.11
1202	2.60	0.88	3.39	1.12
1215	2.65	0.87	3.39	1.12
1230	2.79	0.88	3.39	1.11
1246	2.86	0.86	3.39	1.11
1300	2.87	0.82	3.40	1.11

Iceberg Positions

25 August 1968

	Iceberg 3		Iceberg 4	
Time	X Nautical Mi.	Y Nautical Mi.	X Nautical Mi.	Y Nautical Mi.
0835	2.70	1.30	1.45	0.87
0845	2.74	1.28	1.49	0.87
0900	2.97	1.32	1.55	0.86
0915	2.98	1.30	1.63	0.86
0930	3.10	1.31	1.66	0.83
0945	3.28	1.35	1.69	0.80
1000	3.11	1.27	1.65	0.75
1015	3.12	1.24	1.64	0.73
1030	3.11	1.26	1.91	0.84
1045	3.19	1.24	1.84	0.78
1100	3.19	1.22	1.84	0.77
1115	3.21	1.20	1.79	0.73
1130	3.44	1.26	1.80	0.73
1145	3.46	1.23	1.92	0.76
1202	3.50	1.21	2.01	0.78
1215	3.51	1.19	2.01	0.77
1230	3.51	1.19	2.02	0.76
1246	3.50	1.20	2.04	0.74
1300			2.12	0.75
1315			2.22	0.77
1330			2.31	0.77
1345			2.35	0.77
1400			2.36	0.74

Iceberg Positions

6 March 1969

	Iceberg 1		Iceberg 2	
Time	Angle	Distance	Angle	Distance
0945	-6°19'	0.20	1°17'	0.04
1000	-2°33'	0.25	3°15'	0.10
1015	-3°02'	0.33	5°37'	0.12
1030			10°09'	0.13
1045			14°32'	0.15
1100			16°40'	0.17

	Iceberg 3		Iceberg 4	
1015	-0°05'	0.24		
1030	10°17'	0.30		
1045	15°12'	0.33		
1100	15°56'	0.35	2°28'	1.13
1115	17°11'	0.38	4°27'	1.12
1130			6°21'	1.15
1145			8°02'	1.23
1200			9°03'	1.34
1215			11°04'	1.46
1230			12°23'	1.60
1245			13°24'	1.69
1300			14°24'	1.85

Iceberg Positions .

6 March 1969

	Iceberg 5		Iceberg 6	
Time	Angle	Distance	Angle	Distance
0945	4°33'	1.60		
1000	4°17'	1.72		
1015	4°23'	1.75		
1030	4°28'	1.89		
1045	4°26'	1.96		
1100	4°09'	1.96		
1115	3°54'	1.93		
1130	3°45'	2.05	0°13'	0.91
1145	3°32'	2.19	1°13'	0.89
1200	3°36'	2.19	2°18'	0.97
1215	3°23'	2.24	3°23'	0.99
1230	3°22'	2.24	5°02'	1.08
1245	3°14'	2.19?	6°26'	1.12
1300	3°13'	2.35	7°43'	1.13

APPENDIX D

```
      DIMENSION OS(48)
    1 FORMAT(2F5.2,2F5.4,3I5)
    2 FORMAT(3F5.2)
    3 FORMAT(20X,12F5.2)
    4 FORMAT(2F10.2)
    5 FORMAT(F10.2)
    6 FORMAT(F10.5)
    7 FORMAT(2X,2HX=,F5.2,2X,2HY=,F5.2)
      READ(1,1)F,FO,BETA,HI,NO,IFORE,SIDE
      DO 10 I=1,NO,12
   10 READ(1,3)OS(I),OS(I+1),OS(I+2),OS(I+3),OS(I+4),OS(I+5),OS(I+6),OS(
     1I+7),OS(I+8),OS(I+9),OS(I+10),OS(I+11)
      READ(1,2)DL,DB,DDB
   70 FO2=FO/2.
      DB=10.*DB
      DL=10.*DL
C DISTANCE FROM CENTER OF PHOTOGRAPH
      DISTB=DB-FO2
      DISTL=DL-FO2
C ANGLE BETWEEN BERG AND LANDMARK
      ALPHA=ATAN(DISTB/F)-ATAN(DISTL/F)
      BEFORE=IFORE
      TEST=(-0.01745)*BEFORE
C FINDING OPPOSITE SHORE DISTANCE AND CONV. TO NAUT. MI.
      DO 20 J=1,NO
      IF(ALPHA-TEST)21,30,22
   30 I=J
      OPPOS=OS(I)
      GO TO 40
   21 TEST=TEST-0.01745
      GO TO 220
   22 TEST=TEST+0.01745
  220 IF(ABS(ALPHA-TEST)-.01745)30,30,20
   20 CONTINUE
C FINDING DEPRESSION OF APPARENT HORIZON AND DISTANCE TO BERG
   40 AH=F*HI/OPPOS
      DA=HI*F/(AH+DDB)
C CALCULATE X AND Y
      X=DA*COS(-BETA-ALPHA)
      SC=1
      IF (SIDE)60,60,50
   50 SC=-1
   60 Y=SC*DA*SIN(-BETA-ALPHA)
      WRITE(3,5)DA
      WRITE(3,7)X,Y
      READ(1,2)DL,DB,DDB
      IF(DL-999.99)70,80,80
   80 CALL EXIT
      END
```

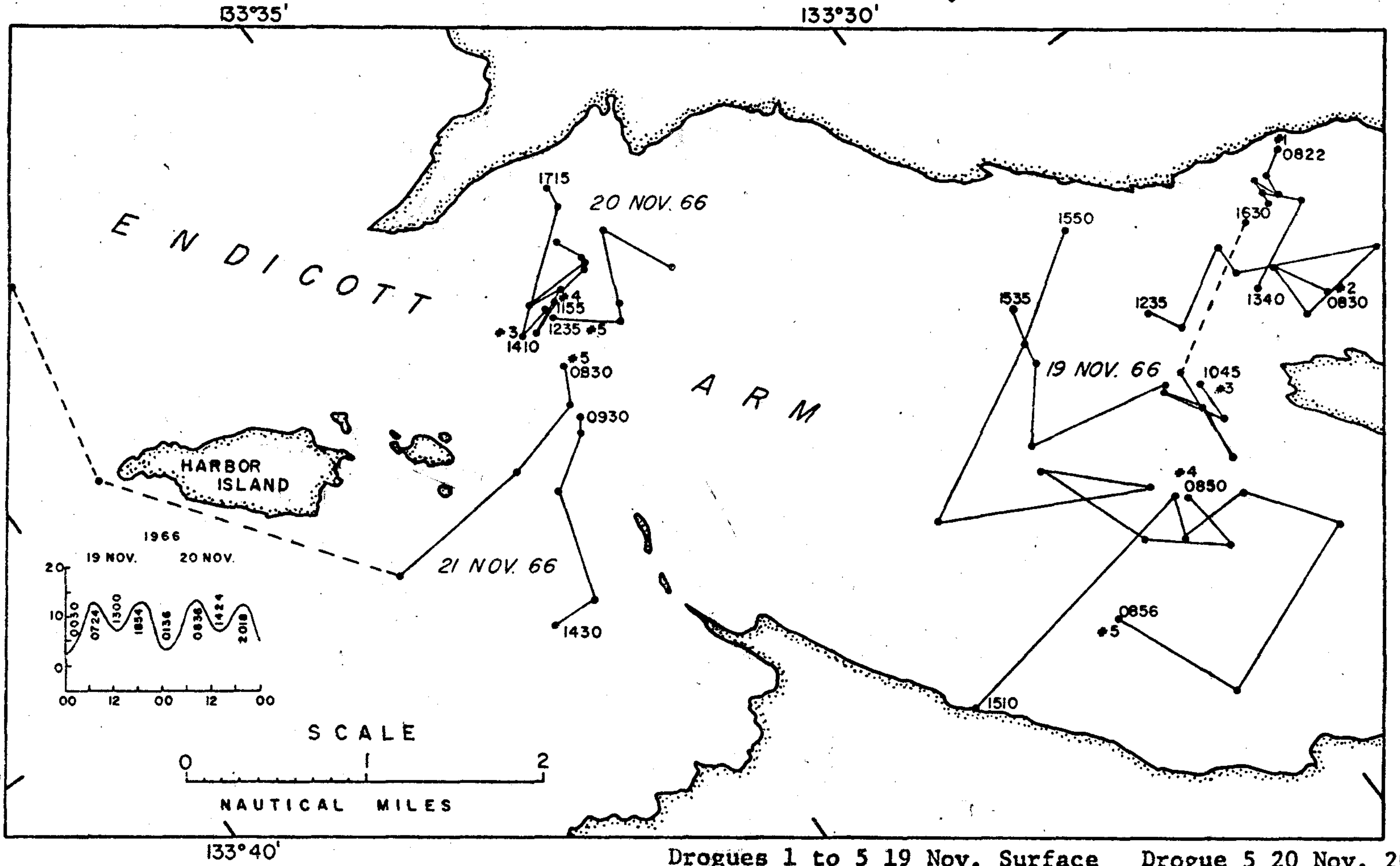

Figure El Drogue Drift Plot
19 to 21 November 1966

Drogues 1 to 5 19 Nov. Surface
Drogue 3 20 Nov. 20 m
Drogue 4 20 Nov. 10 m
Drogue 5 20 Nov. 20 m
Drogue 5 21 Nov. 20 m
Drogue 6 21 Nov. 40 m

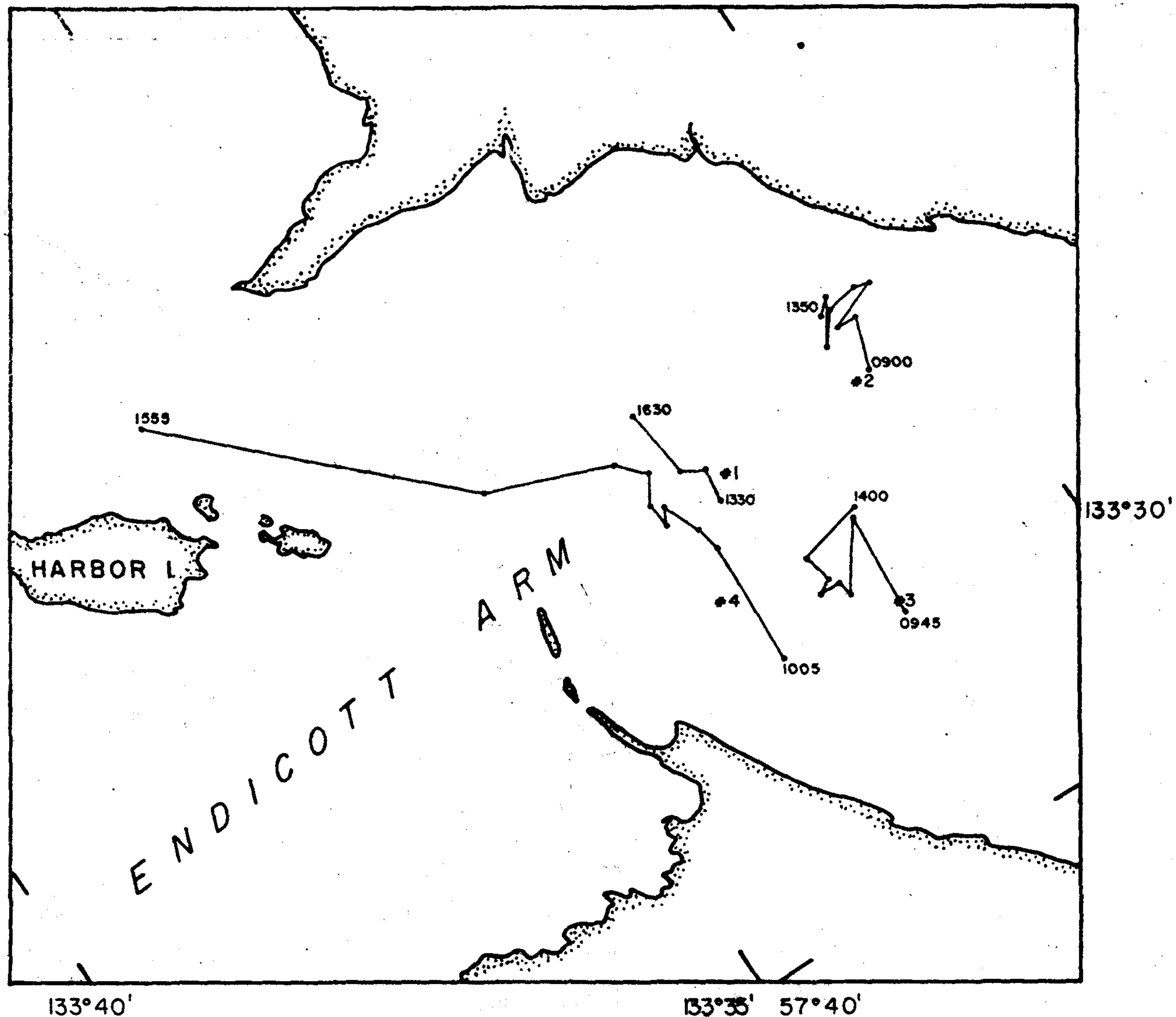

Figure E2. Drogue Drift Plot 6 March 1967 Drogues 1, 2 and 4 Surface Drogue 3 50 m.

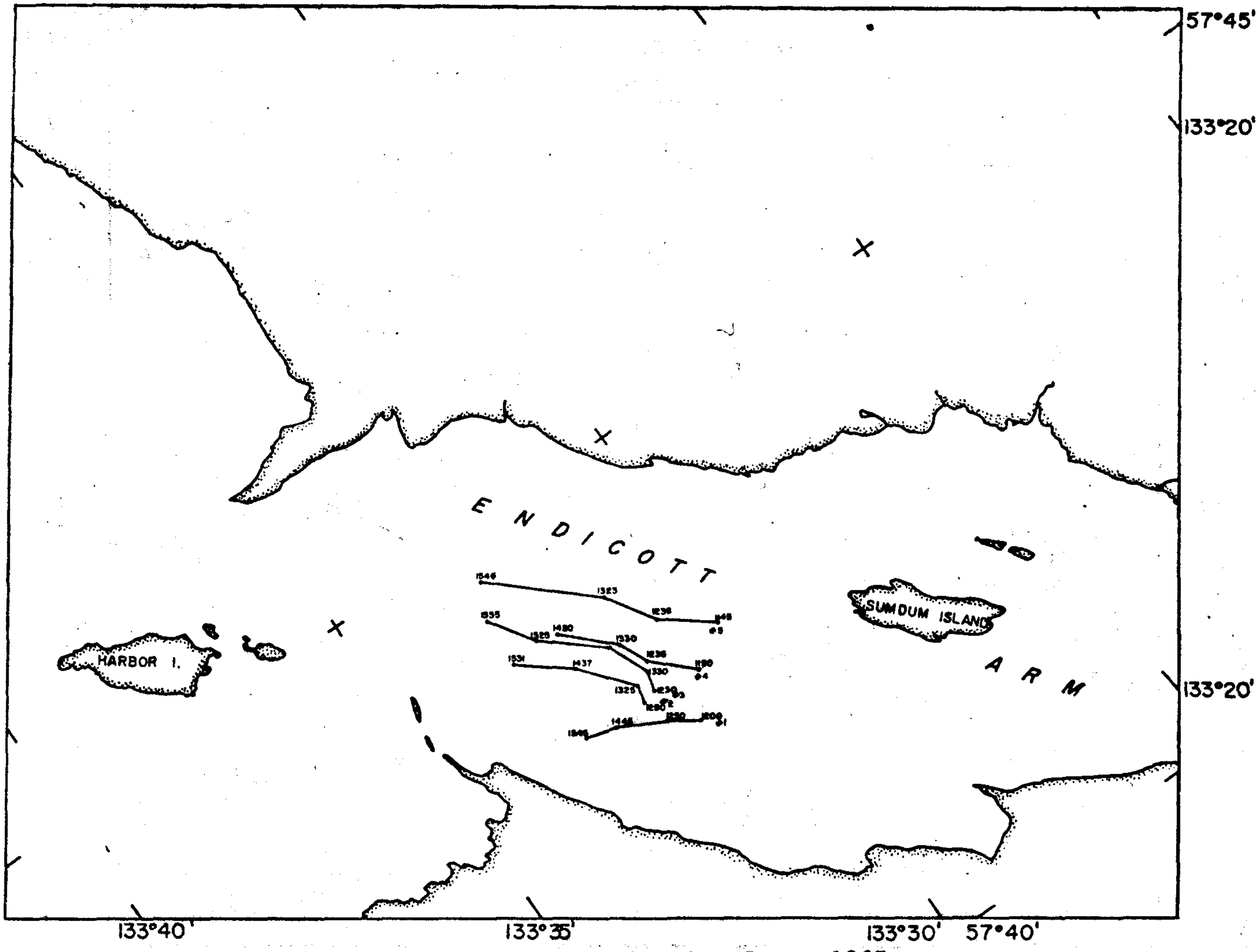

Figure E3 Drogue Drift Plot 5 May 1967
Drogues 1 to 5 Surface

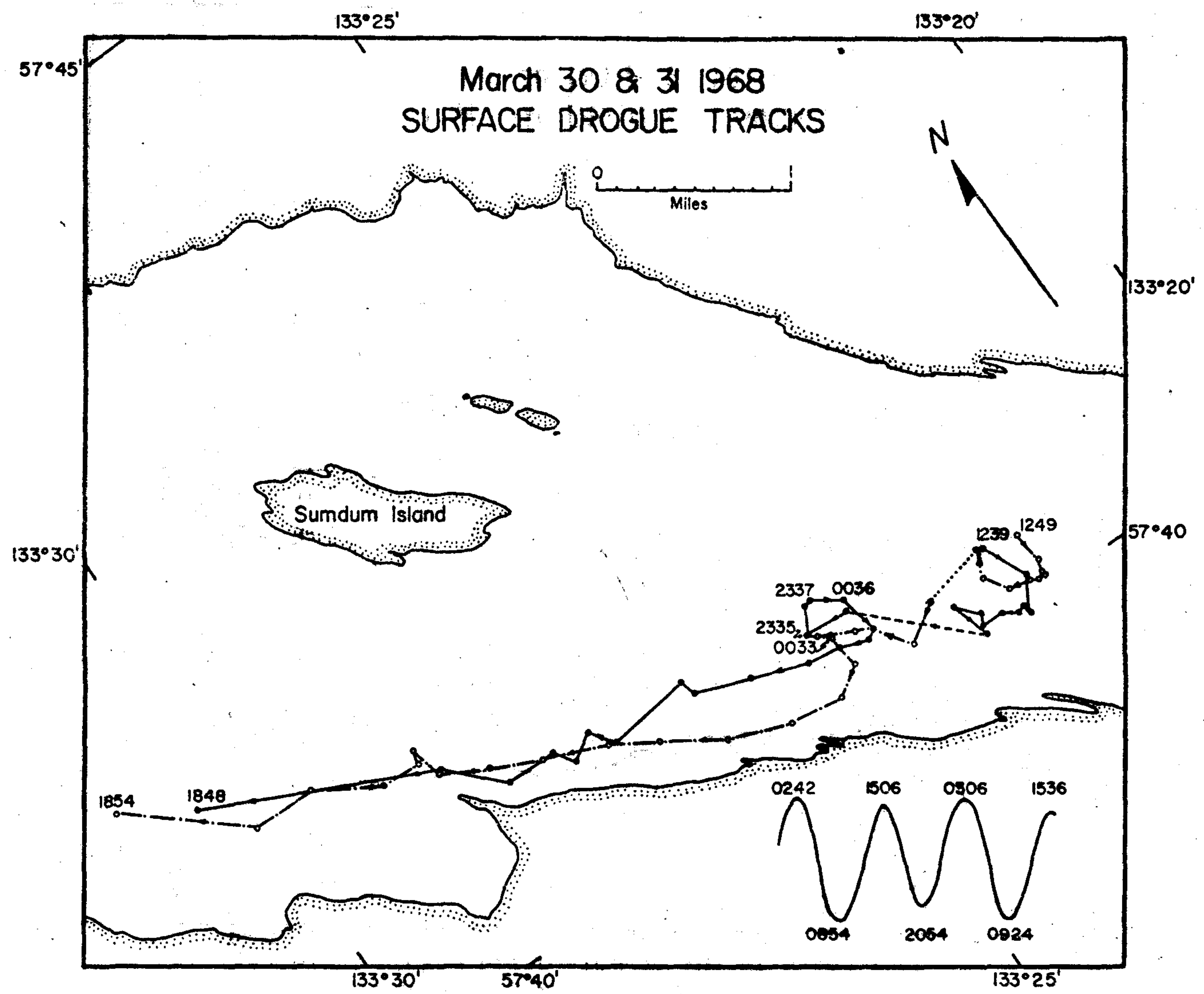

Figure E4 Drogue Drift Plot 30 and 31 March 1968
Drogues 1 and 2 Surface

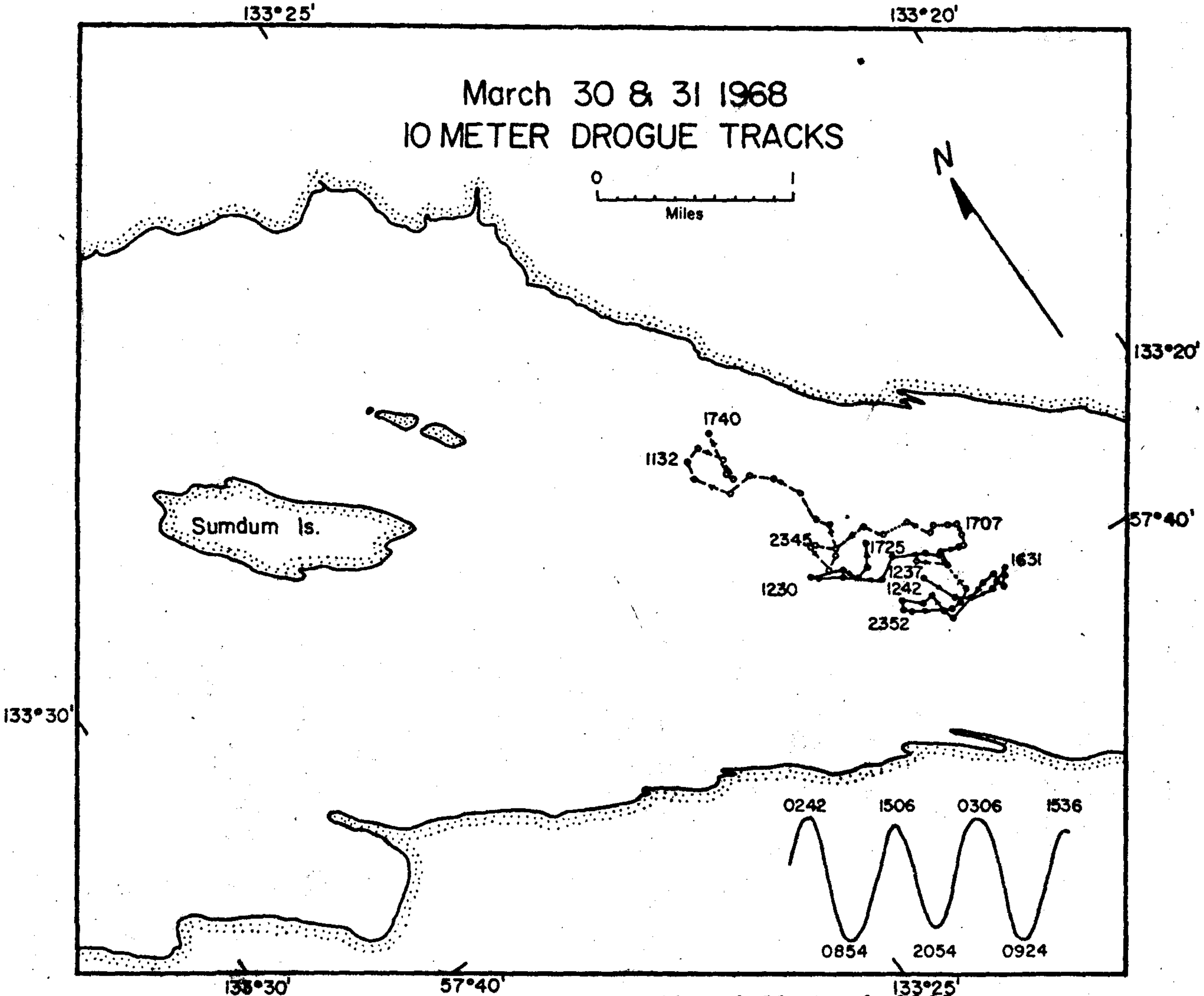

Figure E5 Drogue Drift Plot 30 and 31 March 1968
Drogues 3 and 4 10 m

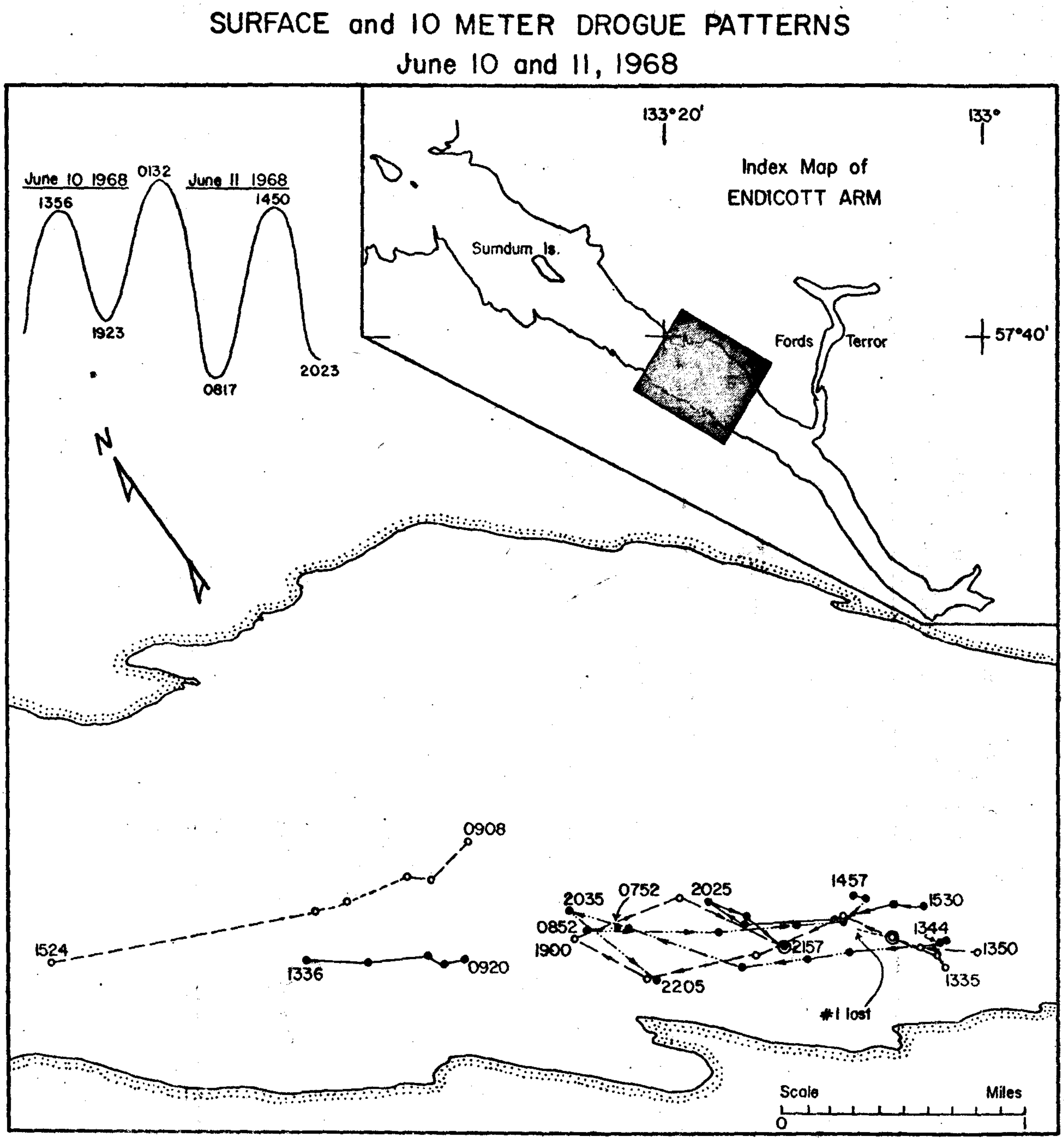

Figure E6 Drogue Drift Plot 10 and 11 June 1968
Drogues 2 and 4 Surface
Drogue 3 10 m

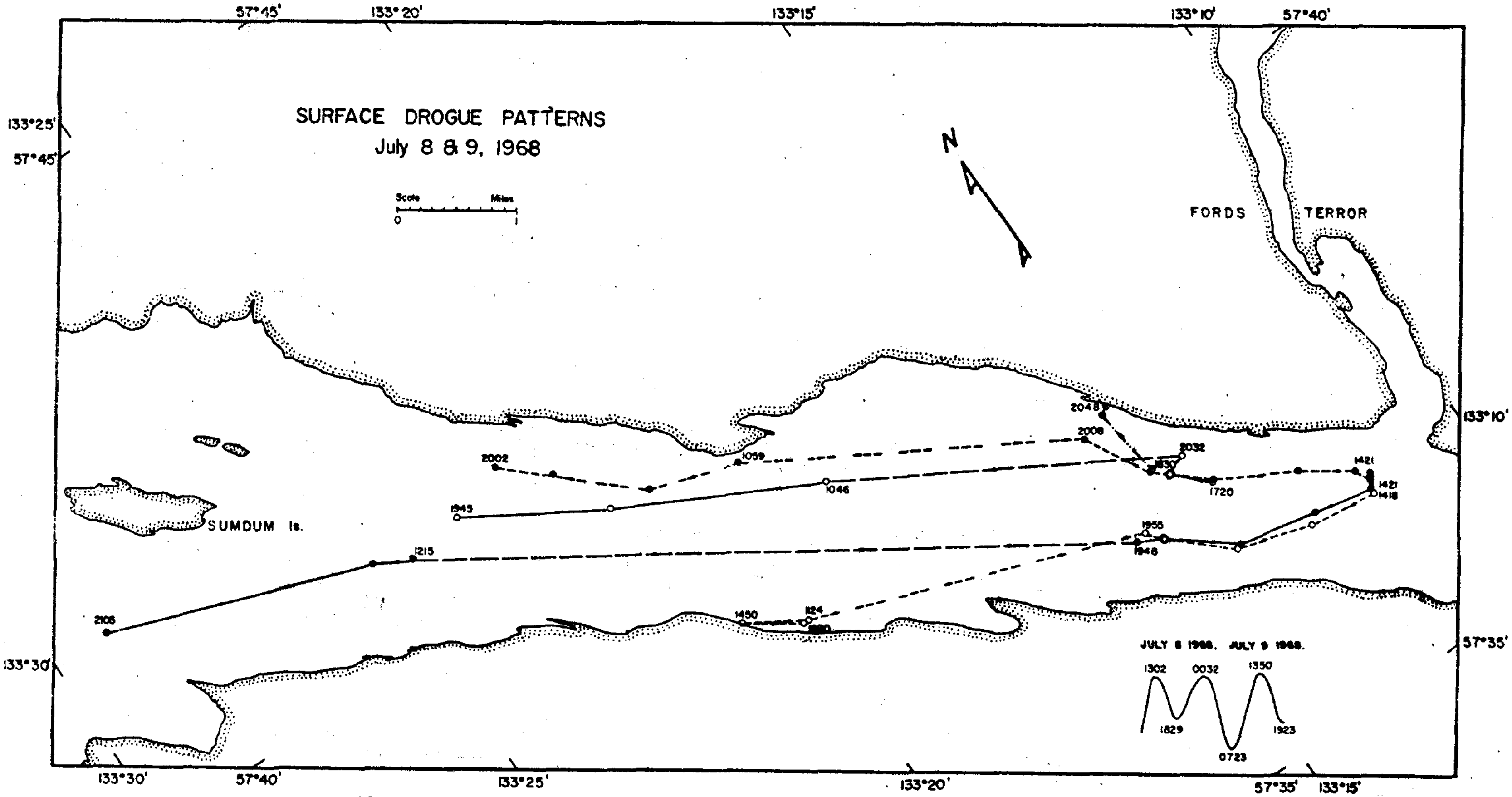

Figure E7 Drogue Drift Plot 8 and 9 July 1968
Drogues 1, 2, 4 and 5 Surface
Drogue 3 10 m

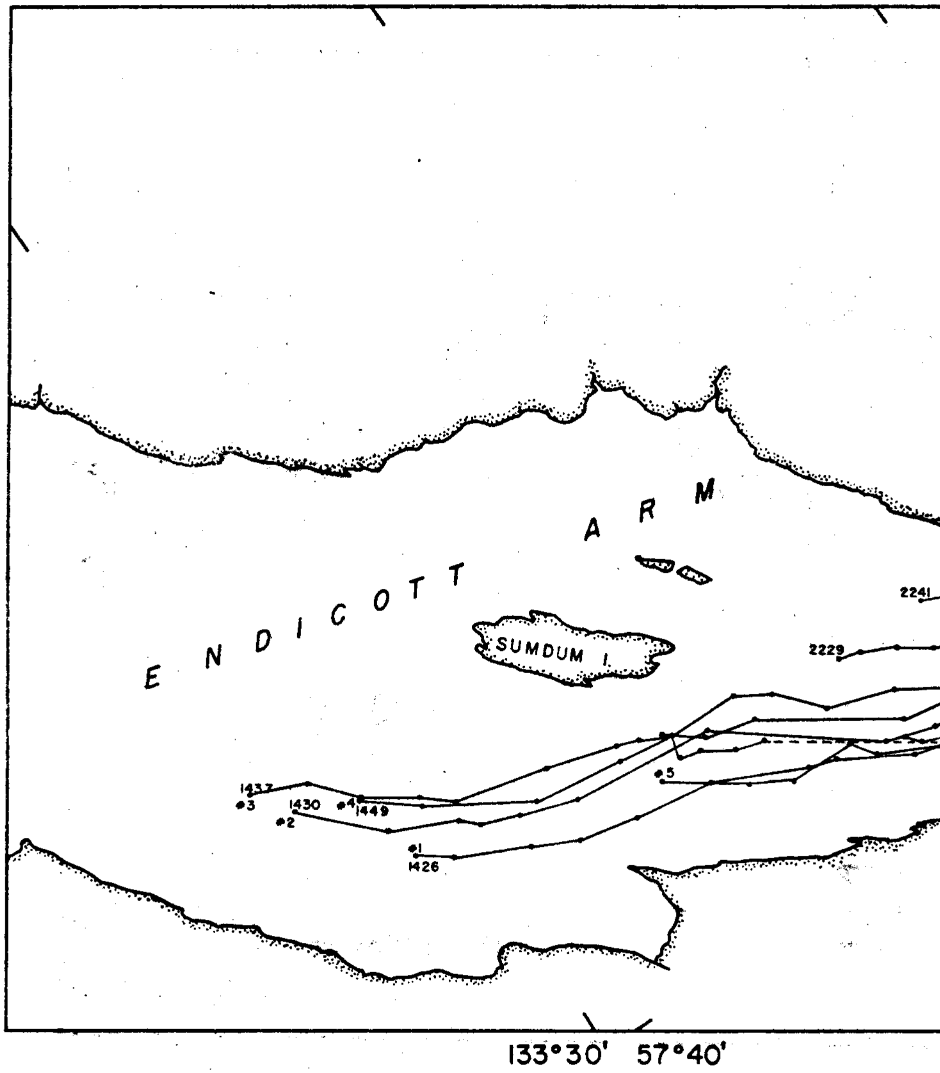

Figure E8 Drogue Drift Plot 25 and 26 February 1969

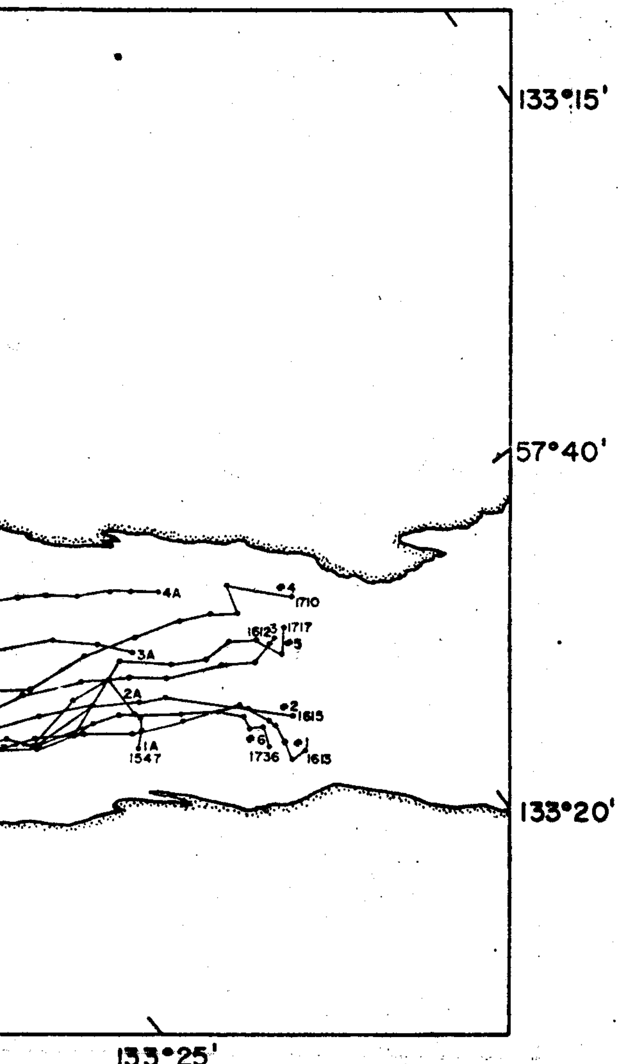

Drogues 1, 2, 3 and 4 Surface
Drogue 5 and 6 10 m
Drogues 1A and 4A Surface

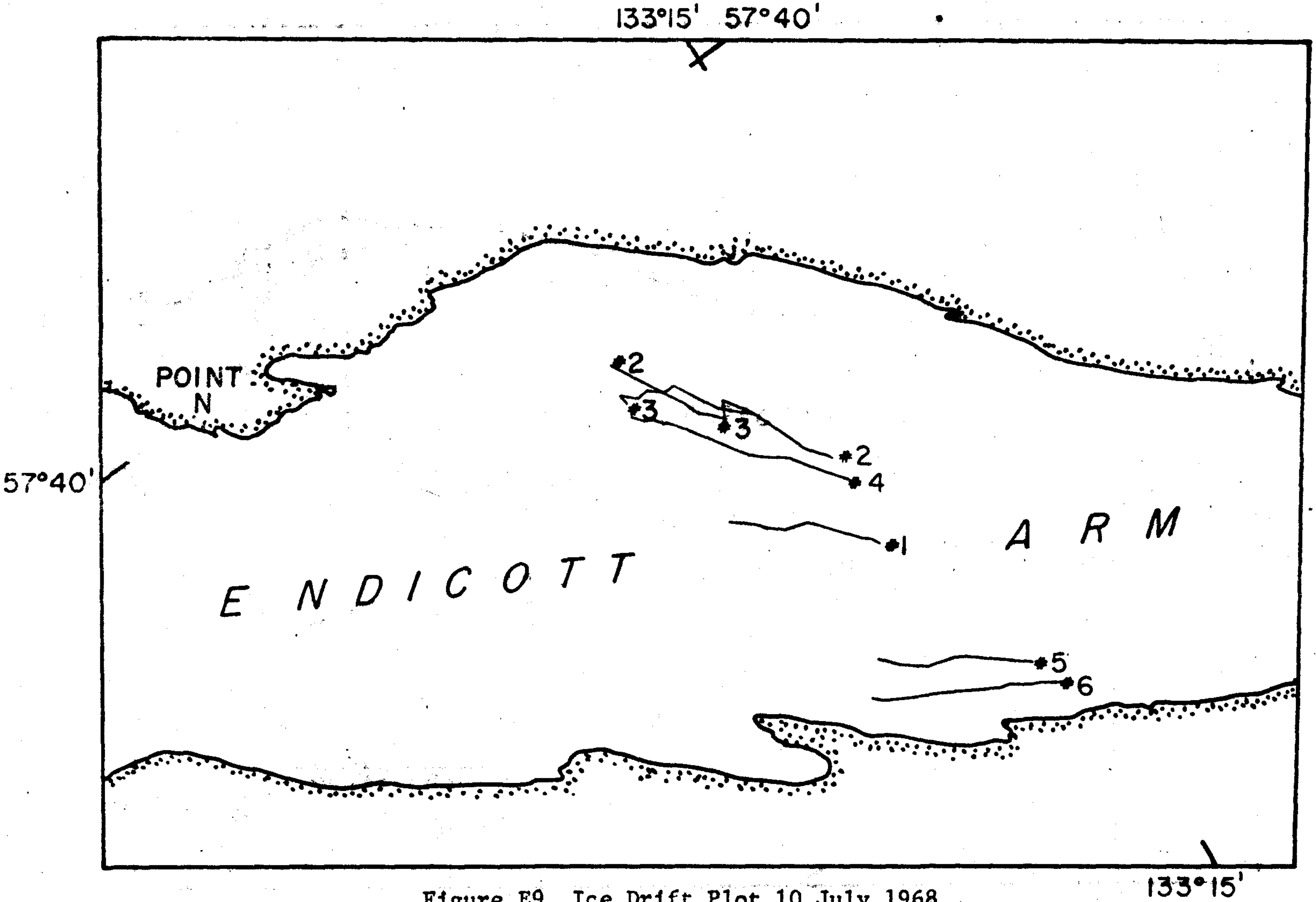

Figure E9 Ice Drift Plot 10 July 1968
Iceberg Sizes in Figure 23

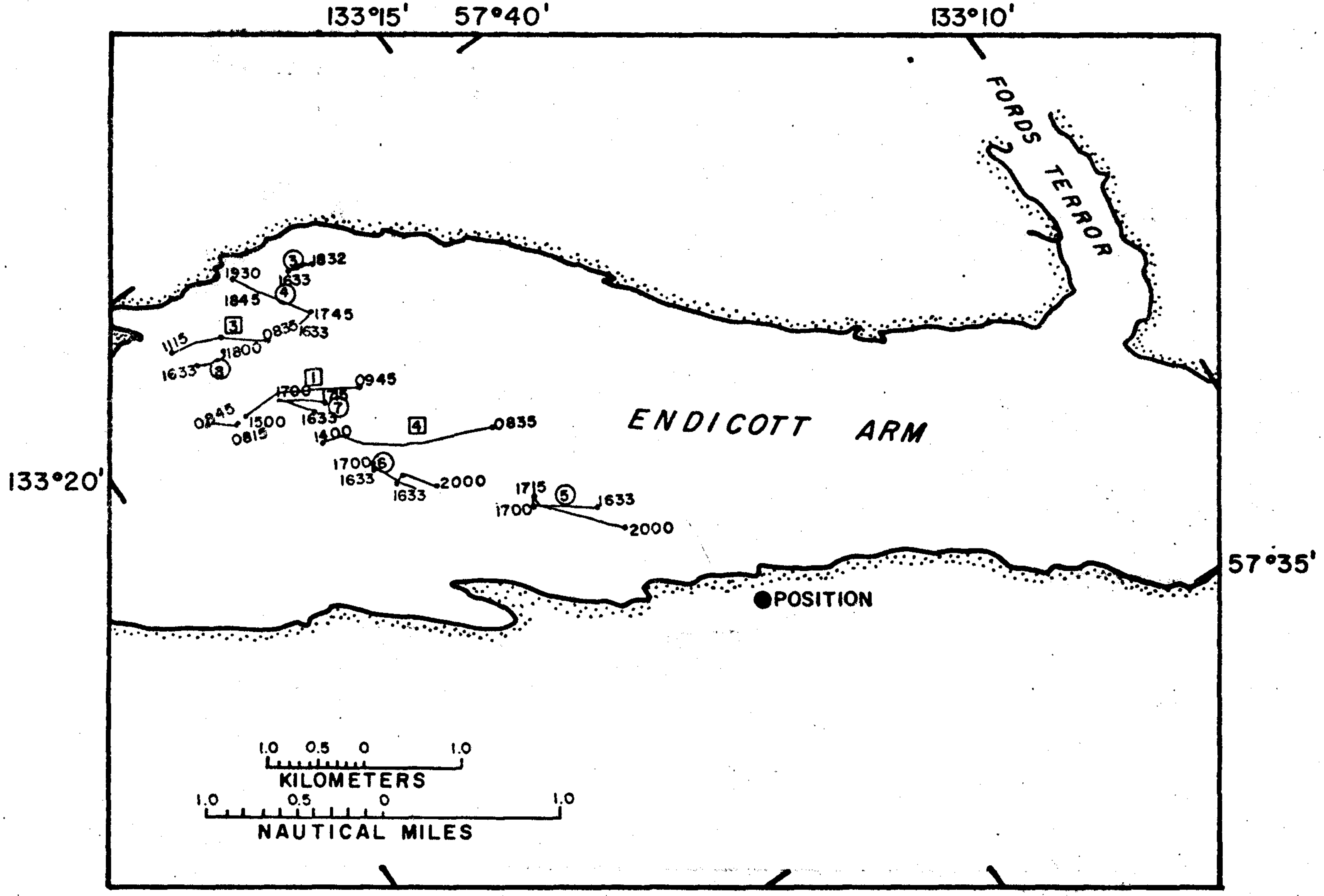

Figure E10 Ice Drift Plot 24 and 25 August 1968

Circled Numbers 24 August
Boxed Numbers 25 August
Iceberg Sizes in Figure 23

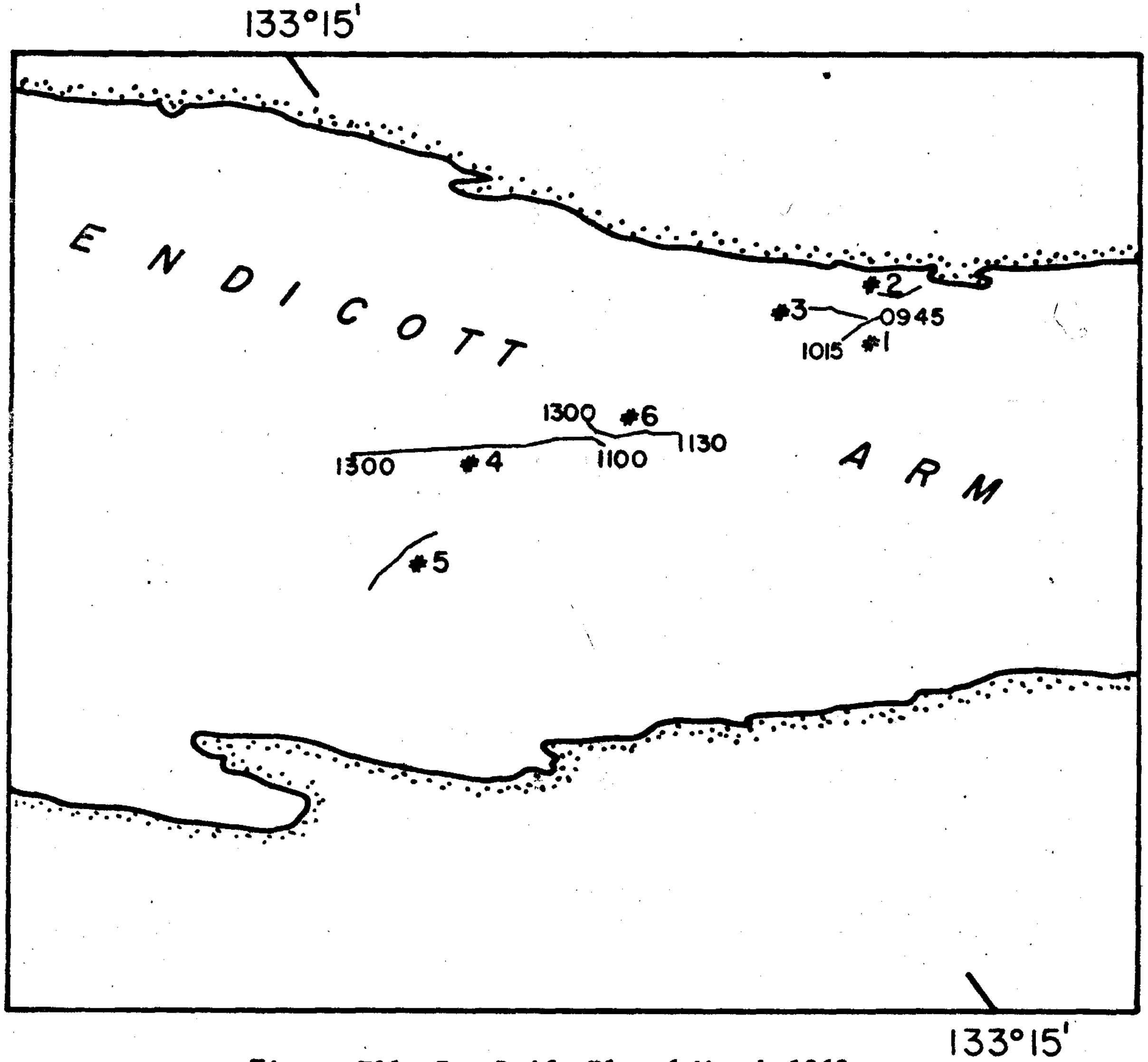

Figure E11 Ice Drift Plot 6 March 1969
Iceberg Sizes in Figure 23

APPENDIX F

MISCELLANEOUS

F.1 Tide Staff Readings Taken in North Dawes on 28 March 1968

Time	Height	Observer
1346	29' 1"	Installation
1455	28' 3"	Gleason
1555	25' 4"	"
1647	22' 3"	"
1758	17' 6"	"
1852	14' 6"	"
2000	13' 3"	"
2100	14' 4"	Hahn
2155	17' 1"	Rosenberg
2255	22' 2"	"

F.2 Drogue Reversals

	From	To	Difference	Flood Current	Predicted Flood
	30 and 31 March 1968 -- Surface				
Drogue 1	2233	0242	4^h09^m	0038	0026
Drogue 2	2335	0133	1^h58^m	0034	0026
	30 and 31 March 1968 -- Ten Meter				
Drogue 3	2352	0405	4^h13^m	0158	0026
Drogue 4	2345	0200	2^h15^m	0053	0026
	31 March 1968 -- Ten Meters				
Drogue 3	1230	1505	2^h35^m	1348	1220
Drogue 4	1132	1345	2^h13^m	1238	1220

F.3 The Correction of Drogue 4, March 1967 to Outflow at High Tide

Drogue 4D left the inlet in March 1967 at near maximum ebb current. Its movement was influenced by both tidal outflow and the mean outflow within the inlet. To indicate the volume of mean outflow within the inlet the drogue's outflow speed was corrected to high tide.

From drogue 4 (figure 2, Appendix E) the current speed within the inlet at high tide and the current through the mouth at maximum ebb current was calculated. (These were 11.9 and 70.3 cm/sec respectively.) From drogue 1 the current at ebb tide within the inlet was calculated. (This was 15.0 cm/sec.) Since drogue 1 was not on the same streamline as drogue 4 it was corrected to that streamline. This was done by observing that drogue 1 was at 23% of the distance from drogue 4 to drogue 2 (which showed little motion). Thus assuming a linear speed-distance relationship drogue 1 represented 77% of drogue 4's speed. (Correcting drogue 1's speed by this factor gave it an ebb current speed of 19.5 cm/sec.)

The current speed at high tide through the mouth was calculated as follows: the current speed measured at ebb stage (being tidal current plus outflow current) minus the current speed measured at high tide (being only mean outflow current) gave the tidal current at ebb stage. (This was 7.6 cm/sec.) This tidal current was 39% of the total ebb current within the inlet. The out-of-inlet current speed was reduced by 39% giving a high tide outflow current speed of 43 cm/sec. This corresponded to a mean outflow volume of $8.0 \cdot 10^3 m^3/sec$.

F.4 Error Curves

The error curves are shown in figures F-1 to F-3.

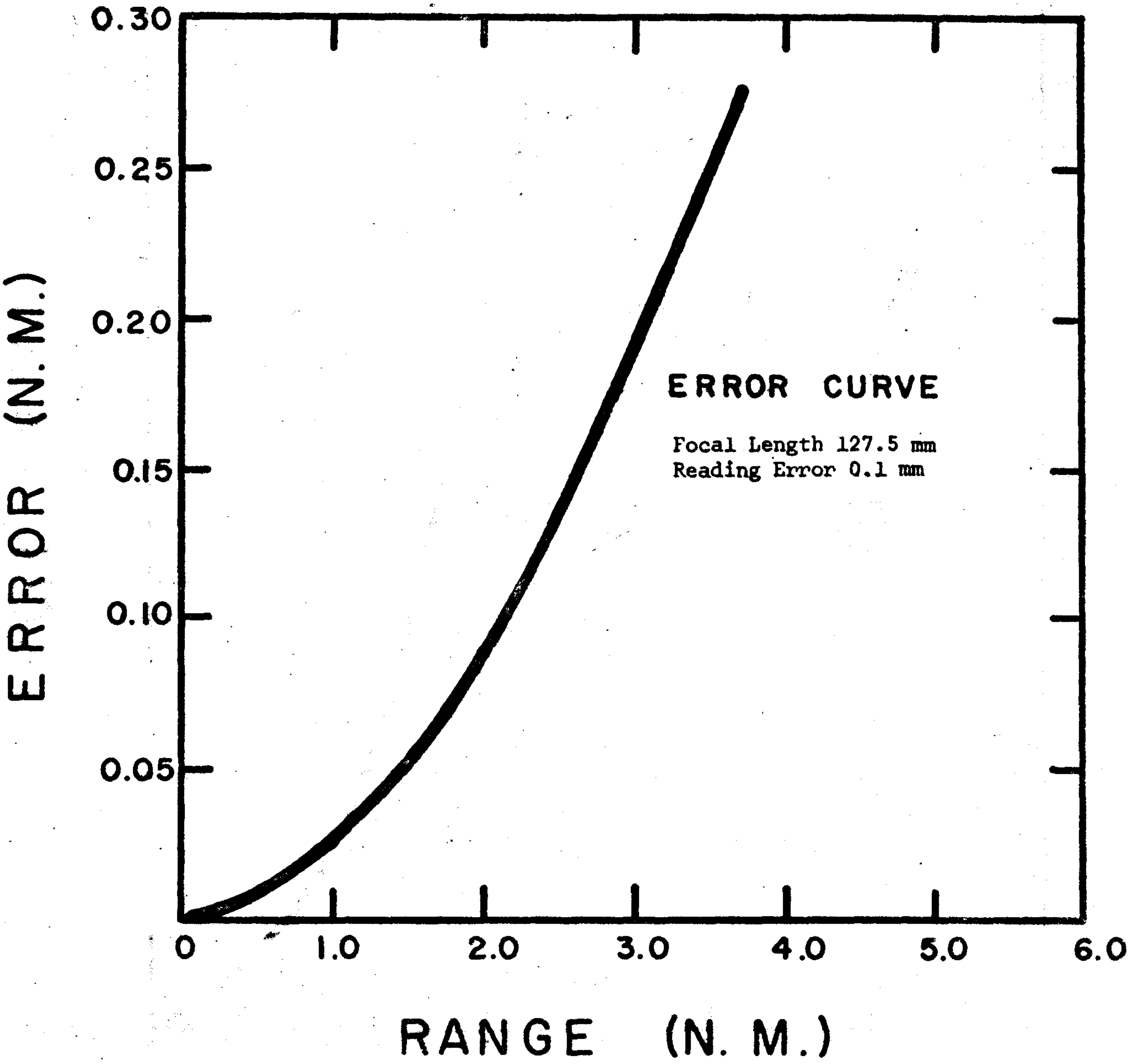

Figure F1 Error Curve 10 July 1968

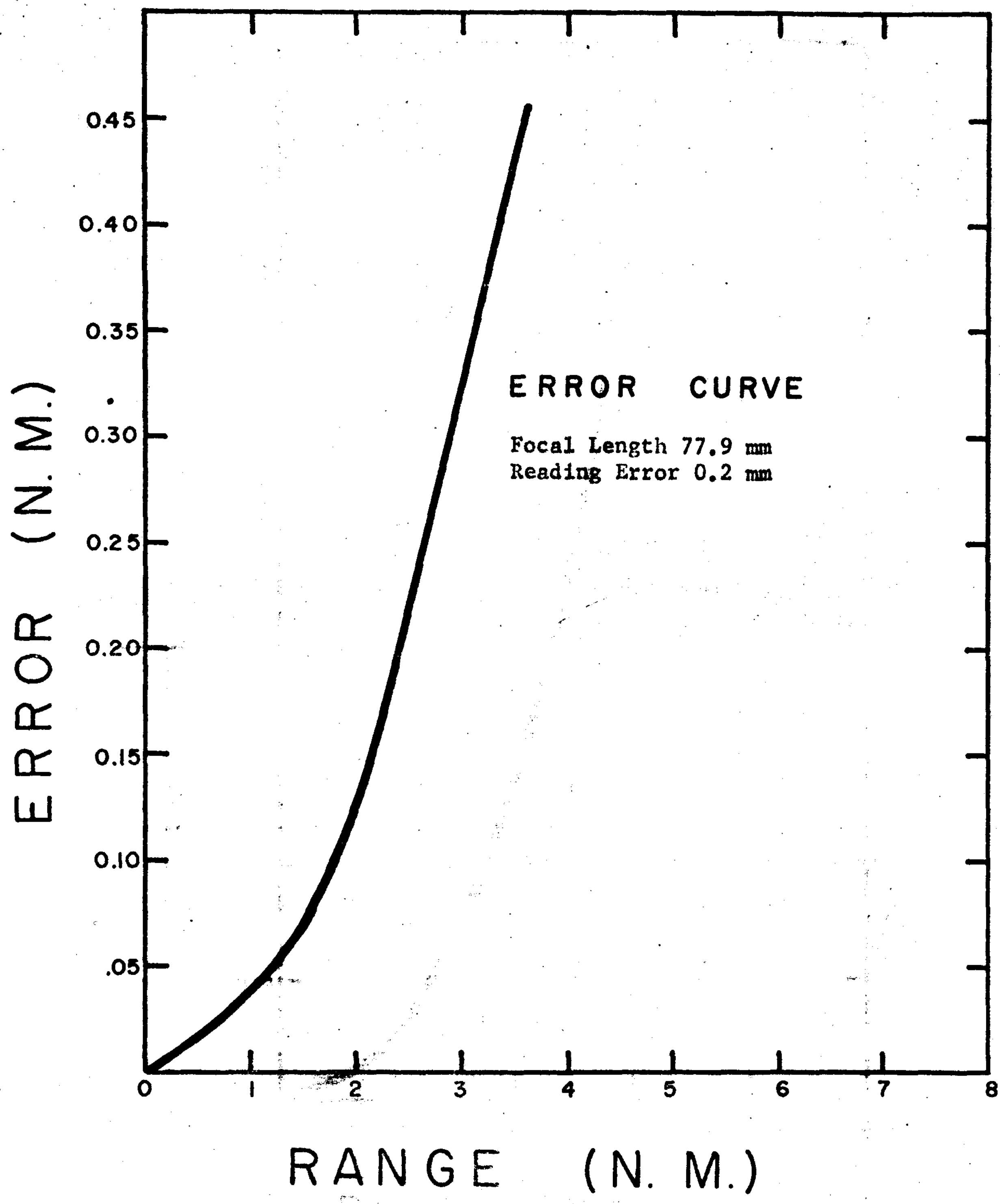

Figure F2 Error Curve 24 and 25 August 1968

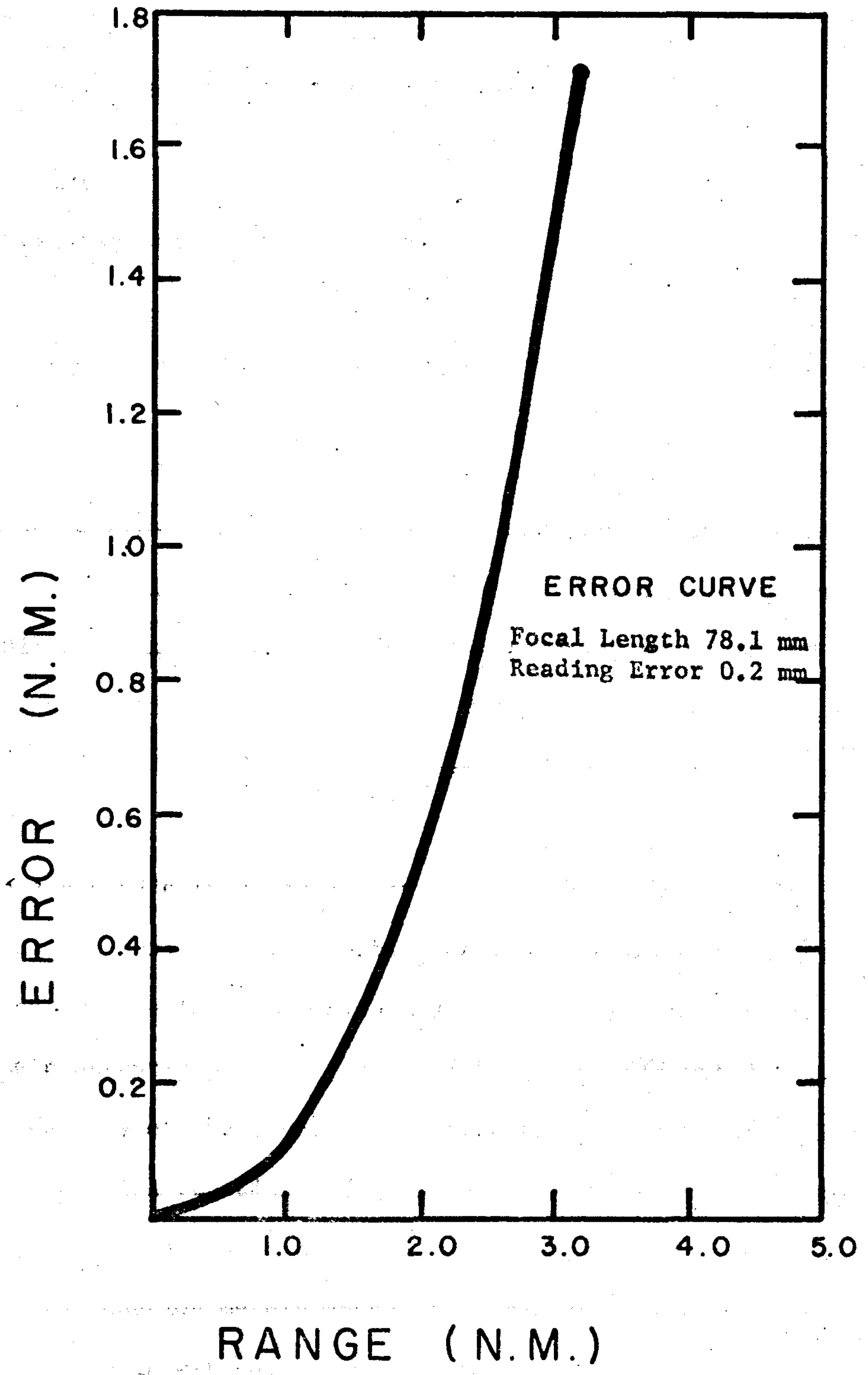

Figure F3 Error Curve 6 March 1969

APPENDIX G

ANALOG SIMULATION OF TIDAL ICEDRIFT

G.1 The Equation

The equation as stated in section 2.2.2 is

$$\frac{dv}{dt} = -k\ \mathrm{sign}(v-v_o \sin\omega t)\cdot(v-v_o \sin\omega t)^2$$

This is a non-linear first order differential equation. At this point it is worth noting what the sign function is and how it was used herein.

The quantity $(v-v_o \sin\omega t)$ or U is normally a periodic function and in this case has a tidal period. The quantity v can bias U somewhat but cannot change the period. This is true because v is the integrated product of dv/dt. This acceleration is caused by the tidal acceleration which is periodic.

When a periodic function is squared it becomes constantly positive with double the period. (The doubled period is caused by the negative oscillations of the function being made positive by squaring (figure G-1). The constantly positive, doubled frequency did not fit with the tidal periodicity of the iceberg's acceleration; this condition was righted by the sign function. (The iceberg's acceleration is proportional to U^2 in magnitude but not in direction.)

The sign function merely generates a square wave of +1 and -1 magnitudes in phase with U. When this sign function is applied to U^2 it converts it back to a function of tidal frequency and U^2 amplitude.

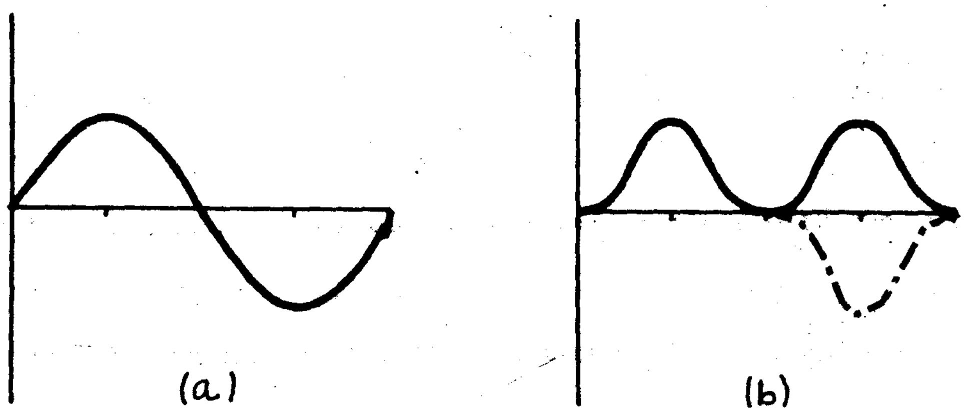

Figure G1 (a) Sine function
(b) Sine function squared. (Solid line) Sine function squared with sign function applied shows positive and negative oscillations as sine function. (Dashed line)

(See dotted lines in figure G-1(b). On the computer the sign function amplifies U, in two stages, by 100 times and limits it to +1 and -1 volt. The result is a square wave in phase with U.

G.2 Diagram of the Problem and Explanation

The diagram of the problem, as set up on the analog computer for oscilloscope, is contained in figure G-2.

$\dot{U}$ is generated starting with the sine generator. The generator produces the sine wave which is modified in amplitude by potentiometer v_o. This sine function is fed into the amplifier along with the output of the integrator -v. The amplifiers in this machine invert the imput functions and add the inputs when there are two. Thus -v and $v_o \sin\omega t$ come out $v - v_o \sin\omega t$ or U.

The U function is fed into both the sign function and the squaring multiplier. The squaring function converts U into the aforementioned square wave. Since it is two stage (involving two amplifiers) the output is in phase with U. The U is fed into the squaring function, is squared, and since the function contains an amplifier, the U is converted to $-U^2$.

The output of these two components is fed into the -XY multiplier. This multiplier merely multiplies the two inputs and changes the sign. The output is $\text{sign}(U)U^2$.

The output of the -XY multiplier is fed through the potentiometer k, through an amplifier and into an integrator. The potentiometer reduces the function by the appropriate constant and the amplifier changes the sign of the function. The output of this amplifier is dv/dt or -k

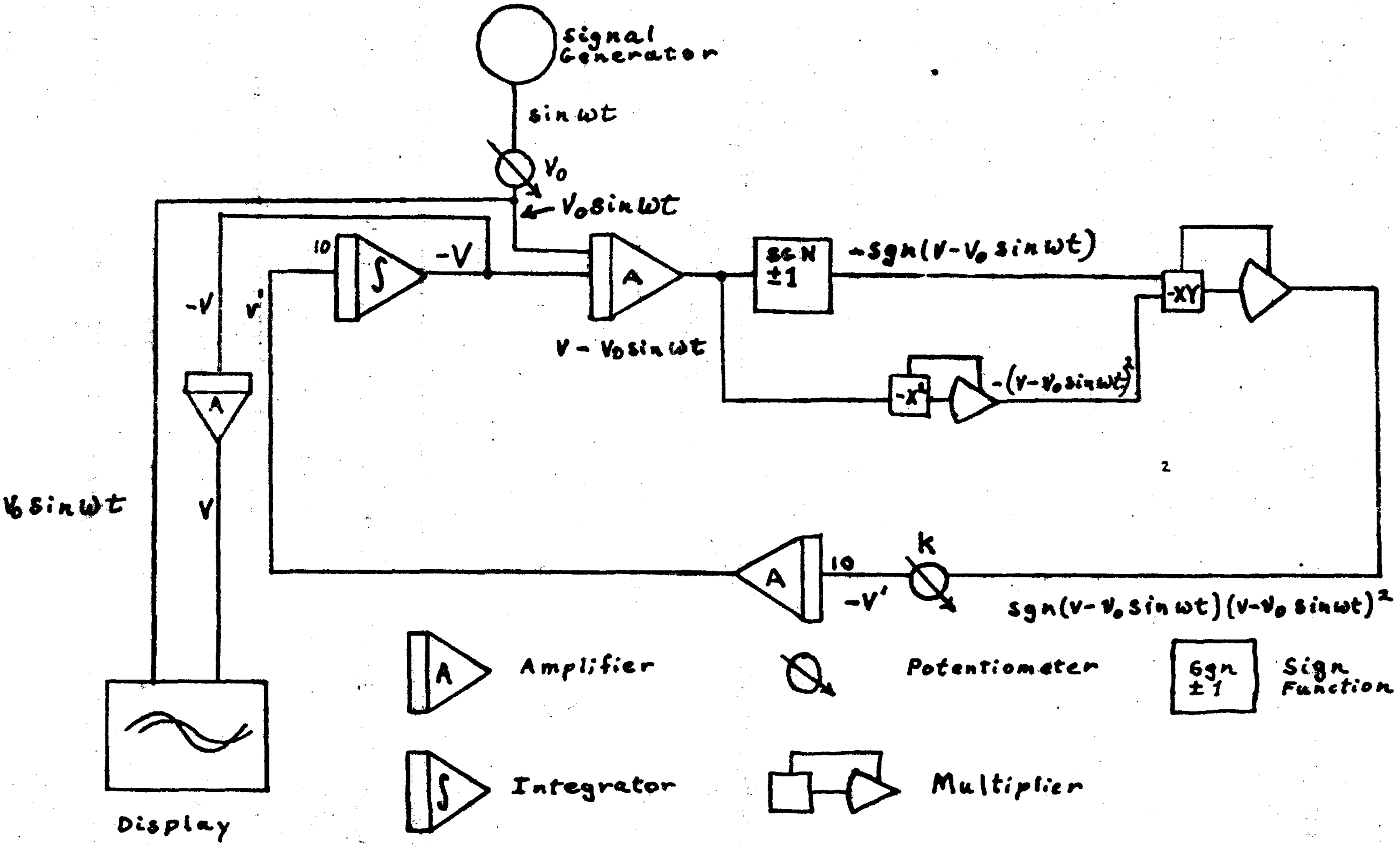

Figure G2 Diagram of problem as set-up for oscilloscope sign(U) $(U)^2$. This derivative is put into the integrator, integrated, and the resultant $-v$ (minus since the integrator contains an amplifier) completes the circuit.

Minus v, however, is the inverse of v, the iceberg's tidal speed so this signal was fed through a further amplifier before displaying it on the oscilloscope. With the v, the tidal signal, $v_o \sin\omega t$ was displayed giving the curves which were later plotted.

G.3 Scaling

The problem of making the real variables of v_o, k, and time compatible with the machine was the problem of scaling.

The v_o term was kept as it was, 0.2 and 0.1 representing 0.2 and 0.1 m/sec, the tidal current speed amplitudes.

The time term was one cycle per 12 hours or 2.32×10^{-5} cycles per second. This time was increased to 11.6 cycles per second by increasing the scaling perameters by 5×10^5 times. Initially the fast function of the computer was used which allows integration at 500 times normal speed. In addition, two amplifiers were allowed to amplify by 10 times each and the potentiometer k was set 10 times high, taking care of the other 1000 times (figure G-2).

Increasing amplification for scaling is permissible since time is a variable in the function as is v. When the derivative $dv/d\tau$ (τ is machine time) is increased by 10^3 the derivative is increased so time and velocity are increased. Since velocity is dependent upon time the net effect is to increase the problem's speed without altering its characteristics (EAI 380 Analog/Hybrid Computer Handbook).

The 10^3 term was introduced by the amplifier, the k potentiometer and the integrator as previously stated. The real and machine values are given as follows:

Real Units	Machine Units
$v_o = 0.2$ m/sec	$v_o = 0.2$
$k = 0.0010$ to 0.1000	$k = 0.010$ to 1.000
$f = 2.32 \times 10^{-5}$ cyc/sec	$f = 11.6$ cyc/sec

G.4 Plotting Set-up

The X-Y plotter required a different set up. Plotting required a speed slow enough for the machine to work accurately; 0.116 cyc/sec was used. Further it required sine generation within the machine, a time base to drive the plotter and repetition mode on the machine.

Generation of the sine function was a combination of two integrators, an amplifier, and a potentiometer. (See figure G-3. The initial condition, marked as a battery, biases the integrator's capacitor with a positive voltage. When the machine is started the capacitor discharges through the amplifier. The amplifier, in turn inverts the signal from positive decreasing to negative increasing. This current charges the second integrator's capacitor. When the first integrator has discharged the second integrator has charged and reverses the current flow. The rate of this function is regulated by the potentiometer. (The sine function was calibrated against the sine generator.)

The time base for the plotter was generated by integrating a positive voltage (figure G-4). The positive voltage charges the capacitor

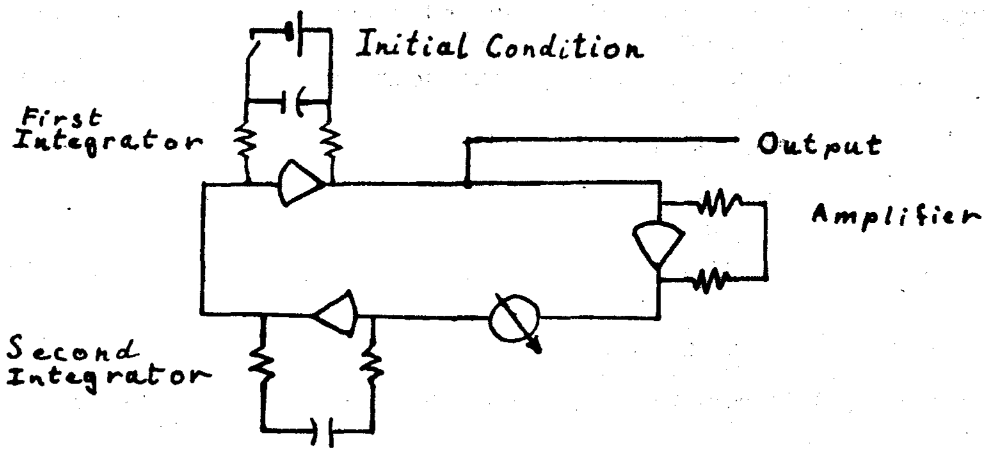

Figure G3 Sine Generator

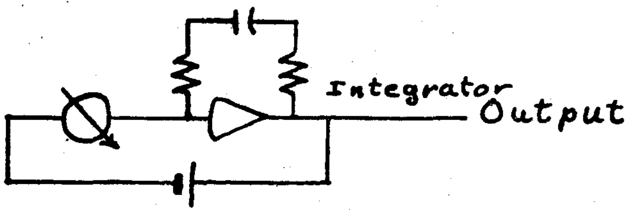

Figure G4 Time Base Generator

and generates an increasing voltage at the output terminal. The machine must reset, however, for when the capacitor is fully charged, the machine indicates overload. (The machine resets the amplifiers to prevent their burning out.)

With the internal sine generator supplying the problem (and providing the sinωt curve for the plotter) and the time base integrator providing the time (or X-motion) for the plotter, the problem may be plotted in repeat mode.

On the plotter the sine function starts at 1 volt and decreases to zero. The v function starts at zero and goes toward the sine curve. (This was clipped from the standard plots. See figure G5 for an unclipped plot.) The v-curve reverses direction as it crosses the sine curve and continues in the proper relation to the sine curve afterward. There is a slight error associated with this mode of operation in that v does not reach its full magnitude before reversing. This means there is roughly 5% error in the amplitude of the first peak of the v-curves (on the clipped plot). This error is considerably less than the errors incurred by use of the oscilloscope's 60 x 100 millimeter screen (error of about 10%) and was allowed to stay in the plots.

G.5 Plots

Plots of the tidal current speed (cm/sec) and iceberg drift speed (cm/sec) versus time (in hours) are figures G-6 to G-19. Figures G-6 to G-12 use a tidal current amplitude of 10 cm/sec and figures G-13 to G-19 use 20 cm/sec tidal amplitude. The k-number varies from 0.0010 to 0.1000.

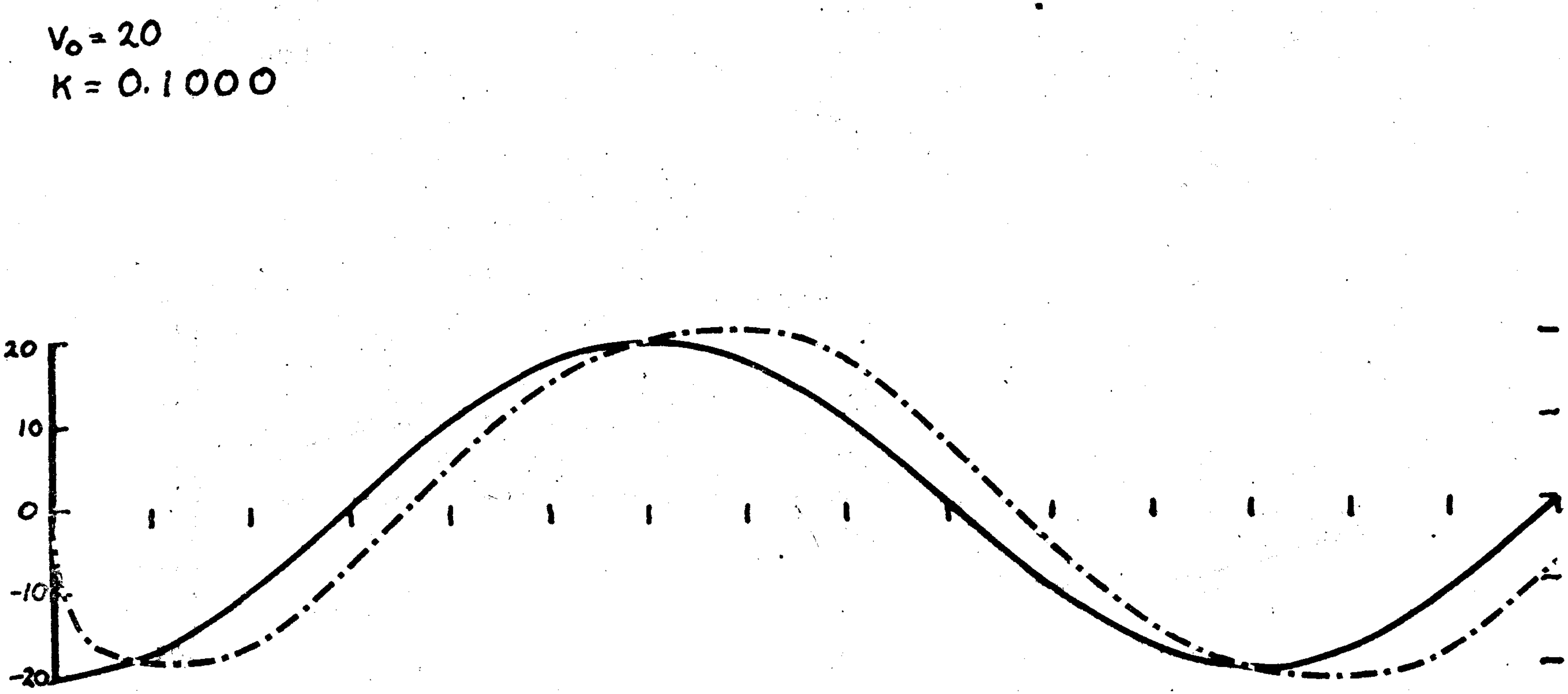

Figure G5 Unclipped Plot Current Speed and Iceberg Drift Speed vs. Time V_o=20 cm/sec, K=0.1000

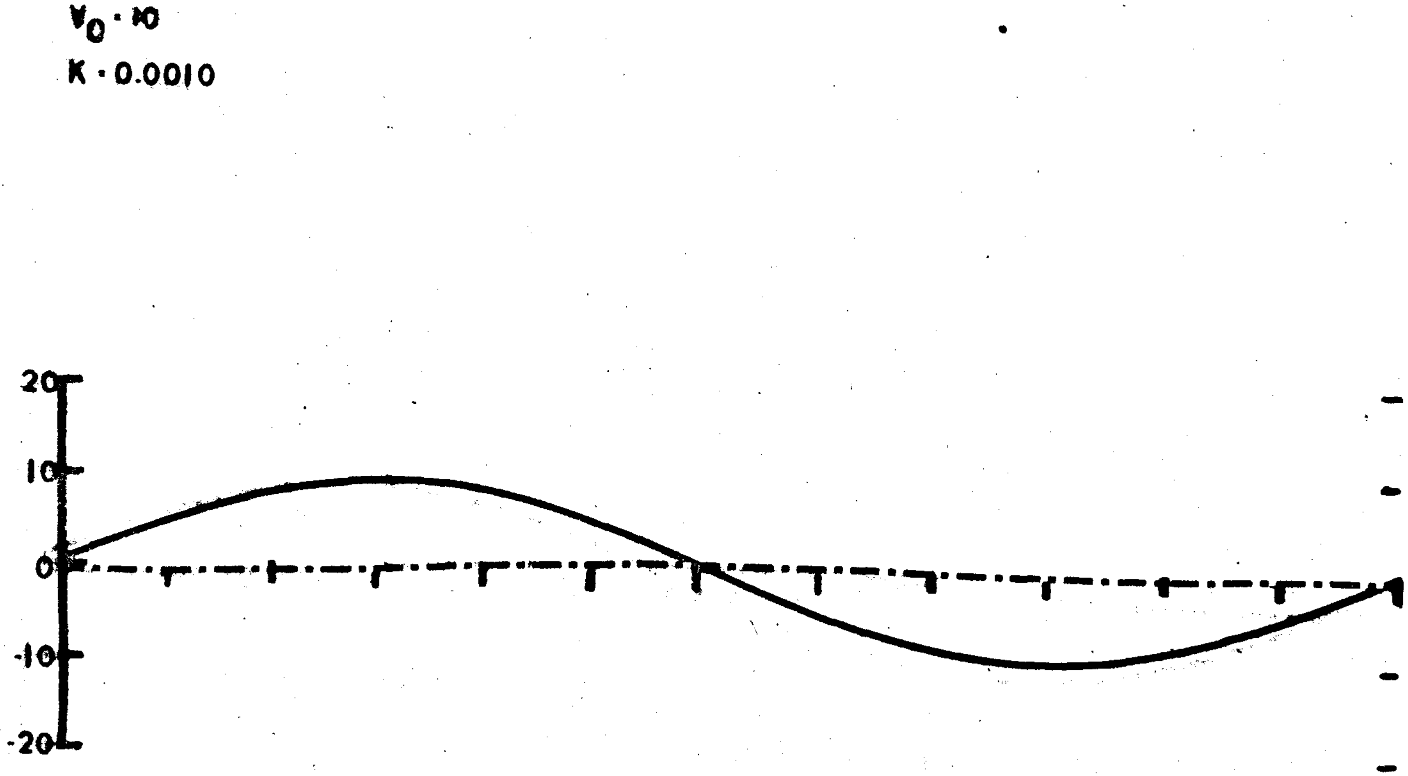

Figure G6 Current Speed and Iceberg Drift Speed vs. Time
V_o=10 cm/sec, K=0.0010

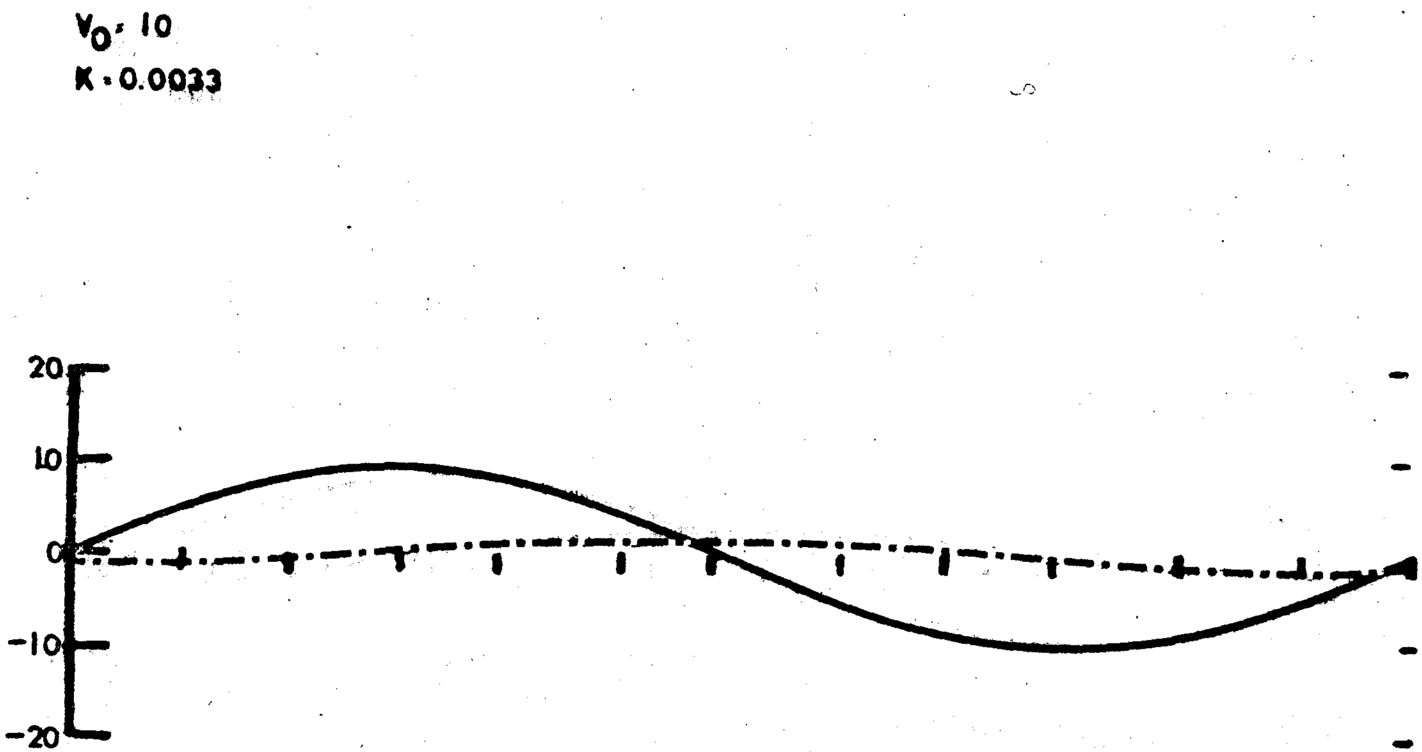

Figure G7 Current Speed and Iceberg Drift Speed
V_o=10 cm/sec, K=0.0033

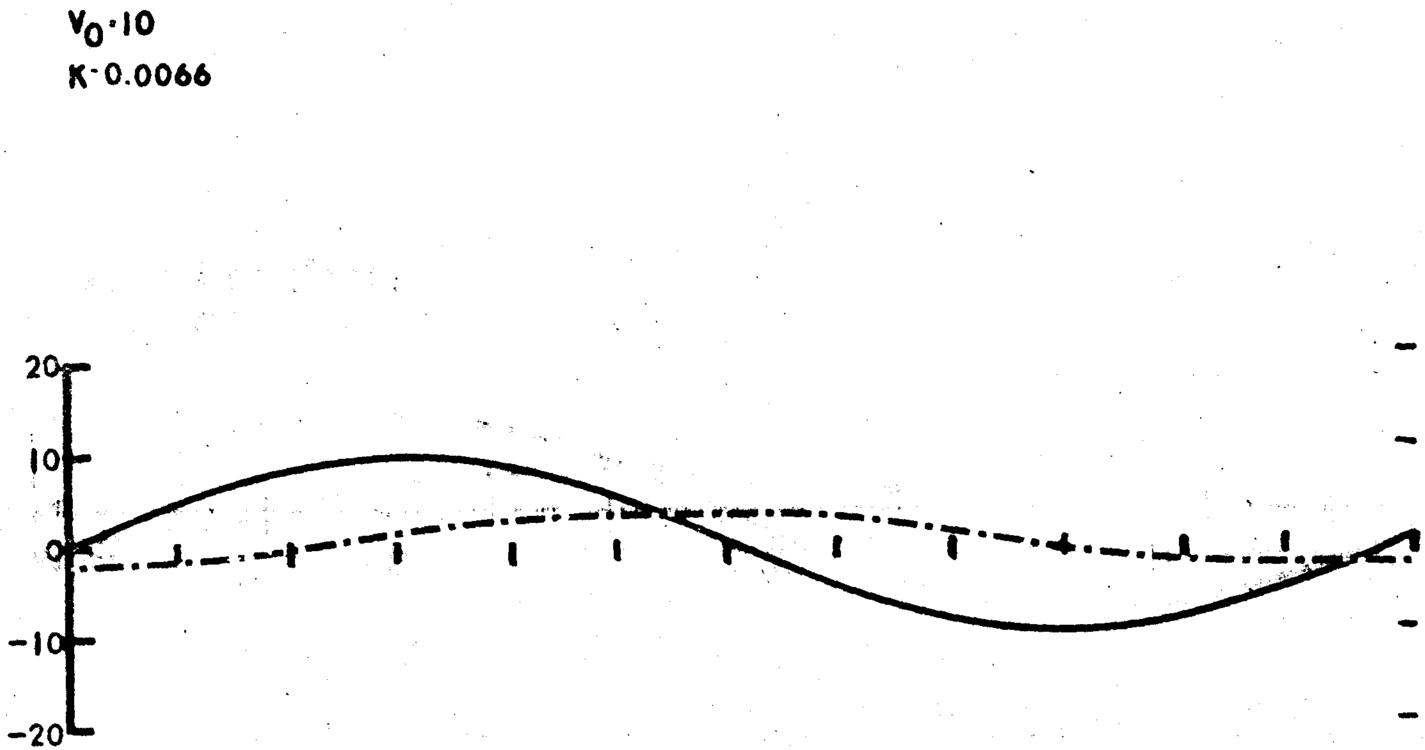

Figure G8 Current Speed and Iceberg Drift Speed vs. Time
V_o=10 cm/sec, K=0.0066

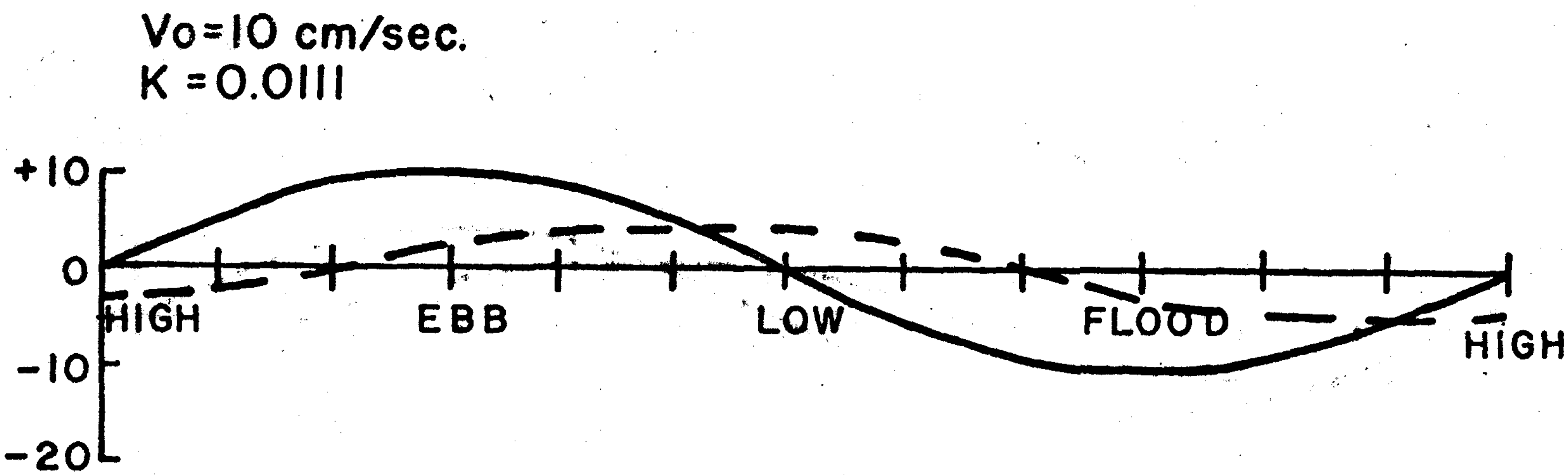

Figure G9 Current Speed and Iceberg Drift Speed vs. Time
V_o=10 cm/sec, K=0.0111

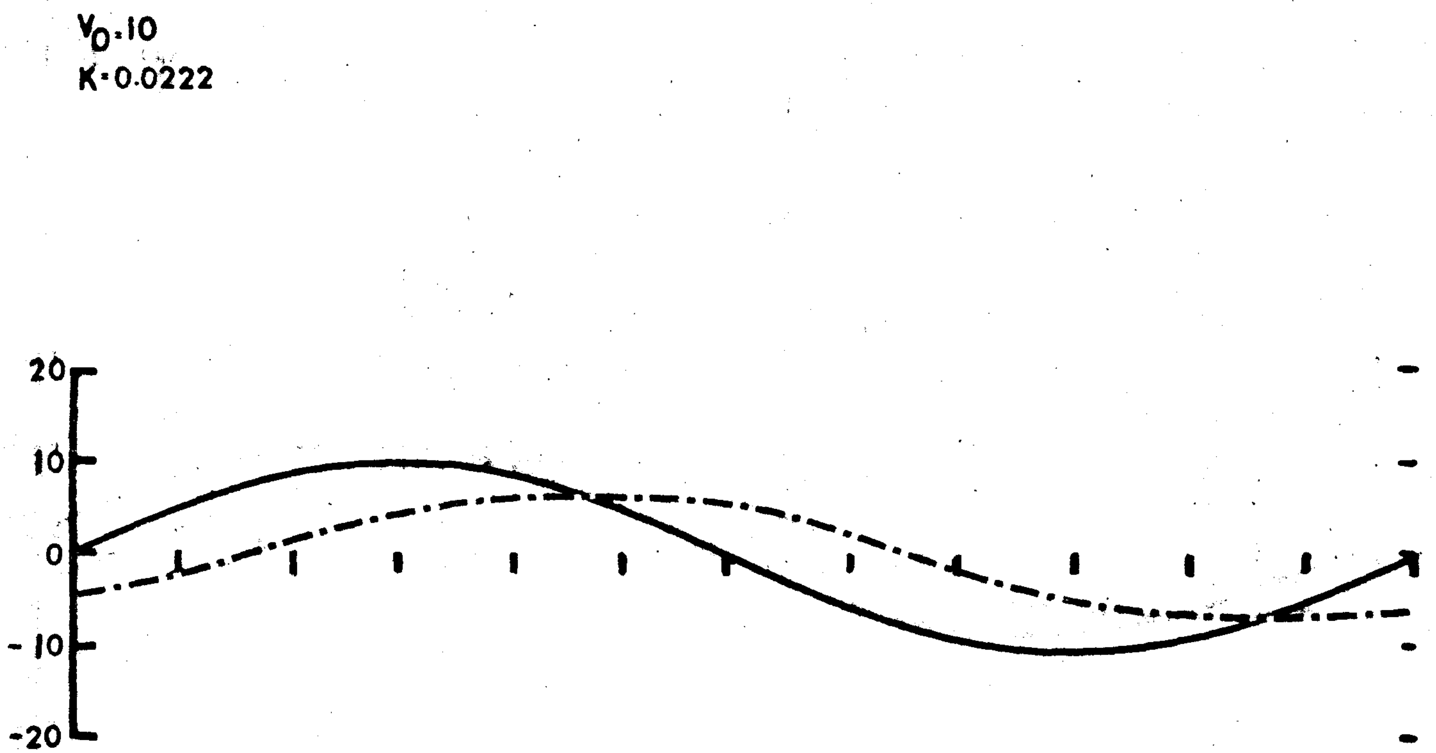

Figure G10 Current Speed and Iceberg Drift Speed vs. Time
V_o=10 cm/sec, K=0.0222

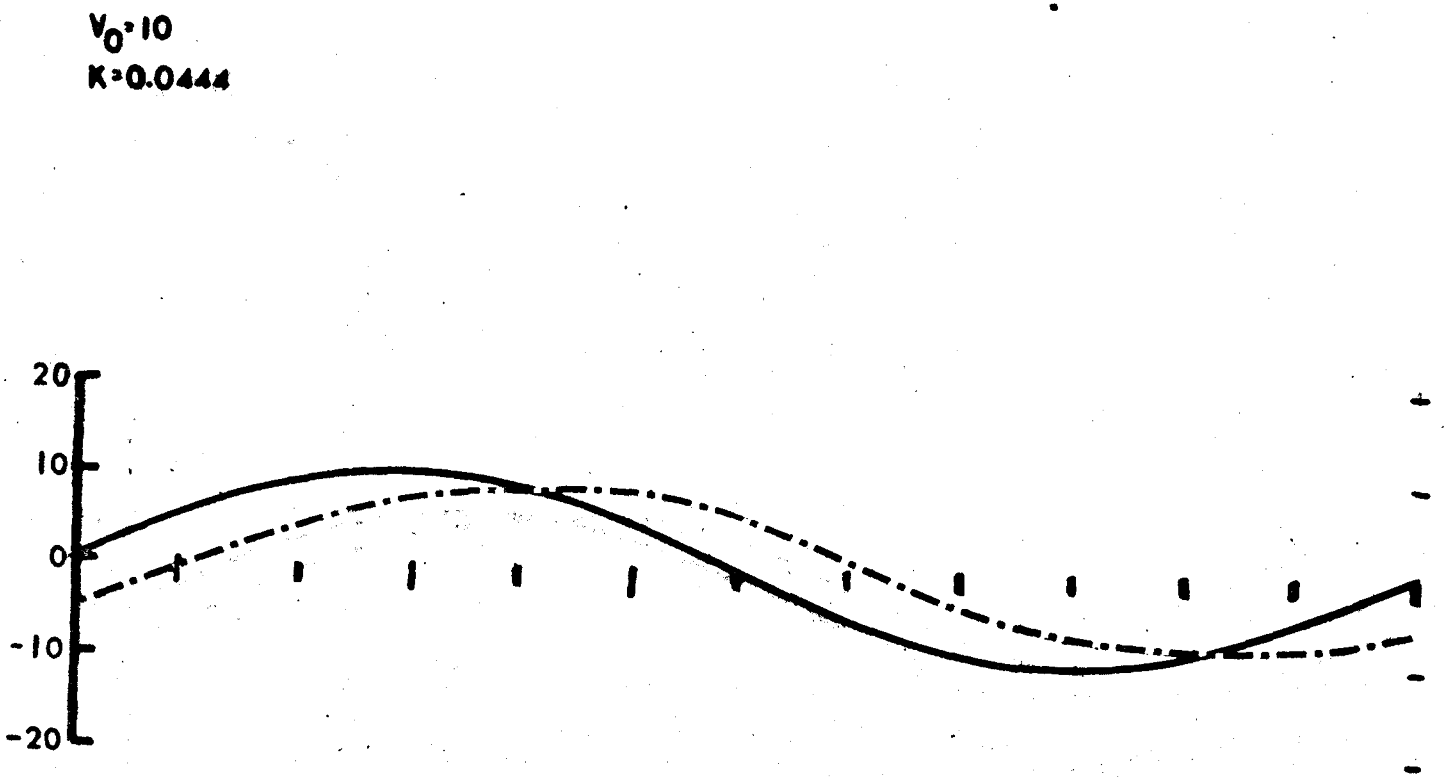

Figure G11 Current Speed and Iceberg Drift Speed vs. Time
V_o=10 cm/sec, K=0.0444

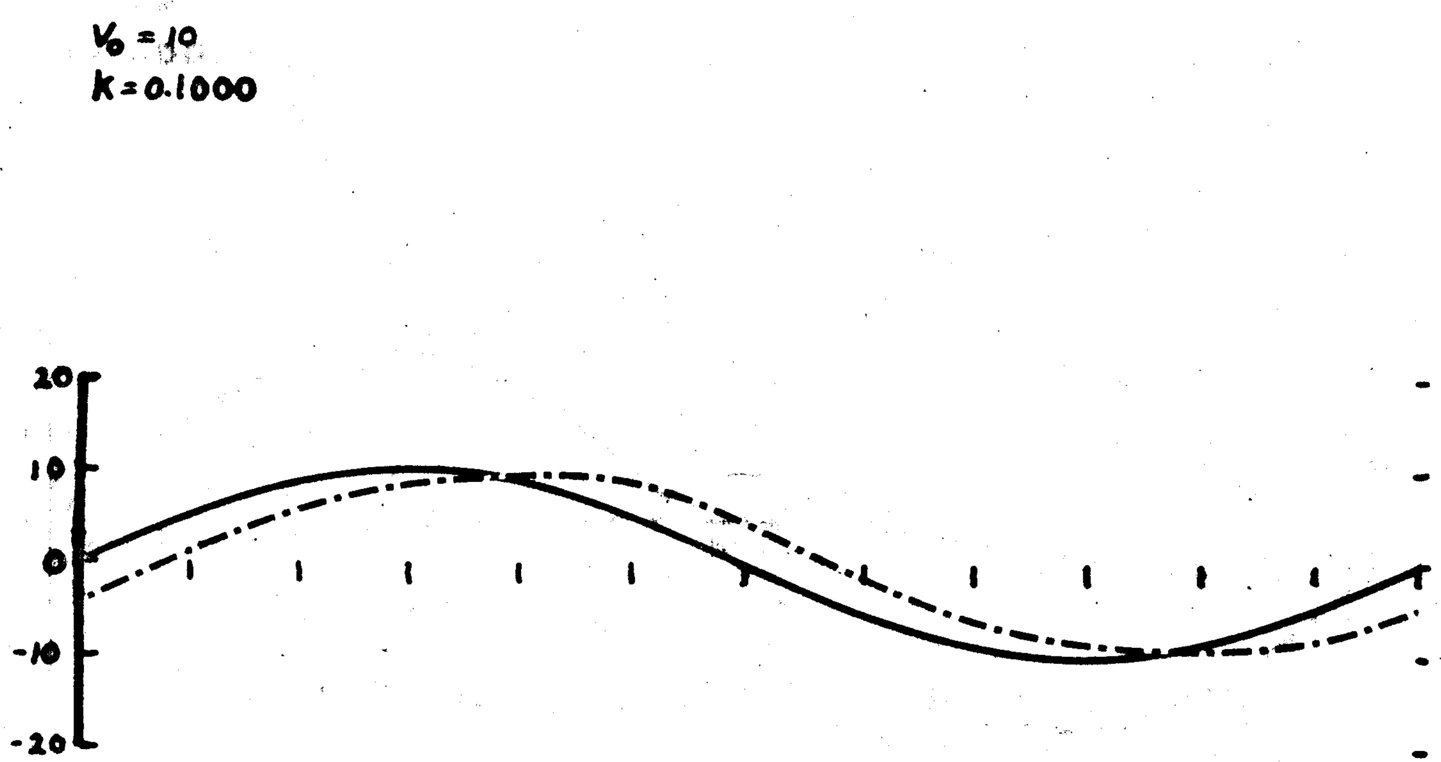

Figure G12 Current Speed and Iceberg Drift Speed vs. Time
V_o=10 cm/sec, K=0.1000

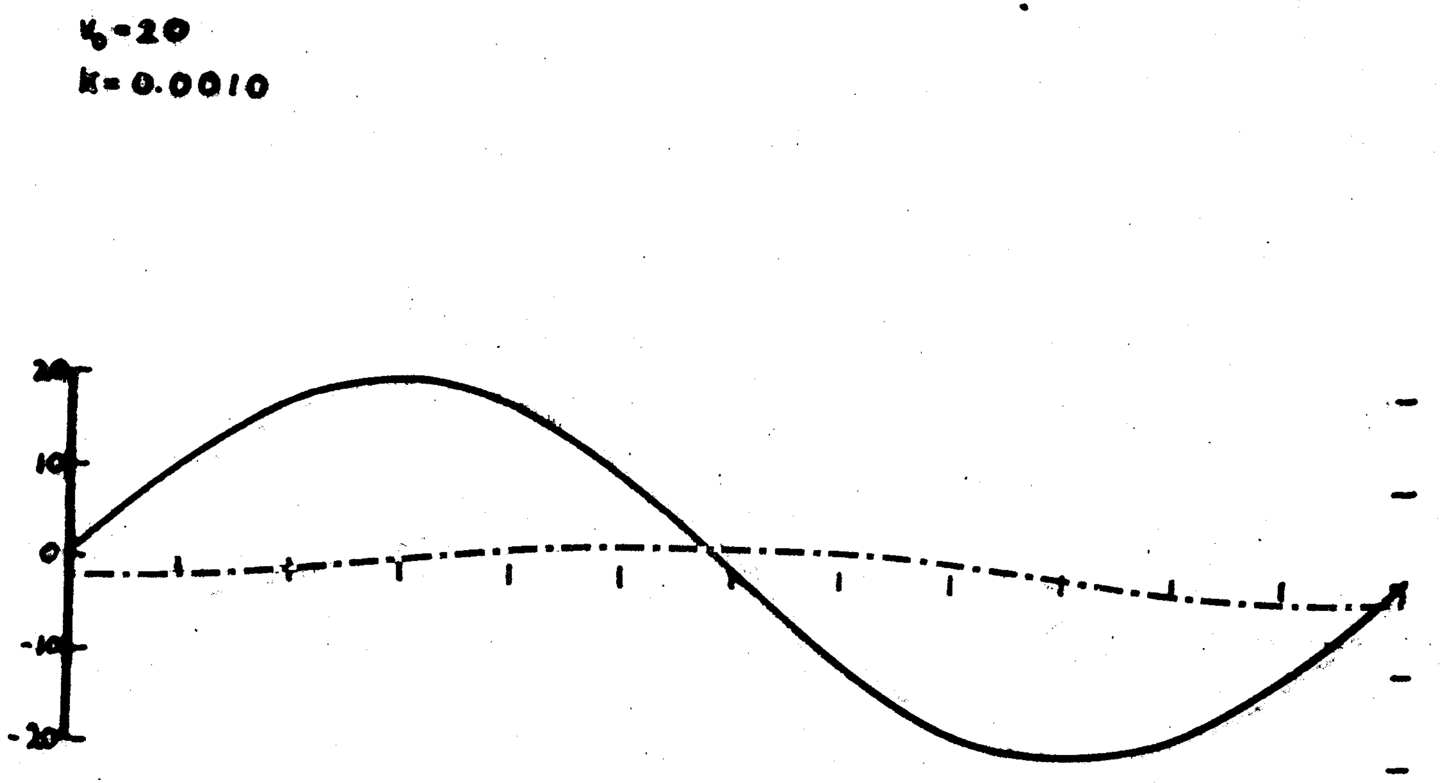

Figure G13 Current Speed and Iceberg Drift Speed vs. Time
V_o=20 cm/sec, K=0.0010

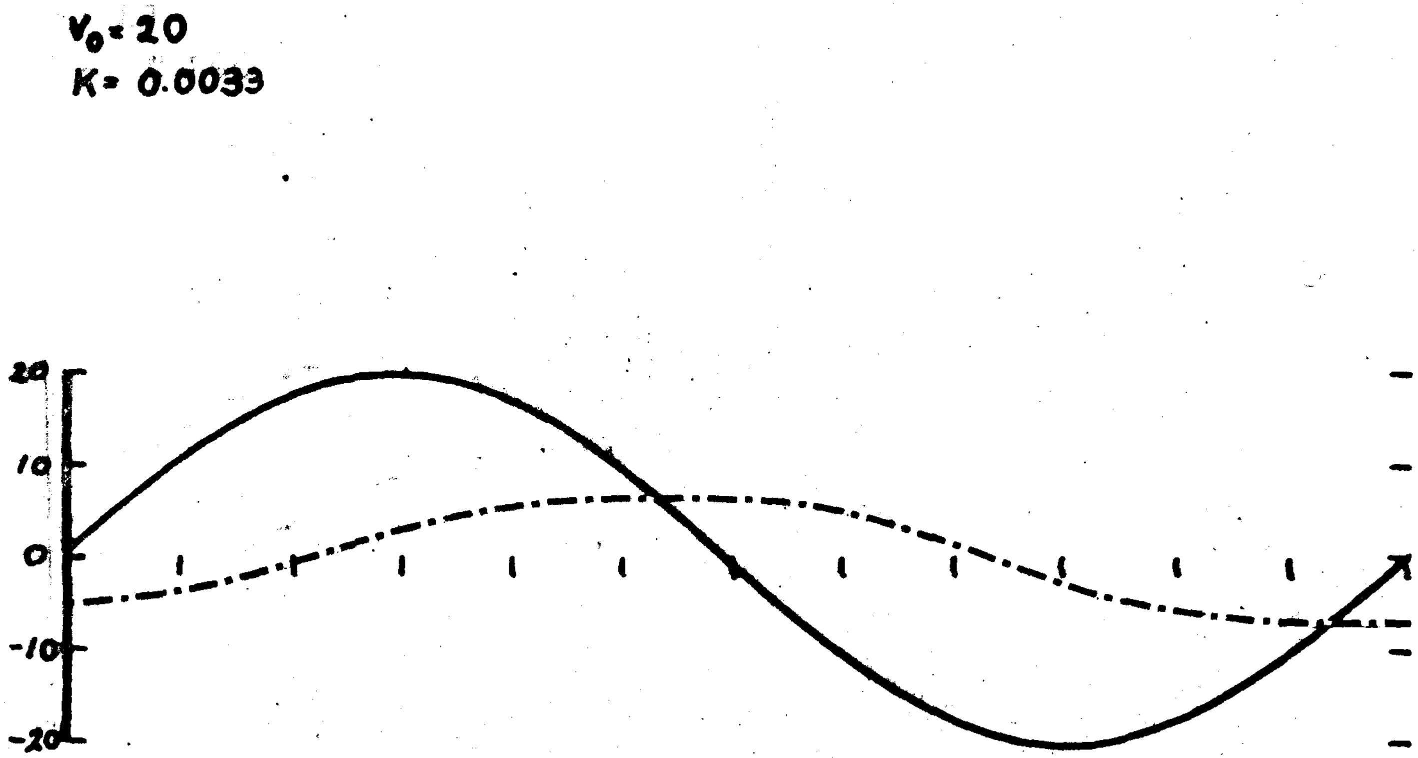

Figure G14 Current Speed and Iceberg Drift Speed vs. Time
V_o=20 cm/sec, K=0.0033

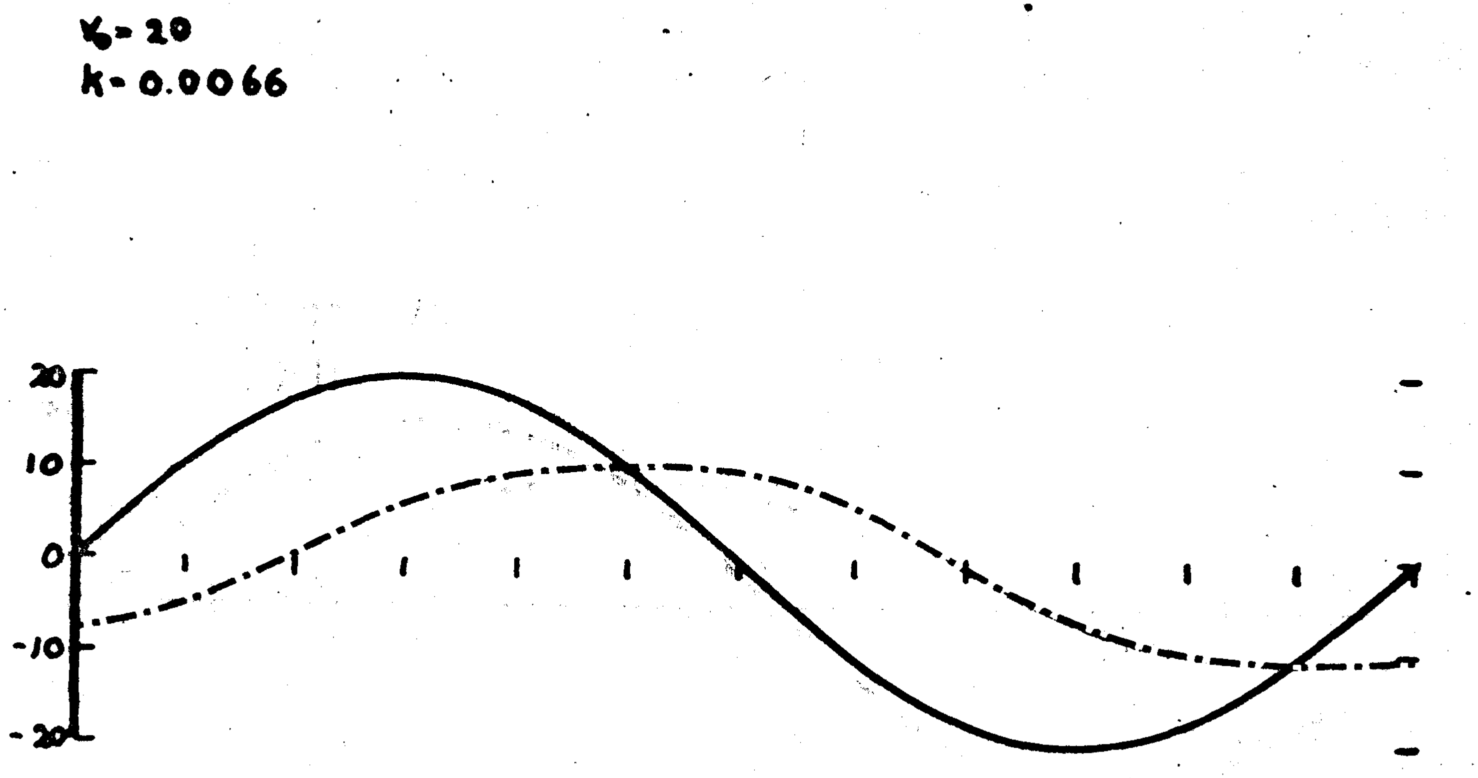

Figure G15 Current Speed and Iceberg Drift Speed vs. Time
V_O=20 cm/sec, K=0.0066

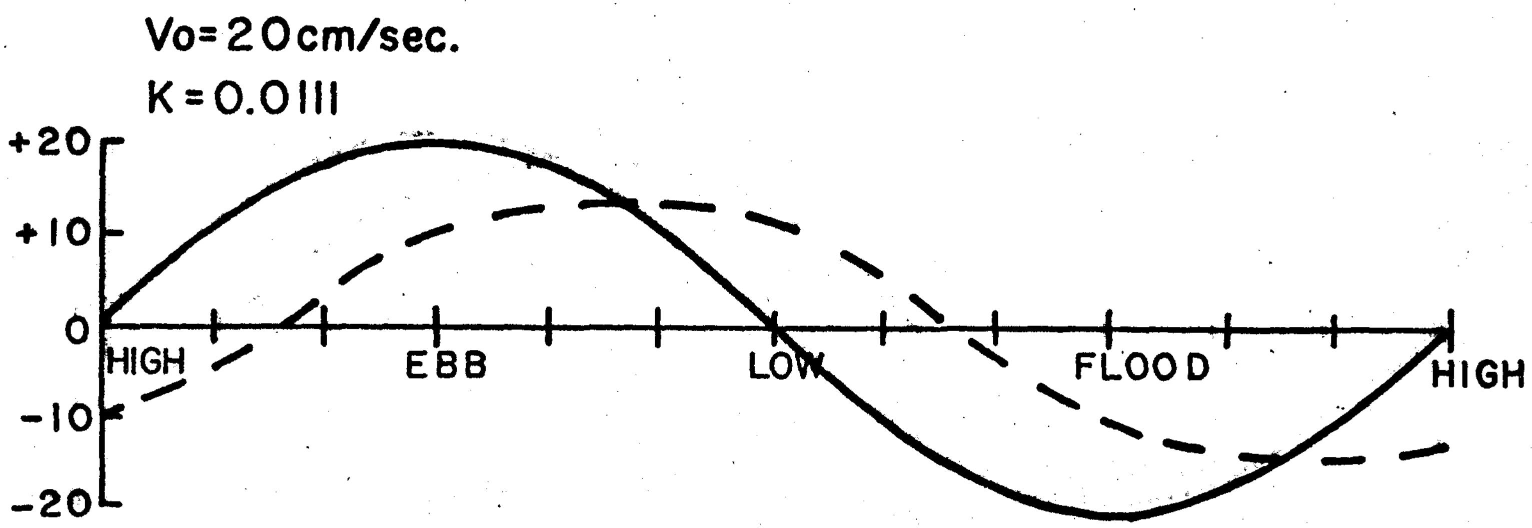

Figure G16 Current Speed and Iceberg Drift Speed vs. Time
V_o=20 cm/sec, K=0.0111

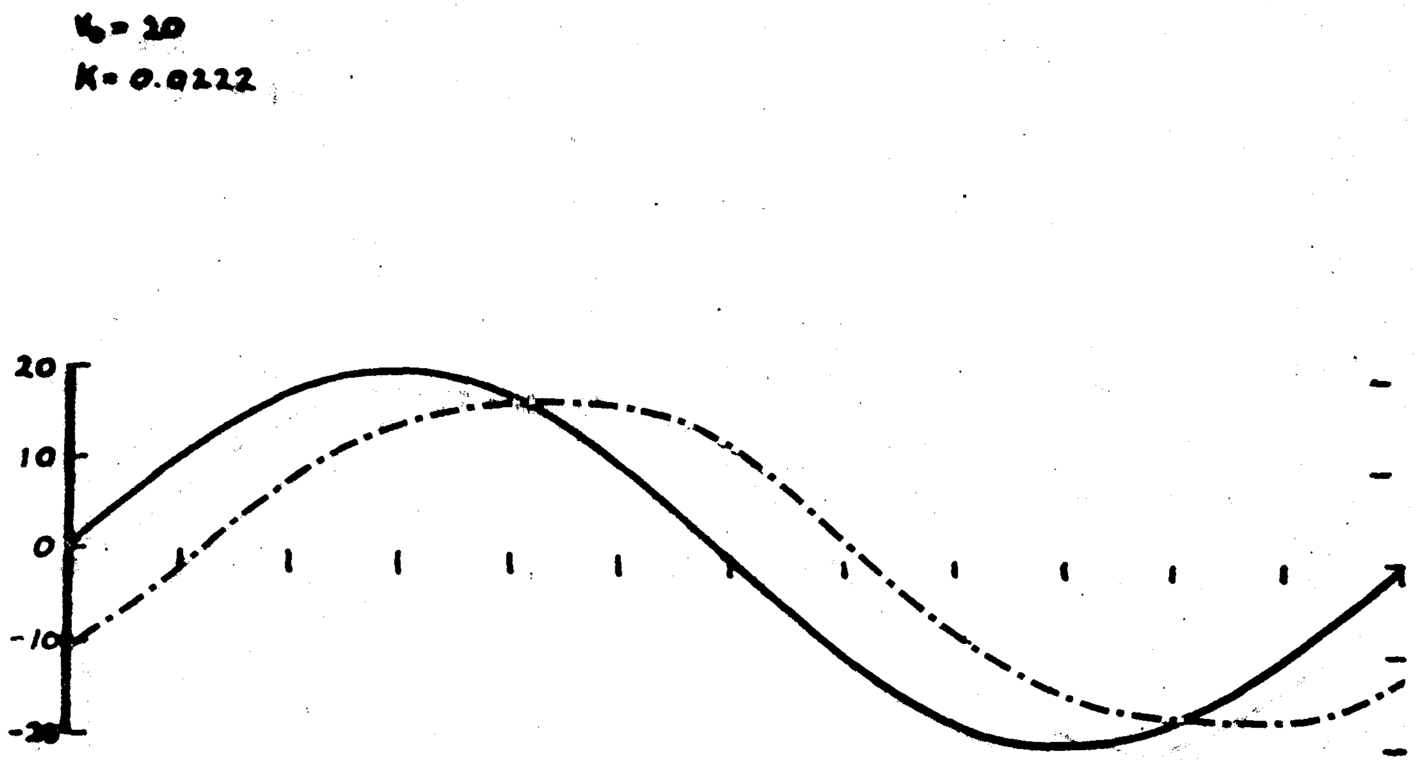

Figure G17 Current Speed and Iceberg Drift Speed vs. Time
V_o=20 cm/sec, K=0.0222

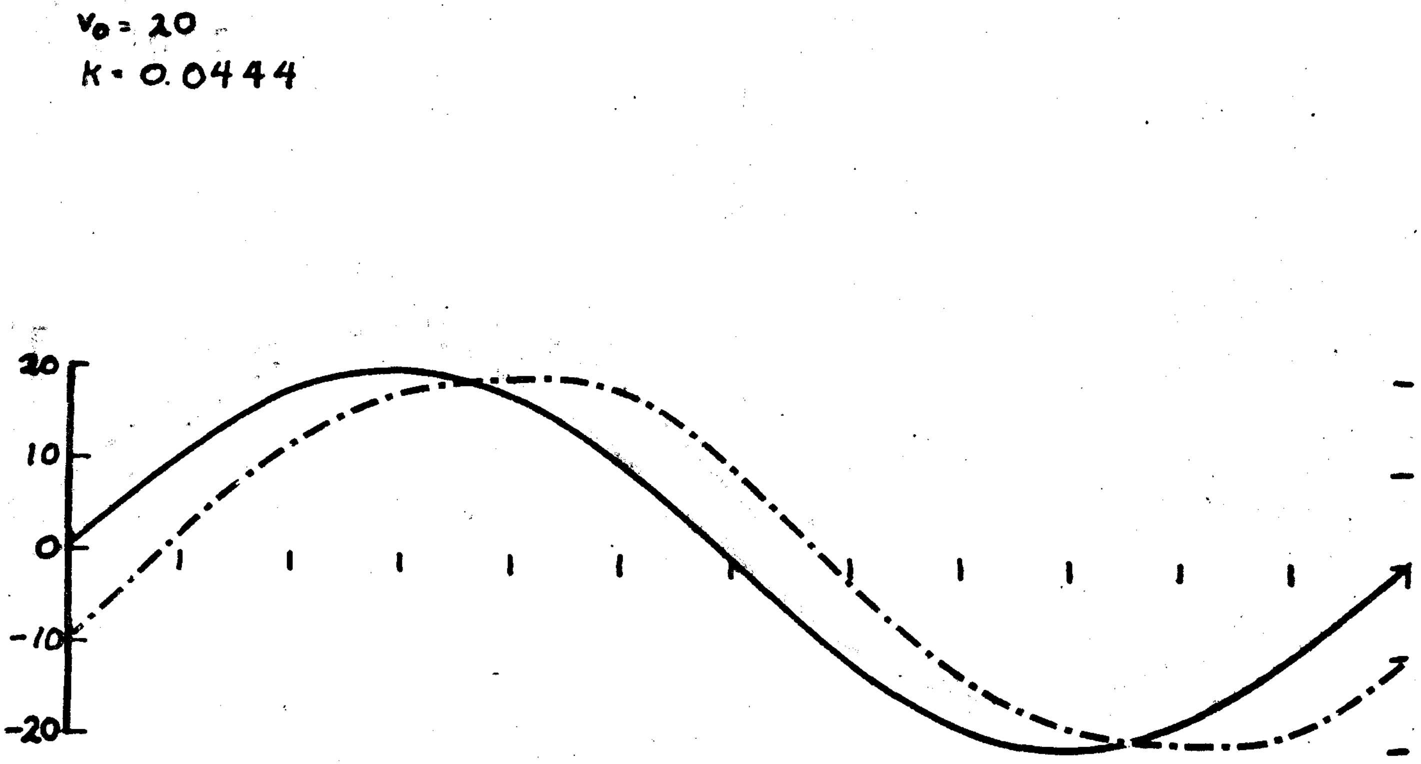

Figure G18 Current Speed and Iceberg Drift Speed vs. Time
V_o=20 cm/sec, K=0.0444

Figure G19 Current Speed and Iceberg Drift Speed vs. Time
V_o=20 cm/sec, K=0.1000

SELECTED BIBLIOGRAPHY

Aagaard, K. and L. K. Coachman, 1968. The East Greeland Current North of Denmark Strait, Part I, Arctic, 21, 182-200, Part II, Artic, 21, 276-290.

Abbott, M. R., 1960. Salinity Effects in Estuaries, J. Mar. Res., 18, 101-111.

Agnew, R., 1961. Estuarine Currents and Tidal Streams, Proc. 7th Conf. Coastal Engr., The Hague, 1960, 2, 510-535.

Arons, A. B. and H. Stommel, 1951. A Mixing Length Theory of Tidal Flushing, Trans. Am. Geophys. U., 32, 419-421.

Avery, D. E., 1968. An Integrating Current Meter, Deep Sea Res., 15, 235-236.

Beyer, F., E. Foyn, T. J. Ruud, and E. Totland, 1967. Stratified Current Measured in Oslofjord by Means of a New Continuous Depth-Current Recorder: The Bathyrheograph, J. Du Conseil, 31, 5-26.

Bowden, K. F., 1963. The Mixing Process in a Tidal Estuary, Int. J. Air and Water Poll., 7, 343-356.

Bowden, K. F. and L. A. Fairbairn, 1952. A Determination of the Frictional Forces in a Tidal Current, Proc. Roy. Soc., A 214, 317-392.

Bowditch, N., 1966. American Practical Navigator, U.S. Navy Hydrographic Office, U.S. Govt. Print. Office.

Brown, D. M., 1965. Results of Current Measurements with Drogues, Scripps Inst. Ocean., U. of Cal. 65, 28 p.

Budinger, T. F., 1960. Wind Effect on Icebergs, Int. Ice Patrol., U.S. Coast Guard.

Burt, W. V. and J. Queen, 1957. Tidal Overmixing in Estuaries, Science, 126 (3280), 973-974.

Cameron, W. M., 1951. On Tranverse Forces in a British Columbia Inlet, Trans. Roy. Soc., Canada, 45, 1-8.

Cameron, W. M. and D. W. Pritchard, 1963. Estuaries, The Sea, M. N. Hill, Ed., Interscience, New York, 2, 306-324.

Cameron, G. A., 1968. The Anatomy of an 86 hour Current Velocity Record from a Coastal Plain Estuary, Ocean Sci. and Engr. of the Atlantic Shelf Symposium, Mar. Tech. Soc., Delaware Valley Sect., 63-69.

Crean, P. B., 1967. Physical Oceanography of Dixon Entrance, B.C., Canada Fish. Res. Bd. No. 126.

Dem'yanov, N. I. and S. I. Stepanov, 1966. Comparison of Data Obtained with Different Types of Current Meters, Oceanology, 6, 289-294.

Duncan, C. P., 1965. Disadvantages of the Olson Drift Card and Description of a Newly Designed Card, J. Mar. Res., 23, 233-236.

Forrester, W. D., 1960. Plotting of Water Current Patterns by Photogrammetry, Photogram. Engr., 26 (12).

Frassetto, R., 1967. A Neutrally Buoyant, Continuously Self Recording Ocean Current Meter for Use in Compact Deep Moored Systems, Deep Sea Res., 14, 145-158.

Gerard, R. D. Some New Techniques in Parachute Drogue Technology, Lamont Geophys. Obs., Columbia U. Contrib. 851, 1088-1094.

Glenne, B. and T. Simensen, 1963. Tidal Current Chokeing in the Land-locked Fjord of Nordasvatnet, Sarsia 11.

Godin, G., 1967. The Analysis of Current Observations, The Int. Hydro Review, 44, 149-165.

Gordon, A. L., Dye Observations in the Upper Few Meters of Ocean, Trans. Am. Geophys. U., 50, 182.

Hansen, D. V., 1965. Currents and Mixing in the Columbia River Estuary, Ocean Sci. and Ocean Engr., 1, Trans. of Joint Conf. Mar. Tech. Soc. and Am. Soc. of Limnology and Ocean., 943-955.

Hansen, D. V. and M. Rattray, Jr., 1965. Gravitational Circulation in Straits and Estuaries, J. Mar. Res., 23, 104-122.

Ingram, R. G., O. M. Johannessen and E. R. Pounder, 1969. Pilot Study of Ice Drift in the Gulf of St. Lawrence, J. Geophys. Res., 74, 5453-5459.

Inglis, C. C. and F. H. Allen, 1957. The Regimen of the Thames Estuary as Affected by Currents, Salinity and River Flow, Proc. Inst. Civil Engr., 7, 827-878.

Johannessen, O. M., 1968. Some Current Measurements in Drobak Sound, The Narrow Entrance to the Oslofjord, Hvalrddets Skrifter Scientific Results of Marine Biological Res., Univer. Institutt for Marin Biologi and Statens Institutt for Hvalforakning Nr. 50, Oslo, 38 p.

Keller, M., 1963. Tidal Current Surveys by Photogrammetric Methods, U.S. Coast and Geod. Surv. Tech. Bull. N 22, 20 p.

Kent, R. E. and D. W. Pritchard, 1956. A Method for Determining Longitudinal Velocities in a Coastal Plain Estuary, J. Mar. Res., 15, 81-91.

Khundzhua, G. C., A. G. Vaskanyan, and A. A. Pivovarov, 1967. Methods for Remote Recording of the Velocitiy and Direction of Currents in the Upper Layers of the Sea, Oceanology, 7, 137-141.

Kinsman, B., 1965. Notes on Tides, Seiches and Long Waves, The Johns Hopkins U., Chesapeake Bay Inst., Balt. Md., 258 p.

Kinsman, B., 1965. Kinsman's Notes on Lectures on Estuarine Oceanography Delivered by D. W. Pritchard, 3 Oct. - 14 Dec. 1960, Johns Hopkins U., Chesapeake Bay Inst. of Ocean., Balt. Md., 154 p.

Knauss, J. A., 1963. Drogues and Neutral-Buoyant Floats, The Sea, M. N. Hill, Ed., 2, 303-305.

Korshunov, Yu. S., 1963. Oblique Wave Photography with a single Aerial Survey Camera from a Plane, Trans. of Marine Hydrophys. Inst., Acad. of Sci., USSR.

Malkus, W. V. R., A Recording Bathypitometer, J. Mar. Res., 12, 51-59.

Manual of Photogrammetry, American Society of Photogrammetry, Box 286, Benj. Franklin Sta., Wash., D.C., 1952.

Matthews, J. B. and D. R. Rosenberg, 1969. Numeric Modelling of a Fjord Estuary, Progress Report of the Off. of Naval Res., Contract No. 3010(05), U. of Alaska, 24-40.

McAllister, W. B., M. Rattray, Jr., and C. A. Barnes, 1968. The Dynamics of a Fjord Estuary: Silver Bay, Alaska, Tech. Rept., Dept. Ocean., U. of Wash., No. 62, 70 p.

Montgomery, R. B., 1968. Oceanic Leveling by a Vessel Crossing a Current J. Mar. Res., 26, 80-81.

Neyman, V. G., 1966. Measurement of Currents from a Drifting Vessel, Oceanology, 6, 132-134.

Niskin, S. J., 1968. A Method and Arrangement for Recording Current Fields and Total Volume Transport in Vertical Profiles from Sea Surface to Any Desired Depth, Mar. Sci. Instrumentation 4, 15-18.

O'Brien, M. P., 1952. Salinity Currents in Estuaries, Trans. Am. Geo. Un., 33, 520-522.

Ommanney, C. S. L., G. Holdsworth and O. H. Loken, 1970. Iceberg Production Survey of Arctic Canada, Preprint of Paper Presented to Bering Sea Symposium, U. of Alaska, 10 p.

Pickard, G. L., 1953. Oceanography of British Columbia Mainland Inlets, Prog. Rept. of Pacific Coast Sta., J. Fish Res. Bd., Canada, 907-999.

Pickard, G. L. and K. Rodgers, 1959. Current Measurements in Knight Inlet, British Columbia, J. Fish Res. Bd., Canada, 635-678.

Pritchard, D. W., 1952. Salinity Distribution and Circulation in the Chesapeake Bay Estuarine System, J. Mar. Res., 11, 106-123.

Pritchard, D. W., 1954. A Study of the Salt Balance in a Coastal Plain Estuary, J. Mar. Res., 13, 133-144.

Pritchard, D. W., 1957. Discussion of "On Estimating Streamflow in a Tidal Estuary," by David K. Todd and Leung-Ku Lau, Trans. Am. Geophys. Un., 38, 581-583, Reply, 583-584.

Pritchard, D. W., 1958. The Equations of Mass Continuity and Salt Continuity in Estuaries, J. Mar. Res., 17, 412-423.

Pritchard, D. W. and W. V. Burt, 1951. An Inexpensive and Rapid Technique for Obtaining Current Profiles in Estuarine Waters, J. Mar. Res., 10, 180-189.

Pritchard, D. W. and R. E. Kent, 1956. A Method for Determining Mean Longitudinal Velocities in a Coastal Plain Estuary, J. Mar. Res., 15, 81-91.

Rattray, M. Jr., 1967. Some Aspects of the Dynamics of Circulation in Fjords, Estuaries, George H. Lauff, Ed., AAAS Pub. 83, 52-62.

Reid, J. L. Jr., 1958. A Comparison of Drogue and GEK Measurements in Deep Water, Limn. and Ocean. 3, 160-165.

Richardson, W. S., A. R. Carr, and H. J. White, 1967. Description of a Freely Dropped Instrument for Measuring Current Velocity, J. Mar. Res., 27, 153-157.

Rosenfield, G. H., 1967. Horizon Camera Orientation, Photo. Engr. 33.

Saelen, O. H., 1967. Some Features of the Hydrography of Norwegian Fjords, Estuaries, George H. Lauff, Ed., AAAS Pub. 83, 63-70.

Shvede, Ye. Ye., 1966. Icebergs of the Northwest Atlantic, Oceanology, 6, 499-504.

Stewart, R. W., 1957. A Note on the Dynamic Balance in Estuarine Circulation, J. Mar. Res., 16, 34-39.

Stommel, H. and H. G. Farmer, 1953. Control of Salinity in an Estuary by a Transition, J. Mar. Res., 12, 13-20.

Swanson, L. W., M. Keller and S. D. Hicks, 1963. Photogrammetric Measurement of Tidal Currents, USC&GS, presented at Int. Un. of Geod. and Geophys., 13 Gen. Assembly.

Swallow, J. C., 1955. A Neutral-Buoyancy Float for Measuring Deep Currents, Deep Sea Res., 3, 74-81.